Slow Electromechanical Interference Links Division Geometry, Differentiation Bias, and Senescence-like Arrest

Alfonso De Miguel Bueno

Independent Researcher, Madrid, Spain
ORCID: 0009-0000-5420-3805
ademiguelbueno@gmail.com

Preprint, November 11, 2025

Abstract

This work develops a biophysical theory in which a bioelectric field $V(x,t)$ and a cortical stress field $\sigma(x,t)$ are weakly and reciprocally coupled. In the fast band, the dynamics are captured by *two weakly coupled first–order latent modes* that produce two damped carriers $f_\pm$ and a measurable slow beat $f_{\text{slow}} = |\Omega_+ - \Omega_-|/(2\pi)$. Sampling the dynamics at the neutral moment (the recurring near–symmetric crossing between V and σ) yields an even circle map (mod π) for the slow phase with forcing Ω and even–harmonic coupling K_2. To first order, Ω is controlled by the fast–band carrier ratio $r_{\text{eff}} = \Omega_-/\Omega_+$ via $\Omega \simeq \frac{\pi}{2}(1 - r_{\text{eff}})$, while K_2 is obtained by neutral–moment regression.

We define a functional order parameter $\Lambda \equiv C_{V\sigma}(f_{\text{slow}})$ as the cross–spectral coherence between V and σ at f_{slow}. We hypothesize that high Λ within (or repeatedly re–entering) the 2/21 Arnold tongue is associated with stable spindle orientation and cortical anchoring during division, whereas drifting away suggests two generic failure modes: (i) persistent unlocking with low Λ and elevated spindle–angle dispersion, and (ii) over–locked, low–plasticity states with a rigid slow cadence. Appendix E formalizes this as a cycle–resolved "re–entry" analysis.

The theory yields preregisterable, falsifiable predictions. (P1) Homeostatic epithelia exhibit two fast–band carriers together with a narrow shared slow–band peak and elevated $\Lambda = C_{V\sigma}(f_{\text{slow}})$. (P2) The pair (Ω, K_2), obtained from the fast–band carriers (for Ω) plus neutral–moment stroboscopy (for K_2), lies inside the 2/21 tongue while avoiding broad low–order tongues. (P3) A weak, frequency–specific electrical or mechanical drive at f_{slow} increases Λ and reduces spindle–angle dispersion relative to an energy–matched off–resonant control, with efficacy governed by alignment to the tissue–specific f_{slow}.

In addition (P3.c), a small persistent bias ε_b breaks even parity, mixes harmonics, raises even components and $(f_0, f_0 \to 2f_0)$ bicoherence, and produces a non–monotonic power–versus–coherence response, as reproduced by our numerical surrogate.

This study provides analytical bounds and preregistered analysis code, enabling direct experimental tests using combined optical electrophysiology and mechanical readouts.

Keywords: tissue electromechanics; bioelectricity; cortical tension; weak coupling; latent modes; carrier splitting; slow beat; neutral moment; even circle map; neutral–moment stroboscopy; parity mixing; $(f_0, f_0 \to 2f_0)$ bicoherence; mode locking; Arnold tongues; 2/21 rotation number; helical quantization; Ω (forcing); K_2 (even coupling); cross–spectral coherence Λ; cycle–by–cycle re–entry; synchronization/desynchronization; phase–targeted entrainment; preregistered analysis; in–silico prevalidation; voltage imaging; optical electrophysiology; traction force microscopy (TFM); atomic force microscopy (AFM); epithelial organoids.

Contents

1 Introduction **4**

2 Background and gaps the model addresses **6**

2.1 Relation to prior bioelectric models 7

3 Physical identity of the fields and oscillatory reduction consistent with the dual-field model **7**

3.1 Governing equations and oscillatory splitting 7

3.2 Phase-map reduction and parity switching 9

4 Even circle map and rotation number **10**

5 Helical quantization without fitted integers **11**

6 An experimental coherence observable **11**

7 Mechanistic link to division and differentiation **11**

7.1 Testable pathology signatures (aging and proliferative unlocking) 12

7.2 Phase-guided modulation (phase-targeted entrainment) 13

7.3 Regenerative bioelectrical stimulation: empirical frequencies and dynamical specificity 13

8 Falsifiable experimental targets **14**

9 Materials and methods **15**

9.1 Electrical and mechanical parameters 15

9.2 Candidate systems and parameter acquisition 15

9.3 Spectral estimation and coherence 16

9.4 Rotation number and stroboscopic regression 16

9.5 Statistical model for the coupling K_2 17

9.6 Biological King plot: common-curvature test (pre-experimental) 17

9.7 Experimental candidates and realism 17

9.8 Preregistered reanalysis on public datasets (Level-1 verification) 18

10 In-silico validation: continuum sandbox and cell-based models **20**

10.1 Reference implementation (concept and usage) 20

11 Reproducible in-silico regimes: implementation and outputs **21**

12 Results: analytical and numerical evidence **26**
12.1 Analytical width bounds . . . 26
12.2 Sensitivity and low-order exclusion for P2 . . . 26
12.3 Phase-locking geometry in the even convention . . . 27
12.4 Slow-band spectra and coherence (P1) . . . 28
12.5 Common-curvature signatures (preliminary, *in silico*) . . . 28
12.6 Fast-band spectra (carriers $f_{\pm}$) . . . 29
13 Pre-Experimental Validation of Mode Selection **29**
13.1 First-order control of the slow forcing without physical inertia . . . 29
13.2 Biological meaning of the phase map (one-minute recap) . . . 31
13.3 Definition of the neutral moment and slow-phase map . . . 31
13.4 Quantitative check with independently chosen parameters . . . 31
13.5 Falsifiable outcomes for P1–P3 . . . 31
14 Relation to the original c and c' formalism **32**
15 Robustness, physiological levers, and scope to other helices **33**
16 Limitations **34**
16.1 Scope, extensions, and mechanistic context . . . 34
17 Conclusion **35**
Appendix A Common-curvature diagnostics (SVD and alternation) **37**
Appendix B Numerical simulation of the overdamped continuum coupler (Eqs. 19–21) **38**
B.1 Overdamped continuum electromechanical coupler . . . 38
Appendix C Molecular integration of the electromechanical tissue model **39**
Appendix D Biological basis of the 2/21 lock **40**
D.1 Why 2/21 matters biologically (evolutionary canalization) . . . 40
D.2 Prevalidation and falsifiability: how the lock is tested . . . 41
D.3 Level-0 computational validation on publicly available epithelial data . . . 42
D.4 Level-1 dual-channel analysis pipeline (synthetic demonstration and public applicability) . . . 44
D.5 Parameter dictionary (experimental interpretation) . . . 47
D.6 Bidirectional correction loops (homeostatic control) . . . 47
D.7 Relation to canonical signalling pathways . . . 47
Appendix E Cycle-resolved neutral-phase analysis, re-entry, and sliding-window map fits **48**
E.1 Neutral crossings and slow-phase sampling . . . 49
E.2 Local windows A / B / C around each neutral crossing . . . 49
E.3 Sliding-window estimation of (Omega-hat, K2-hat) . . . 50

E.4 Cycle-resolved timing of the sync transition and division phases 51
E.5 Diagnostic figure (conceptual layout) 52
E.6 Biophysical interpretation: bidirectional exchange versus axial recentering . 52

Appendix F Capture kinetics across time scales: quantitative predictions and in-silico prevalidation 53

F.1 Averaged slow-phase flow and capture time 53
F.2 Testable timing for division-scale phases 54
F.3 Minimal in-silico prevalidation 54

Appendix G Computational prevalidation of P3 (weak entrainment and resonant recovery of slow-phase locking) 55

G.1 Readouts for recovery by entrainment: Delta Lambda and Var map 55
G.2 Weak-drive protocol in silico (extension of Case D) 56
G.3 Resonance curve in a reduced noisy circle map 57
G.4 Cross-system plausibility from human iPSC-derived cardiomyocyte syncytia 58
G.5 Preregistered falsification criteria 58

Appendix H Speculative protocols for bench-scale tests of P3 59

Appendix I Popperian falsification of linearity and nonlinear predictions 60

I.1 Computational test of falsifiability 60
I.2 P3.a — Phase-locked neutral crossings 62
I.3 P3.b — Transition sharpness modulates slow-band power 63
I.4 P3.c — Persistent bias: parity mixing, rectified pumping, and a non-monotonic response 63
I.5 Neutral-crossing bias and parity mixing 63
I.6 Breakdown of parity cancellation under amplitude skew 64

18 Supplementary Code Listings (reproducibility) 64

18.1 Listing S0. Dual-field pseudo-spectral sandbox and analysis pipeline. . . . 64
18.2 Listing S1. Level-0 analysis script (public epithelial movie). 69
18.3 Listing S2. Level-1 dual-channel pipeline script (synthetic benchmark). . . 76
18.4 Listing S3. P3_sandbox computational prevalidation of P3 (weak resonant drive at f_slow) 83
18.5 Listing S4. Popper falsifiability (H1–H4) 87
18.6 Listing S5. Capture kinetics across time scales 94

19 Glossary of symbols 99

1 Introduction

Biological tissues exhibit coupled electrical and mechanical dynamics. Bioelectric potentials shape patterning, growth, and large-scale morphogenesis, while cortical tension and poroelastic stresses govern force transmission, division geometry, and tissue-scale mechanics [3, 5, 6, 8]. Controlled bioelectric cues can actively reshape tissues *in vivo* and

in vitro, and multicellular responses to electrophysiological perturbations can be captured quantitatively by bioelectrical models [3, 4, 5]. Here we treat these two sectors explicitly as fields: a bioelectric field $V(\mathbf{x}, t)$ and a cortical stress field $\sigma(\mathbf{x}, t)$ that are weakly and *reciprocally* coupled.

In the fast band, the observable dynamics arise from *two weakly coupled first-order latent modes* that generate two damped carriers in the 1–3 Hz range. Their slight detuning produces a measurable slow beat $f_{\text{slow}} = |\Omega_+ - \Omega_-|/(2\pi)$ at the mesoscale set by the effective thickness ℓ (i.e., $k^* = \pi/\ell$). This two-mode coupling succinctly accounts for the apparent second-order features in the measured time series—namely, voltage-imaging traces $V(t)$ and traction/AFM-based stress reconstructions $\sigma(t)$ in epithelial monolayers.

Sampling the dynamics at the *neutral moment*—the recurring near-symmetric crossing between V and σ where the relative phase ψ passes through 0 (mod π) with positive slope—yields an *even* circle map (mod π) for the slow phase. In this reduced description, the forcing Ω and the even-harmonic coupling K_2 are defined directly from data: to first order,

$$\Omega \simeq \tfrac{\pi}{2}\big(1 - r_{\text{eff}}\big), \qquad r_{\text{eff}} = \frac{\Omega_-}{\Omega_+},$$

with r_{eff} obtained from the fast-band carriers, while K_2 is estimated by neutral-moment regression.

Within this framework we propose that the slow electromechanical phase does not just exist spectrally, but coordinates two biological scales that are usually treated separately. On one side, it constrains spindle geometry and cortical anchoring during mitosis, limiting spindle-angle dispersion and chromatin torsional load at division checkpoints. On the other side, it provides a dynamical compatibility window for helical coordination. We focus on a narrow high-order lock, the 2/21 tongue, used here as a concrete target whose center is $\Omega_{2/21} = \pi \cdot 2/21$. We do not assume a direct forcing of molecular helical pitch by a tissue-scale cadence; any apparent alignment remains to be established empirically. The analysis concerns tissue-level observables (f_{slow}, Λ, and (Ω, K_2)), with cross-scale links treated operationally via the cycle-resolved neutral-reset analysis (Appendix E).

A central observable is the cross-spectral coherence $\Lambda \equiv C_{V\sigma}(f_{\text{slow}})$ between V and σ at f_{slow}. High Λ indicates that the bioelectric and mechanical sectors share a common slow cadence and remain phase-locked across neutral moments, whereas low Λ indicates slow-cadence drift between sectors. Together with the neutral-moment map parameters (Ω, K_2), Λ provides a concrete test of whether tissue sits within a specific high-order Arnold tongue (notably 2/21) and whether departures from that window correlate with pathological states.

Physiological tissue is not expected to sit forever in a perfectly locked, stationary regime. Instead, Appendix E formalizes a *cycle-resolved* analysis in which healthy tissue repeatedly *re-enters* the 2/21 band on each slow cycle. Operationally, we identify each neutral moment, compute local slow-band coherence around it, and track the sliding estimates $(\widehat{\Omega}, \widehat{K}_2)$ over many cycles. Failure to re-enter takes two characteristic forms. First, *persistent unlocking*: the system drifts out of 2/21, Λ collapses, and spindle orientation becomes erratic. Second, *aging-like overlock*: the system remains trapped near the neutral state, Λ stays high but rigid, and adaptability is lost. In this reading, cancer-like genomic instability and aging-like loss of plasticity are opposite dynamical arrests of the same electromechanical cycle.

The theory yields three preregisterable predictions (P1–P3) with direct experimental readouts. P1: homeostatic epithelia exhibit two fast-band carriers together with a narrow shared slow-band peak and a coherence maximum $\Lambda = C_{V\sigma}(f_{\text{slow}})$. P2: the forcing/coupling

pair (Ω, K_2), obtained from the fast-band carriers (for Ω) and neutral-moment stroboscopy (for K_2), lies inside the predicted 2/21 Arnold tongue while avoiding broad low-order tongues. P3: a weak, frequency-specific electrical or mechanical drive at f_{slow} should increase Λ and reduce spindle-angle dispersion relative to an energy-matched off-resonant control. Appendix G gives a preregistered assay for P3 and an *in silico* prevalidation in which a synthetic unlocked state is driven weakly at f_{slow}, showing selective recovery of slow-phase locking (higher Λ) and reduced angular noise in the neutral map, while off-band controls at $f_{\text{slow}}(1 \pm 0.10)$ fail to reproduce both effects together. Small persistent biases are also considered: a tonic offset breaks the π-symmetry of the neutral map, mixes parities, elevates even harmonics and $(f_0, f_0 \to 2f_0)$ bicoherence, and produces a non-monotonic power versus coherence response (Appendix I).

Within P3 we also preregister three mechanistic subtests—**P3a** (phase-locked neutral crossings), **P3b** (transition sharpness vs. slow-band power), and **P3c** (bias-induced parity mixing and rectified pumping)—which share the same weak-drive paradigm and serve as falsifiers of linear, phase-preserving alternatives (see App. I and App. G).

All analysis code, the preregistered workflow, and the cycle-resolved diagnostics are provided in App. E and App. G; the main text is self-contained.

2 Background and gaps the model addresses

Current explanations for helical pitch selection and tissue-scale coordination tend to live at two extremes. One is molecular and statistical, treating double-helix structure and transcriptional programs as self-contained while largely ignoring tissue mechanics. The other is phenomenological and tissue-level, modeling collective mechanics, division geometry, or cortical tension without explicitly referencing the double-helix code. Both perspectives miss a cross-scale mechanism that is *dynamical*, directly *falsifiable*, and does not require manual integer tuning. Our dual-field framework is designed to bridge that gap in three specific ways:

1. **Mechanistic cross-scale link.** A measurable slow cadence f_{slow} emerges from the interaction between a bioelectric field $V(\mathbf{x}, t)$ and a cortical-stress field $\sigma(\mathbf{x}, t)$ that are weakly and reciprocally coupled. In the fast band, the observable dynamics are captured by *two weakly coupled first-order latent modes* (Eqs. 1–4) that produce two damped carriers with slight detuning; their interference defines $f_{\text{slow}} = |\Omega_+ - \Omega_-|/(2\pi)$. This slow cadence is predicted to coordinate checkpoints and spindle geometry at the tissue scale. The same neutral-moment (even) map that describes that slow phase fixes the effective rotation number ρ_π, with the high-order lock $\rho_\pi = 2/21$ used here as a concrete, testable target. Crucially, the 2/21 lock *emerges* from the even map and the measured carriers; it is not imposed as an ad hoc quantization rule.
2. **Parity control.** Sampling the fast electrical phase specifically at recurring near-symmetric crossings between V and σ (the *neutral moments*) produces an *even* circle map (mod π) whose Arnold–tongue structure is distinct from the *odd* (full-cycle) strobe. This built-in parity switch (even vs. odd) provides an internal falsification test: the locking and curvature structure we predict should appear under neutral-moment strobing and degrade, in a parity-sensitive manner, under full-cycle strobing.[1]
3. **Parameter provenance.** All quantities entering the reduced slow-phase map

[1] Operationally, neutral moments are the recurrent instants when the analytic-phase difference $\psi(t) = \arg Z_V - \arg Z_\sigma$ crosses 0 (mod π) with positive slope; sampling the fast phase there enforces even parity and yields an even (mod π) circle map.

are defined from data. To first order, the forcing is controlled by the carrier ratio $r_{\text{eff}} = \Omega_-/\Omega_+$ via $\Omega \simeq \frac{\pi}{2}(1 - r_{\text{eff}})$, and the even-harmonic coupling K_2 is obtained by neutral-moment regression (Eq. 5). This enables preregisterable tests rather than post hoc tuning. Directly measurable tissue properties (membrane time constant τ_m, cortical stiffness κ, viscosity η, diffusivities D_V, D_σ, and weak electromechanical gains γ, β_R, β_I) inform priors and channel projections; they do not require adding extra state variables to the observable equations.

Figure 21 summarizes this logic. Weak reciprocal coupling between V and σ produces two damped carriers $\Omega_\pm$ whose slight detuning defines a slow beat $f_{\text{slow}} = |\Omega_+ - \Omega_-|/(2\pi)$. Strobing at neutral moments yields an even circle map (mod π) with parameters (Ω, K_2) obtained from the measured carriers (for Ω via r_{eff}) and from neutral-moment regression (for K_2), avoiding manual integer tuning. From that map we obtain both (i) a predicted high-order locking tongue at $\rho_\pi = 2/21$ and (ii) a functional order parameter Λ, defined as the cross-spectral coherence between V and σ at f_{slow}, $\Lambda = C_{V\sigma}(f_{\text{slow}})$. High Λ indicates a shared slow cadence and stable phase locking between the electrical and mechanical sectors; low Λ indicates electromechanical drift. We interpret spindle-angle dispersion, cortical anchoring at division, and helical-phase stability as downstream readouts of the same locking structure, rather than as unrelated phenomena.

2.1 Relation to prior bioelectric models

Classical bioelectric frameworks emphasize voltage gradients, ionic currents, and patterning cues, often without including an explicitly reciprocal mechanical field. In contrast, the present dual-field reduction (i) treats V and σ as weakly but reciprocally coupled, (ii) predicts two underdamped carriers plus a slow interference cadence f_{slow} that is directly measurable rather than purely inferred, (iii) yields an *even* circle map at neutral moments, providing a built-in parity switch (even vs. odd strobing) that acts as an internal falsification control, (iv) computes (Ω, K_2) from directly measurable electrical and mechanical properties of the tissue, with no ad hoc quantization step, and (v) enables common-curvature "biological King plots" across observables (slow-band voltage power, slow-band stress power, and the functional order parameter Λ) as a compact universality test.

This is intended to complement bioelectric accounts of growth control, morphogenesis, and large-scale tissue coordination [3, 7], and to align with recent work showing that bioelectric control of tissue shape is quantitatively testable *in vivo* and *in vitro* [4], and that multicellular responses to electrophysiological perturbation can be captured by explicit predictive bioelectrical models [5].

3 Physical identity of the fields and oscillatory reduction consistent with the dual-field model

3.1 Governing equations and oscillatory splitting

We model the fast band as two weakly coupled first-order latent modes. In complex-amplitude form,

$$\dot{u}_1 = (-\alpha_1 + i\omega_1)\, u_1 + J\, u_2 + \xi_1(t), \qquad \dot{u}_2 = (-\alpha_2 + i\omega_2)\, u_2 + J\, u_1 + \xi_2(t), \tag{1}$$

with decay rates $\alpha_k > 0$, damped carrier frequencies $\omega_k > 0$, and a small complex coupling J. The two measured channels are real projections of these modes:

$$V(t) = \Re\{h_{V1}u_1 + h_{V2}u_2\}, \qquad \sigma(t) = \Re\{h_{S1}u_1 + h_{S2}u_2\}, \tag{2}$$

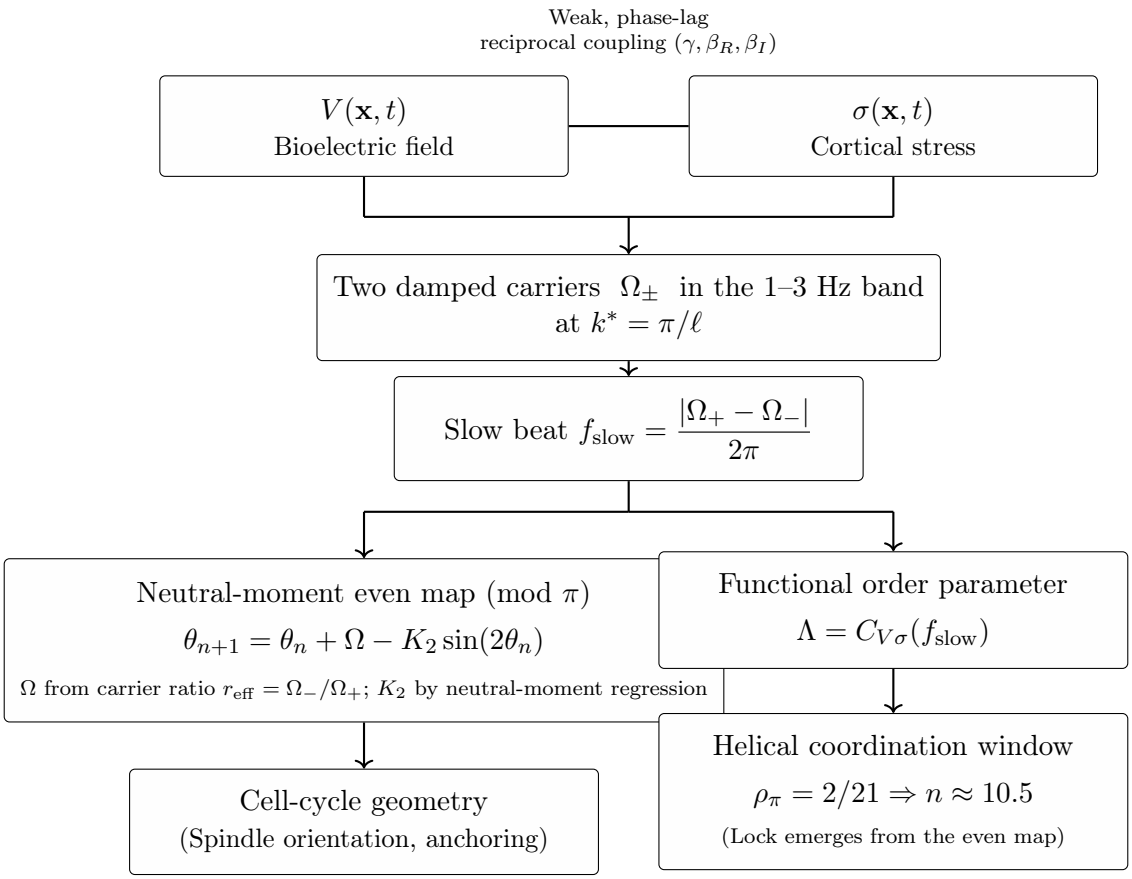

Figure 21: Conceptual pipeline linking (i) weakly and reciprocally coupled bioelectric and cortical-stress fields, (ii) two damped carriers $\Omega_\pm$ and their slow beat $f_{\text{slow}} = |\Omega_+ - \Omega_-|/(2\pi)$, (iii) the neutral-moment even map (mod π) with parameters (Ω, K_2) obtained from the measured carriers (for Ω via r_{eff}) and neutral-moment regression (for K_2), and (iv) two proposed biological readouts: spindle orientation / cortical anchoring and a narrow high-order compatibility window ($\rho_\pi = 2/21$). The 2/21 lock emerges from the even map rather than being imposed.

where $h_{(\cdot)k} \in \mathbb{C}$ collect instrument/mixing factors. Apparent second-order behavior in the fast band is captured here by the two-mode coupling itself (Eqs. 1–4), which already generates complex poles and a measurable f_{slow}.

Writing $\bar{\alpha} = \frac{\alpha_1+\alpha_2}{2}$, $\bar{\omega} = \frac{\omega_1+\omega_2}{2}$, $\Delta\alpha = \alpha_1 - \alpha_2$, and $\Delta\omega = \omega_1 - \omega_2$, the exponents of the 4×4 real system are

$$s_\pm = -\bar{\alpha} + i\,\bar{\omega} \;\pm\; \frac{1}{2}\sqrt{(\Delta\alpha - i\,\Delta\omega)^2 + 4\,|J|^2}. \tag{3}$$

Hence there are generically *two* damped carriers with observable frequencies $\Omega_\pm = \Im\, s_\pm$. In the symmetric case $\Delta\alpha = 0$,

$$|\Delta\omega| > 2|J| \;\Rightarrow\; \Omega_\pm = \bar{\omega} \pm \tfrac{1}{2}\sqrt{\Delta\omega^2 - 4|J|^2}, \qquad |\Delta\omega| \le 2|J| \;\Rightarrow\; \Omega_+ = \Omega_- = \bar{\omega}.$$

The slow beat is

$$f_{\text{slow}} = \frac{|\Omega_+ - \Omega_-|}{2\pi} = \frac{1}{2\pi}\left|\Im\sqrt{(\Delta\alpha - i\,\Delta\omega)^2 + 4\,|J|^2}\right|. \tag{4}$$

In summary, two weakly coupled first-order latent modes account for the fast-band structure: when $|\Delta\omega| > 2|J|$ the spectrum exhibits two damped carriers $\Omega_\pm$ with a slow beat $f_{\text{slow}} = |\Omega_+ - \Omega_-|/(2\pi)$, whereas under locking ($|\Delta\omega| \leq 2|J|$) the split collapses to a single carrier and $f_{\text{slow}} \to 0$. The apparent second-order features of the fast band are captured by the two-mode coupling itself (Eqs. 1–4).

Observed phases. If the projections are cross-dominant, $|h_{V1}| \gg |h_{V2}|$ and $|h_{S2}| \gg |h_{S1}|$, each channel follows the phase of the mode that dominates its projection in the desynchronized regime. Under locking, approximately odd/even combinations $h_{V1} \approx -h_{V2}$ and $h_{S1} \approx h_{S2}$ yield phase opposition in V and phase alignment in σ for the locked solution.

Role of nonlinearity (P3). Nonlinearity does not create the carriers; it mixes and rectifies their interference under a weak bias ε_b, raising even harmonics and the $(f_+, f_+ \to 2f_+)$ bicoherence and transmitting the cadence f_{slow} to the slow map.

Falsifiable check for two damped carriers. A brief, spatially uniform impulse followed by traction/stress readout should exhibit a lightly underdamped ring-down at the carrier band if the spectrum contains two complex poles. Fitting the impulse response with a single-carrier vs. two-carrier model discriminates whether a split consistent with Eqs. 3–4 is present. Alternatively, Hilbert-phase relative drift between channels detects a nonzero f_{slow} in the desynchronized regime ($|\Delta\omega| > 2|J|$) and its collapse under locking ($|\Delta\omega| \leq 2|J|$).

3.2 Phase-map reduction and parity switching

In the antisymmetric regime the two underdamped normal modes at $k^* = \pi/\ell$ alternate in dominance. We define the *neutral moment* as the recurrent instant when the instantaneous phase difference between V and σ is $0 \pmod{\pi}$ with a positive crossing slope, i.e. when $\phi_V(t) - \phi_\sigma(t) = 0 \pmod{\pi}$ and $\frac{d}{dt}[\phi_V(t) - \phi_\sigma(t)] > 0$; the signals are locally mirror-symmetric even if amplitudes remain unbalanced.[2] Taking that neutral moment as a Poincaré section identifies $\theta \equiv \theta + \pi$. In this π-quotient the leading nonlinearity is even, and the slow-phase map is:

$$\begin{aligned} \theta_{n+1} &= \theta_n + \Omega - K_2 \sin(2\theta_n) + \mathcal{O}(\sin 4\theta) \pmod{\pi}, \\ \Omega &\simeq \tfrac{\pi}{2}\left(1 - r_{\text{eff}}\right), \\ r_{\text{eff}} &= \frac{\omega_{-,r}(k^*)}{\omega_{+,r}(k^*)} \in (0,1) \qquad \text{(ratio of carrier frequencies } f_-/f_+ \text{ from Eqs. 1–4).} \end{aligned} \tag{5}$$

Type of nonlinearity. Because the neutral-moment section identifies $\theta \sim \theta + \pi$, the reduced phase map (5) must be parity-even; hence the leading nonlinear correction is quadratic and appears as $-K_2 \sin(2\theta)$, with higher even orders $\mathcal{O}(\sin 4\theta)$. Odd harmonics (e.g., $\sin\theta$) are symmetry-forbidden in the unbiased regime and only emerge when parity is broken by a sustained bias (cf. Sec. I.4). In Listing S4 we report two compact empirical checks supporting this classification: the even/odd spectral ratio $P(2f_+)/P(3f_+)$ and the normalized bicoherence at $(f_+, f_+ \to 2f_+)$ with a phase-randomization p-value.

[2] Operationally, this marks a transient balance between inward (electrical) and outward (mechanical) tendencies, minimizing phase asymmetry and resetting the slow cadence.

Bias and parity mixing in the reduced map. A small tonic bias (electrical DC offset or mechanical prestress) does not remove slow alternation; it perturbs the reduced phase map by mixing even and odd harmonics. To leading order,

$$\theta_{n+1} = \theta_n + \Omega \;-\; K_2 \sin(2\theta_n) \;-\; \varepsilon_b\, K_1 \sin(\theta_n) \;+\; \mathcal{O}(\sin 3\theta, \sin 4\theta) \pmod{\pi}, \tag{6}$$

where ε_b measures the tonic offset (ionic or mechanical) and K_1 is the odd-parity projection at neutral moments. In the 2π lift of the section, the odd term is formally 2π-periodic; see Eq. (34) (Sec. I.4) for the explicit form used in the rectification analysis. The odd correction skews dwell times around neutral moments and *rectifies* the phase-gated exchange, which can increase slow-band power. In control-plane terms, mild bias raises the even-harmonic weight in the response while progressively reducing adaptability (Λ) as the operating point approaches tongue boundaries.

Here Ω is obtained directly from the carrier ratio $r_{\text{eff}} = \Omega_-/\Omega_+$ measured in the fast band, and K_2 is estimated by neutral-moment regression (Methods), with no ad hoc integer fitting.

Within this π-circle convention, a p/q phase lock is centered at $\Omega \simeq \pi\, p/q$. In particular, for 2/21,

$$\Omega_{2/21} = \pi \cdot \frac{2}{21} \approx 0.2992 \text{ rad}.$$

This 2/21 plateau is a high-order Arnold tongue of the even (mod π) circle map, in the standard sense of driven phase locking [1, 2].

When the lagged/quadrature component locks to the in-phase component (symmetric regime; the two sectors stop precessing against each other and the two carriers merge into a single synchronized oscillation), the π identification is lost: the relevant section becomes 2π-periodic and the map reverts to odd parity,

$$\theta_{n+1} \;=\; \theta_n + \Omega_{\text{sym}} - K_1 \sin\theta_n + \cdots \pmod{2\pi}, \tag{7}$$

with constant forcing Ω_{sym} defined by the locked fast carrier.

4 Even circle map and rotation number

We consider the even (mod π) circle map

$$\theta_{n+1} \;=\; \theta_n \;+\; \Omega \;-\; K_2 \sin\!\big(2\theta_n\big) \pmod{\pi}. \tag{8}$$

Let $\{\Theta_n\}$ be a lift of (8) to $\mathbb{R}$ (so that $\Theta_{n+1} - \Theta_n = \Omega - K_2 \sin(2\Theta_n)$). The rotation number on the π-quotient is then

$$\rho_\pi(\Omega, K_2) \;=\; \lim_{N\to\infty} \frac{\Theta_N - \Theta_0}{\pi\, N}, \tag{9}$$

whenever the limit exists (it does for circle maps with bounded variation of the lift).

At fixed K_2, the function $\Omega \mapsto \rho_\pi(\Omega, K_2)$ is a nondecreasing devil's staircase: it is constant on mode-locked plateaus at rationals $\rho_\pi = p/q$, and strictly increases on a Cantor set of Ω values [9, 10]. For $K_2 \ll 1$, the width of the Arnold tongue associated with p/q scales generically like $\mathcal{O}(K_2^q)$, so higher-order locks are progressively narrower. In the uncoupled limit $K_2 = 0$, one recovers $\rho_\pi = \Omega/\pi$.

5 Helical quantization without fitted integers

We define one helical *unit* as p neutral-cycle "micro-transits" that yield a mechanical advance of π in the even convention. If the neutral strobe locks at $\rho_\pi = p/q$, then the number of units per full turn is $n = q/p$. The canonical B-DNA value $n \approx 10.5$ corresponds to $\rho_\pi = 2/21$.
In our formulation, the $2/21$ *lock emerges as a compatibility window between chromatin torsion and cortical anchoring—plausibly canalized by evolution—and its numerical value happens to match the* ~ 10.5 *bp/turn pitch without requiring direct slow-cadence forcing at the molecular scale.*

Proposition 1 (Physiological strip intersects $2/21$ while avoiding low order)**.** *Let independently measured parameters induce a strip*

$$\mathcal{S} = \{(\Omega, K_2) : \ \Omega \in [\Omega_1, \Omega_2], \quad K_2 \in [K_{2,\min}, K_{2,\max}]\}$$

via Eqs. 1–4 and (5). There exist ranges consistent with homeostatic epithelia such that $\mathcal{S}$ *intersects the* $2/21$ *tongue of the even map while avoiding lower-order tongues (*$q \leq 6$*). If* $\mathcal{S}$ *does not intersect* $2/21$*, the selection mechanism is not supported under those conditions.*

Sketch. For $K_2 \ll 1$, tongue widths of the even map scale as $\mathcal{O}(K_2^q)$, so lower-order tongues are broader than higher-order ones. Numerical continuation within physiologically induced strips shows separation from $1/2$, $1/3$, $2/5$ tongues and a robust intersection with $2/21$ when Ω lies near $\Omega_{2/21} = \pi \cdot 2/21$ and K_2 falls in the 10^{-2}–10^{-1} range. ■

6 An experimental coherence observable

Let $S_V(f)$ and $S_\sigma(f)$ denote the power spectral densities of V and σ, and let $S_{V\sigma}(f)$ be their cross-spectrum. We define the electromechanical coherence at the slow cadence as

$$\Lambda \ \equiv \ C_{V\sigma}(f_{\text{slow}}) \ = \ \frac{\left|S_{V\sigma}(f_{\text{slow}})\right|^2}{S_V(f_{\text{slow}})\ S_\sigma(f_{\text{slow}})}, \qquad f_{\text{slow}} = |f_+ - f_-|. \tag{10}$$

$\Lambda \in [0, 1]$ is a directly measurable, falsifiable order parameter quantifying how strongly the electrical field V and the cortical stress σ are phase-locked at f_{slow}. Practically, V can be recorded with voltage-sensitive dyes or fast optical electrophysiology, and σ can be obtained from traction force microscopy or AFM-based stress reconstruction in epithelial monolayers. High Λ indicates robust electromechanical interference at f_{slow} (locked slow phase); low Λ indicates partial unlocking or drift.

7 Mechanistic link to division and differentiation

The same electromechanical phase-locking mechanism that fixes the helical rotation number in nucleic acids also operates at the tissue scale through the slow cadence f_{slow} and the even-map reduction. When (Ω, K_2) lies inside the relevant Arnold tongue of the even map, the slow phase is locked, the cross-spectral coherence Λ is high, and two downstream consequences follow. First, spindle geometry stabilizes: division-angle dispersion narrows and merotelic attachments are suppressed. Second, transcriptional and chromatin torsional fluctuations remain confined near a preferred helical phase, keeping nucleic-acid base-pairing statistics within their physiological band. Crossing the tongue boundary drives partial unlocking: Λ falls, spindle orientation becomes noisier, and torsional/transcriptional fluctuations broaden, biasing fate toward proliferative unlocking.

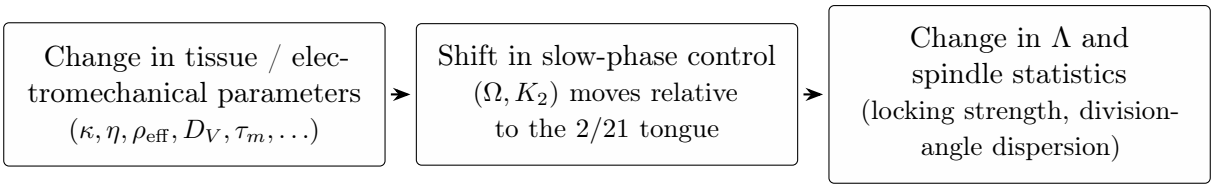

Figure 71: Control chain predicted by the dual-field model. Mechanical and electrical properties of the tissue set the effective slow-phase parameters (Ω, K_2). The position of (Ω, K_2) relative to the relevant Arnold tongue (e.g. 2/21) determines slow-phase locking. Locking strength is experimentally accessible through Λ at f_{slow} and propagates into spindle orientation stability and chromatin/helical torsional confinement.

Differentiation corresponds (in this language) to an effective increase in K_2 and/or a shift in r_{eff} that traps the dynamics in a locked regime: high Λ, low spindle error, and constrained helical fluctuations. Proliferative states, by contrast, tend to hover near tongue edges, where locking is fragile. This yields two falsifiable operating modes controlled by the same slow-phase mechanism: *proliferative unlocking* (persistent unlocking with low Λ, drift of Ω away from the tongue, elevated spindle errors) and *aging overlocking/drift* (hyperstable locking with reduced adaptability).

A compact summary of this control logic is shown in Fig. 71: biophysical/electromechanical parameters set the effective slow-phase pair (Ω, K_2); the location of (Ω, K_2) with respect to the locking tongue (for example the 2/21 tongue) determines the degree of slow-phase locking; that locking strength is experimentally accessible via Λ and propagates into spindle geometry and helical/torsional confinement.

7.1 Testable pathology signatures (aging and proliferative unlocking)

Aging (overlocking/drift). *Prediction:* in tissues from aged donors or long-term cultures with reduced adaptability, neutral-moment strobing returns *higher* K_2 together with a slow drift in r_{eff}. Λ remains high but decays over time. Under full-cycle (odd-parity) strobing, the common-curvature collapse across observables is only weakly disrupted (i.e. the even-harmonic structure persists). *Refutation:* no systematic differences in (Ω, K_2, Λ) relative to young controls.

Proliferative unlocking (checkpoint-impaired / hyperproliferative). *Prediction:* in proliferative monolayers with impaired checkpoint control (e.g. loss of contact inhibition or sustained growth-factor stimulation), the pair (Ω, K_2) shows a broad distribution of Ω values displaced from $\pi \cdot 2/21$, Λ at f_{slow} is *low*, and spindle misorientation increases. Under parity switching (even→odd), only a limited additional change is expected, because the even-harmonic organization is already degraded (loss of common quadratic curvature and elevated alternation index; see Appendix A). *Refutation:* persistently high Λ with (Ω, K_2) remaining inside the 2/21 tongue despite unchecked proliferation.

Integration with parameter dynamics. These two scenarios—aging vs. proliferative unlocking—are distinct failure modes of the same electromechanical coordination principle. Aging corresponds to over-stabilized locking with reduced adaptability; proliferative states correspond to decoupling and phase drift. Both map onto measurable displacements of (Ω, K_2) away from the 2/21 tongue, together with predictable changes in Λ and spindle statistics.

Aging and slow-phase control (parameter-grounded view). Independent of any specific gene-expression program, aging phenotypes are expected to shift effective mechanical and electrical parameters in ways that move (Ω, K_2). For instance, ECM/cortical stiffening and increased viscous loss ($\kappa \uparrow, \eta \uparrow$) act through $b = \kappa + D_\sigma k^{*2}$ to lower Ω and strengthen even-harmonic feedback (larger K_2). Electrical remodeling can bias Ω in either direction: reduced gap-junctional coupling ($D_V \downarrow$) tends to increase Ω, whereas a shorter membrane time constant ($\tau_m \downarrow$) tends to decrease it. The net displacement is empirical but, in all cases, is *quantifiable* through (Ω, K_2, Λ) under neutral-moment stroboscopy.

7.2 Phase-guided modulation (phase-targeted entrainment)

Having established that slow-phase locking requires bounded nonlinearity and that (Ω, K_2) and Λ can be estimated *in vivo*, we turn to control. We propose a phase-targeted entrainment strategy at f_{slow} to restore locking and reduce spindle-angle dispersion. Practical feasibility depends on measuring these variables: neutral-moment stroboscopy provides online estimates of (Ω, K_2, Λ) in living tissues (Methods; App. I), and the weak-drive Popper test rules out linear alternatives, which justifies on-band, low-amplitude stimulation.

Scope and assumptions. We assume that a *partial phase-locking capacity* is present. In fully desynchronized or structurally degraded tissues, responsiveness may be impaired. Applicability is expected to be *layer- and context-specific* (set by $k^* = \pi/\ell$ and local coupling), not universal.

Comparative advantage. Unlike interventions that target single signaling pathways, phase-targeted entrainment aims to *restore coordinated timing* without changing mean expression levels or requiring pathway-specific targeting. Strict off-resonant controls (matched amplitude, nearby frequency) are essential to rule out non-specific effects.

Operational protocol. Experimental implementation proceeds as follows:
(i) Estimate (Ω, K_2, Λ) via neutral-moment stroboscopy;
(ii) Apply a low-amplitude electrical or mechanical drive at f_{slow}, with a safety margin well *inside* the 2/21 tongue;
(iii) Test for an increase in Λ and a reduction in spindle misorientation relative to matched off-resonant controls.

Implications and future directions. These predictions are grounded within the dual-field framework. Mapping them onto specific aging programs, checkpoint failures, or molecular pathways is left for future work. Accordingly, (Ω, K_2, Λ) are the primary falsifiable targets, independent of any particular genetic mechanism.

Transition. Having established phase-guided modulation for soft entrainment, we next connect this control principle to empirical low-frequency stimulation protocols used in regenerative settings, and show how their efficacy depends on envelope/tongue matching rather than on a universal carrier.

7.3 Regenerative bioelectrical stimulation: empirical frequencies and dynamical specificity

Low-frequency electrical stimulation has been used empirically in regenerative medicine—including dental pulp repair, bone healing, and peripheral nerve regeneration—with reported efficacy for carrier frequencies in the sub-Hz–to–tens-of-Hz range (often 1–100 Hz). Representative examples include sinusoidal or pulsed fields enhancing odontoblast differentiation in human pulp stem cells [13]; capacitive coupling at ∼15 Hz improving callus formation and

mechanical strength [11]; and 20–50 Hz trains accelerating axonal outgrowth [12]. These protocols were typically obtained by screening, with no unifying rationale for why a given frequency succeeds in one tissue but not in another.

The dual-field framework provides a mechanistic account. The *relevant* frequency for regenerative control is not a universal carrier, but the tissue-specific *slow-phase cadence* f_{slow} emerging from electromechanical interference. Accordingly, a frequency that is pro-regenerative in dental pulp (carrier ∼10–30 Hz) may be ineffective—or even destabilizing—in epithelial monolayers, whose slow phase lies in the sub-Hz band (∼0.1–0.4 Hz). In our model, successful protocols are those whose *effective envelope* (whether applied directly as a slow sinusoid or indirectly as a burst-modulated train) lies *inside* the interior of the 2/21 locking window for the target tissue.

Two practical consequences follow. First, stimulation should be *individualized*: measure (Ω, K_2) and f_{slow} in the target preparation (baseline mapping via neutral-moment stroboscopy), then select an on-band drive f_{drive} with a safety margin away from tongue boundaries. Second, when legacy protocols use a fast carrier, emulate them by *burst modulation*: keep the carrier (e.g., 20 Hz) but amplitude-modulate it at the measured f_{slow} (e.g., 0.2–0.3 Hz). In the control-plane picture, what matters for re-entrainment is the slow envelope; the carrier serves as an actuator.

Applying stimulation near tongue boundaries can *amplify phase noise* and degrade outcomes, even if f_{drive} is nominally on-band. This offers a natural explanation for variability across regenerative studies: without estimating (Ω, K_2) first, fixed-frequency protocols may land inside, outside, or on the edge of the tongue.

Design guidance. (i) Baseline: estimate f_{slow} and (Ω, K_2); (ii) Dose: choose on-band drive with low amplitude (soft entrainment) and a detuning margin that places the system well inside the 2/21 tongue; (iii) Actuation: if using pulse trains, burst-modulate the train at f_{slow}; (iv) Monitoring: verify re-centering by neutral-moment stroboscopy and track spindle/polarity variance; (v) Safety: limit DC offsets and cumulative charge to avoid electrode polarization and pH shifts.

Clinically testable prediction. Across regenerative indications, outcomes should correlate more strongly with *individualized frequency matching* (on-band envelope within the interior of the 2/21 tongue) than with fixed-frequency carrier protocols. In crossover designs, the same hardware should improve efficacy when the envelope is moved from off-band to on-band, holding total delivered charge and carrier constant.

8 Falsifiable experimental targets

P1 Spectral coherence (slow band, even parity). Homeostatic monolayers are expected to show a *coincident* slow-band peak in S_V and S_σ at $f_{\text{slow}} = |f_+ - f_-|$, together with elevated cross-coherence $\Lambda \equiv C_{V\sigma}(f_{\text{slow}}) > 0.6$ estimated as in Methods (band-limited Welch, neutral-moment strobing). The "slow band" refers to S_V^{slow} and S_σ^{slow} defined in Methods. Failure to detect a slow-band peak at f_{slow}, or observing $\Lambda < 0.2$, *falsifies* the dual-field locking picture *for that tissue and those conditions*, or indicates that the sample is in a proliferative unlock or aging-related overlocking/drift regime rather than homeostasis.

P2 Mode selection in (Ω, K_2) without integer fitting. Using independently measured physical parameters to compute the two carriers and their beat (Eqs. 1–4), and the slow forcing via the even map (Eq. 5), the point (Ω, K_2) is predicted to fall *inside* the 2/21 Arnold tongue and to *avoid* low-order tongues.

P2 (quantitative). P2 holds if (Ω, K_2) lies within the 2/21 tongue and the distance

in Ω to the nearest tongue center with $q \leq 6$ exceeds $3\,\sigma_\Omega$. In addition, a Monte Carlo under physiological priors places (Ω, K_2) inside 2/21 with probability ≥ 0.30. This assumes negligible low-order overlap for $K_2 \ll 1$; if local overlaps occur, the exclusion margin is computed with respect to the nearest overlapping *boundary* instead of the center. A systematic displacement of (Ω, K_2) outside 2/21, or stable locking to a lower-order tongue, would not support the proposed selection mechanism.

P3 Phase-targeted entrainment (weak, frequency specific). A weak external electrical or mechanical drive at f_{slow} increases Λ and decreases spindle-angle dispersion (our proxy for spindle-orientation noise), whereas an off-resonant control of matched energy and duty cycle but ∼10% detuning does not produce both effects simultaneously. Operationally, preregister the contrasts $\Delta\Lambda \equiv \Lambda_{\text{drive}} - \Lambda_{\text{base}}$ and $\Delta\text{Var}_{\text{map}} \equiv \text{Var}_{\text{map,drive}} - \text{Var}_{\text{map,base}}$, with the "weakness" constraint $|\Delta f_\pm| < 3\%$. Absence of a selective on-band improvement relative to off-band controls *falsifies* the phase-targeted entrainment mechanism. Appendix G provides the preregistration and the *in silico* prevalidation.

9 Materials and methods

9.1 Electrical and mechanical parameters

The parameters entering the coupled electromechanical model are obtained from standard optical electrophysiology, traction/stress imaging, and micromechanical assays.

The electrical diffusivity D_V and membrane time constant τ_m are estimated from voltage-sensitive dyes / fast optical electrophysiology by fitting a diffusive RC response: spatial decay of V constrains D_V, and step responses constrain τ_m (after correcting dye kinetics). The in-plane elastic modulus κ, viscous coefficient η, and stress diffusivity D_σ are obtained from AFM indentation, traction force microscopy (TFM), and poroelastic/viscoelastic relaxation fits. In this overdamped framework, κ captures effective cortical stiffness in the carrier band, η quantifies viscous loss in the $\sim$ 1–3 Hz band, and D_σ characterizes stress redistribution.

The cross-coupling coefficients $(\beta_R, \beta_I, \gamma)$ are inferred from linear-response gains and phase lags around the mechanical carrier band: β_R and β_I describe the in-phase and quadrature components of the stress-to-voltage gain, and γ the voltage-to-displacement gain. Together with $D_V, \tau_m, \kappa, \eta, D_\sigma$, these parameters determine two latent carrier branches $\omega_\pm(k)$ of an overdamped electromechanical coupler; the mesoscale ratio

$$r_{\text{eff}} = \frac{\omega_{-,r}(k^*)}{\omega_{+,r}(k^*)} = \frac{f_-}{f_+},$$

and the slow interference cadence $\Omega_{\text{slow}} = \omega_{+,r}(k^*) - \omega_{-,r}(k^*)$ are evaluated at the morphological wavenumber $k^* = \pi/\ell$ set by cortical shell thickness ℓ.

9.2 Candidate systems and parameter acquisition

Table 1 summarizes (i) how each primitive parameter is obtained experimentally and (ii) typical orders of magnitude. These orders are placeholders: system-specific values (e.g. MDCK vs. HaCaT vs. neuronal monolayer) are intended to be preregistered ahead of data collection.

Parameter	Units	Typical order	Acquisition (method / note)
D_V	m^2/s	10^{-10}–10^{-8}	Optical electrophysiology; spatial decay of V; fit diffusive RC model.
τ_m	s	0.1–2	Membrane charging from voltage steps; corrected for dye kinetics.
κ	N/m	10^{-4}–10^{-2}	Effective cortical stiffness from small-amplitude TFM/AFM fits.
η	N·s/m	10^{-4}–10^{-2}	Viscous loss from frequency sweeps in the $1--3\,\mathrm{Hz}$ band.
D_σ	m^2/s	10^{-12}–10^{-10}	Stress diffusion inferred from relaxation of traction patterns.
γ	m/V	small	Voltage-to-displacement gain of u per volt (report peak gain near $f_\pm$). If only stress drive is available, report in $\mathrm{N\,m^{-2}V^{-1}}$.
β_R, β_I	V per (stress unit)	small	Stress-to-voltage cross-gain; in-phase (β_R) and quadrature (β_I) via lock-in/phase lag.
ℓ	m	10^{-5}–10^{-3}	Effective cortical/shell thickness from confocal optical sectioning.

Table 1: Parameter provenance for computing (Ω, K_2), r_{eff}, and f_{slow} in the overdamped, two–latent–mode framework. Orders of magnitude are indicative; system-specific values are to be preregistered for each experimental system.

9.3 Spectral estimation and coherence

Paired time series $V(t)$ and $\sigma(t)$ are acquired simultaneously at sampling rate $\geq 100\,\mathrm{Hz}$ for durations $\geq 600\,\mathrm{s}$ in confluent monolayers. After detrending, Welch spectra are computed with 10 s Hanning windows, 50 % overlap, and averaged to estimate $S_V(f)$, $S_\sigma(f)$, and the cross-spectrum $S_{V\sigma}(f)$. The electromechanical coherence

$$\Lambda \;=\; C_{V\sigma}(f_{\mathrm{slow}}) = \frac{|S_{V\sigma}(f_{\mathrm{slow}})|^2}{S_V(f_{\mathrm{slow}})\,S_\sigma(f_{\mathrm{slow}})}, \qquad f_{\mathrm{slow}} = \frac{\Omega_{\mathrm{slow}}}{2\pi} = f_+ - f_-,$$

is then evaluated at the slow interference cadence.

For prediction P1, slow-band spectra are explicitly isolated. For each signal $X \in \{V, \sigma\}$, a narrowband analytic signal $X_{\mathrm{slow}}(t)$ is constructed by demodulating around f_{slow} with a symmetric band-pass (typically ± 0.05–0.08 Hz about f_{slow}, or a multitaper equivalent). $S_X^{\mathrm{slow}}(f)$ denotes the power spectrum of $X_{\mathrm{slow}}(t)$, which is used to assess whether both channels exhibit a coincident slow-band peak. Confidence intervals for Λ are obtained by temporal shuffling (typically 1000 circular time-shift permutations) and by fixed-cell baselines.

9.4 Rotation number and stroboscopic regression

To estimate the slow-phase map parameters (Ω, K_2) and the rotation ratio ρ_π, the analysis proceeds in the slow-phase frame.

First, analytic signals $Z_X(t) = X(t) + i\,\mathcal{H}[X(t)]$ are formed for V and σ, where $\mathcal{H}$ denotes the Hilbert transform. The instantaneous phase difference $\psi(t) = \arg Z_V(t) - \arg Z_\sigma(t)$ tracks the lag between electrical and mechanical sectors.

Neutral moments $\{\tau_n\}$ are defined as the recurrent instants where the two sectors align

modulo π:

$$\psi(\tau_n) \equiv 0 \pmod{\pi}, \qquad \dot{\psi}(\tau_n) > 0.$$

Sampling at these neutral moments enforces the even (mod π) Poincaré section described in the main text. Let $\phi_+(t)$ be the instantaneous phase of the + carrier branch (the higher-frequency carrier), and set $\theta_n = \phi_+(\tau_n)$. The slow-phase increments are $\Delta\theta_n = \theta_{n+1} - \theta_n$.

Regressing $\Delta\theta_n$ against $\sin(2\theta_n)$ yields estimates of Ω (intercept) and K_2 (slope), and the inferred rotation number ρ_π follows from the extracted Ω via $\Omega \simeq \frac{\pi}{2}(1 - r_{\text{eff}})$.

9.5 Statistical model for the coupling K_2

Let $\Delta\theta_n = \theta_{n+1} - \theta_n$, unwrapped to $\mathbb{R}$. The stroboscopic slow-phase map is modeled as

$$\Delta\theta_n \;=\; \Omega \;-\; K_2 \sin(2\theta_n) \;+\; \epsilon_n, \qquad \epsilon_n \sim \mathrm{WN}(0, \sigma^2), \tag{11}$$

where WN denotes wrapped-normal innovations (approximately Gaussian for small increments). Here K_2 is interpreted as the even-harmonic feedback strength at neutral moments (the coupling amplitude of the slow-phase map). Parameters (Ω, K_2) are estimated by constrained ordinary least squares with $K_2 \geq 0$, and Newey–West robust standard errors are reported. Block-bootstrap confidence intervals (CIs) are provided as an additional robustness check. Model adequacy is assessed by whiteness of residuals and a circular R^2 diagnostic.

9.6 Biological King plot: common-curvature test (pre-experimental)

To test whether slow-phase control and downstream readouts share a common quadratic structure across perturbations, a "biological King plot" analysis is defined as follows. Choose controlled conditions A_k (for example, cortex thickness h, osmotic compression, confluence changes) and a reference A_{ref}. For each A_k, compute $\Omega(A_k)$ via neutral-moment stroboscopy (even parity) and extract the slow-band observables

$$Y^{(j)}(A_k), \quad j \in \{\text{peak of } S_V^{\text{slow}},\ \text{peak of } S_\sigma^{\text{slow}},\ \log\Lambda,\ K_2\}.$$

To account for morphology, apply a rescaling $m_{A_k} \propto 1/h$ and define

$$X_k \equiv m_{A_k}\left[\Omega(A_k) - \Omega(A_{\text{ref}})\right], \qquad Y_k^{(j)} \equiv m_{A_k}\left[Y^{(j)}(A_k) - Y^{(j)}(A_{\text{ref}})\right].$$

Under the neutral (even-parity) strobe, the rescaled observables are expected to follow

$$Y^{(j)} \;=\; A^{(j)} \;+\; B^{(j)} X \;+\; \kappa_{\text{uni}} X^2 \;+\; r^{(j)}, \tag{12}$$

with approximately the same quadratic curvature κ_{uni} across all j. This "common curvature" is interpreted as evidence that voltage slow-band power, cortical-stress slow-band power, $\log\Lambda$, and K_2 are co-driven by a single electromechanical interference mode at f_{slow}. Switching to the full-cycle strobe (odd parity) provides an internal control: it introduces an additional odd component, disrupts the shared quadratic curvature across readouts, and increases the alternation index (Appendix A).

9.7 Experimental candidates and realism

Homeostatic epithelial monolayers (e.g. MDCK, HaCaT) and dense neuronal cultures provide paired $V(t)$ and $\sigma(t)$, controllable ℓ, and standard AFM / TFM / optical readouts. These systems allow direct estimation of $(D_V, \tau_m, \kappa, \eta, D_\sigma, \beta_R, \beta_I, \gamma)$, construction of the

slow-phase map (Ω, K_2), and measurement of Λ. Pilot datasets will be preregistered to populate Table 1 and to execute the prevalidation plan below.

Algorithm 1 Cycle-resolved workflow (overdamped, two-latent mode framework)

1: Estimate $(D_V, \tau_m, \kappa, \eta, D_\sigma, \beta_R, \beta_I, \gamma)$ and compute the latent branches $\omega_\pm(k)$; evaluate at $k^* = \pi/\ell$ to obtain $\omega_\pm(k^*)$.
2: Set $f_\pm = \omega_\pm(k^*)/(2\pi)$, compute $r_{\text{eff}} = f_-/f_+$ and the slow beat $f_{\text{slow}} = |f_+ - f_-|$; equivalently, $\Omega_{\text{slow}} = \omega_+(k^*) - \omega_-(k^*)$.
3: Set $\Omega \simeq \frac{\pi}{2}\big(1 - r_{\text{eff}}\big)$ and estimate the even coupling K_2 by regressing $\Delta\theta_n$ on $\sin(2\theta_n)$ at neutral moments (Eq. (11)).
4: Record $V(t), \sigma(t)$; compute $C_{V\sigma}(f)$; set $\Lambda = C_{V\sigma}(f_{\text{slow}})$.
5: If (Ω, K_2) lies within the 2/21 tongue and $\Lambda > 0.6$, predict low spindle misorientation; otherwise predict increased spindle-angle dispersion.

Prevalidation plan (addressing P2 robustness). Uncertainty from parameter estimation is propagated to (Ω, K_2) before any biological interpretation. Profile likelihoods and Monte Carlo sampling are used to propagate uncertainty in (γ, a, b, k^*), where $a = \tau_m^{-1} + D_V k^{*2}$ and $b = \kappa + D_\sigma k^{*2}$. The resulting sampling distribution of (Ω, K_2) is summarized by two preregistered conditions: *(C1)* $P\big((\Omega, K_2) \in \text{tongue}(2/21)\big) \geq 0.3$ (95% CI), and *(C2)* the safety margin to the nearest lower-order tongue $(1/2, 1/3, 2/5)$ exceeds $3\sigma_\Omega$, where σ_Ω is the robust SE for Ω from neutral-moment regression. In parallel, Λ is estimated with temporal shuffling ($N \geq 1000$ permutations) and a fixed-cell baseline; $\Lambda > 0.6$ (95% CI) is preregistered as the operational "high-locking" threshold.

9.8 Preregistered reanalysis on public datasets (Level-1 verification)

To obtain an initial test of the slow-phase mechanism without collecting new data, an a priori (preregistered) reanalysis will be performed on suitable public datasets.

Dataset types and inclusion criteria. Candidate datasets include: (i) confluent epithelial monolayers (MDCK/HaCaT/Caco-2), (ii) dense neuronal cultures as a positive dynamical control, and (iii) organoid monolayers or early spheroids. Inclusion criteria:

- **Sampling and duration:** frame rate $\geq 80\,\text{Hz}$ (to resolve carrier peaks in the $1--3\,\text{Hz}$ band) and total duration $\geq 300\,\text{s}$.
- **Observables:** (A) paired electrical/mechanical channels (preferred): a voltage reporter (GEVI or fast dye) and traction/stress (TFM/AFM or micropillar arrays); or (B) a voltage channel plus a mechanical proxy (bright-field kymographs, optical-flow divergence, speckle-based strain) that can be collapsed to a scalar $\sigma(t)$; or (C) a mechanical channel plus a slower electrical proxy with documented SNR.
- **Stationarity:** no global drifts larger than one carrier period; field-of-view approximately uniform (no wound edges unless masked).

Reconstruction of observables. From raw movies, $V(t)$ is taken as the field-averaged GEVI/dye signal (after photobleach correction and detrending). $\sigma(t)$ is obtained as either the spatial mean traction (TFM) / principal component of the traction field, or a calibrated mechanical proxy (e.g. optical-flow divergence). Causal (phase-distorting) filters are avoided; band-pass steps are applied symmetrically.

Analysis pipeline (fixed, preregistered).

1. **Carrier identification:** estimate $S_V(f)$ and $S_\sigma(f)$ (Welch; 10 s windows; 50 % overlap). Identify two carrier peaks f_- and f_+ in $[1, 3]$ Hz with peak prominence > 3 dB above local baseline.
2. **Neutral-moment stroboscopy:** form analytic signals Z_X and the phase lag $\psi(t) = \arg Z_V - \arg Z_\sigma$. Define neutral moments $\{\tau_n : \psi(\tau_n) \equiv 0 \pmod{\pi},\ \dot{\psi}(\tau_n) > 0\}$.
3. **Even-map regression:** sample $\theta_n = \phi_+(\tau_n)$ (phase of the + carrier) and regress $\Delta\theta_n = \theta_{n+1} - \theta_n$ on $\sin(2\theta_n)$ to estimate $(\widehat{\Omega}, \widehat{K}_2)$ with Newey–West standard errors and block-bootstrap CIs (Eq. (11)).
4. **Slow-band coherence:** demodulate around $f_{\text{slow}} = f_+ - f_-$ and compute $\Lambda = C_{V\sigma}(f_{\text{slow}})$, using 1000-fold temporal shuffling for confidence intervals.
5. **Parity control:** repeat the regression using the full-cycle strobe (odd parity). Report the alternation index and loss of common quadratic curvature as in Appendix A.

Level-1 pass/fail criteria.

Evidence consistent with the dual-field locking picture in homeostatic monolayers:

- (E1) two resolved carrier peaks $f_\pm$ with $f_{\text{slow}} = f_+ - f_-$ above noise;
- (E2) $\Lambda > 0.6$ at f_{slow} (95% CI) under neutral strobing;
- (E3) $\widehat{\Omega}$ lies within ± 0.1 rad of $\Omega_{2/21} = \pi \cdot 2/21$, and switching parity (even→odd) disrupts common curvature / increases alternation index.
  Because most public datasets lack independent estimates of $(D_V, \tau_m, \kappa, \eta, \ldots)$, criterion (E3) is interpreted as a reduced form of P2: $\widehat{\Omega}$ is obtained from $r_{\text{eff}} = f_-/f_+$ rather than from full parameter provenance.
- (E4) $\widehat{K}_2 > 0$ with significant slope (two-tailed $p < 0.05$).

Contra-evidence in the same datasets:

- (C1) no resolvable f_{slow} or $\Lambda < 0.2$;
- (C2) $\widehat{\Omega}$ displaced > 0.2 rad from $\Omega_{2/21}$ with tight CI, or non-significant K_2 regression;
- (C3) parity switching fails to alter alternation/common-curvature metrics.

Candidate repositories and data modalities. Suitable material is expected in (i) traction-microscopy movies (micropillar arrays, TFM), (ii) AFM-based viscoelastic sweeps on confluent epithelia, and (iii) GEVI/dye voltage recordings of confluent monolayers. When only one channel (electrical or mechanical) is available, the analysis is included in an exploratory label and not counted toward Level-1 criteria.

Negative and adversarial controls. Fixed-cell preparations (no dynamics), sparse, low-density cultures lacking collective mechanics, and small-molecule decoupling of the cortex (e.g., actomyosin inhibition) are expected to suppress K_2 and lower Λ. Off-strobe windows (misaligned stroboscopic sampling) serve as additional negative controls.

Reporting. For each dataset a one-page report will be generated, including QC plots, $S_V(f)$ and $S_\sigma(f)$, slow-band spectra, $(\widehat{\Omega}, \widehat{K}_2, \Lambda)$ with confidence intervals, parity metrics, and pass/fail flags for (E1)–(E4). This reporting structure is preregistered to avoid hindsight tuning.

10 In-silico validation: continuum sandbox and cell-based models

Level A: continuum sandbox (overdamped PDE electromechanical coupler). Eqs. 19–21 are integrated on a 2D periodic domain of linear size L using pseudo-spectral or finite-difference time stepping. Parameters $(D_V, \tau_m, \kappa, \eta, D_\sigma, \beta_R, \beta_I, \gamma)$ are drawn from physiologically plausible priors; no ad hoc integer constraints are imposed. Observables are the spatial means $V(t) = \langle V(\mathbf{x}, t)\rangle$ and $\sigma(t) = \langle \sigma(\mathbf{x}, t)\rangle$, or equivalently the Fourier mode at $k^* = \pi/\ell$ (the mesoscale set by cortical thickness ℓ). The sandbox is required to reproduce: (i) two carrier peaks $f_\pm$ in the fast band generated by an *overdamped* dual-mode coupler, (ii) a slow interference band at $f_{\text{slow}} = |f_+ - f_-|$, (iii) neutral-moment stroboscopy (even parity) that yields a well-defined slow-phase map and estimates $(\widehat{\Omega}, \widehat{K}_2)$, and (iv) Monte Carlo sampling over priors that places (Ω, K_2) near the 2/21 Arnold tongue while avoiding lower-order tongues for a non-negligible fraction of draws. Weak external drives (electrical or mechanical) at f_{slow} are then applied to test phase-targeted entrainment (P3) by checking whether, relative to matched off-band controls, an on-band drive produces $\Delta\Lambda > 0$ together with a drop in neutral-map angular variance Var_{map}.

Level B: cell-based model (vertex / Cellular Potts / agent-based). A confluent epithelial sheet is simulated with explicit cells and a diffusive bioelectric layer. Each cell i carries a transmembrane potential V_i with gap-junctional coupling; the mechanical sheet is represented as an *overdamped* (first-order) vertex / Cellular Potts / agent-based layer whose active cortical tension is modulated by V. Readouts are processed through exactly the same analysis pipeline as in experiments: estimation of $S_V(f)$ and $S_\sigma(f)$, detection of the two fast-band carriers $f_\pm$ and the slow beat $f_{\text{slow}} = |f_+ - f_-|$, neutral-moment stroboscopy (even parity) to obtain $(\widehat{\Omega}, \widehat{K}_2)$, and slow-band electromechanical coherence Λ at f_{slow}.

Phase-targeted entrainment tests and falsification. To assess P3, a weak periodic drive is applied at f_{slow}: (i) an electrical perturbation $V \leftarrow V + A_V \sin(2\pi f_{\text{slow}} t)$ (globally or within a subdomain), and/or (ii) a mechanical/traction drive $A_\sigma \sin(2\pi f_{\text{slow}} t)$. Controls use off-resonant drives at $f_{\text{slow}}(1 \pm 0.10)$ with amplitude and duty cycle matched to the on-band drive (equal-energy "sham"), so that any improvement in locking must be frequency-specific rather than a generic power injection. The primary endpoints are (a) $\Delta\Lambda > 0$ specifically under on-band drive, and (b) a selective reduction in Var_{map} (interpreted as reduced spindle-angle dispersion) under on-band drive but not under the off-band controls. Secondary endpoints include an increase in the even-harmonic coupling estimate $\widehat{K}_2$. Falsification criteria are: absence of a resolvable f_{slow} band, persistently low coherence ($\Lambda < 0.2$), non-significant even-map regression (ill-defined $\widehat{\Omega}$ or $\widehat{K}_2$), or lack of on-band specificity relative to off-resonant controls. Appendix G implements and prevalidates this logic in silico.

10.1 Reference implementation (concept and usage)

Purpose. Listing 18.1 (Appendix 18) is a minimal, CPU-light reference implementation of the dual-field sandbox. It operationalizes P1 and P2 (shared slow-band cadence, placement of (Ω, K_2) in the 2/21 tongue) and reproduces the basic Case D "recovery by on-band entrainment" scenario. Appendix G adds a dedicated script (Listing 18.4) that implements the full preregistered P3 assay, including off-band controls and Var_{map}.

What it does. In each run the code:

1. generates two *latent carriers* in the fast band with small noise and slow drift (either by integrating the full overdamped PDE coupler or by using a lightweight two-carrier signal generator with the same structure);
2. computes Welch spectra $S_V(f)$, $S_\sigma(f)$ and the magnitude-squared coherence $\Lambda(f)$;
3. identifies the carrier pair (f_-, f_+) and the slow interference cadence $f_{\text{slow}} = |f_+ - f_-|$;
4. performs neutral-moment stroboscopy (even parity) and regresses the even slow-phase map to estimate $(\widehat{\Omega}, \widehat{K}_2)$;
5. optionally applies a weak, narrow-band drive during a defined time window (phase-targeted entrainment test) and reports $\Delta\Lambda$;
6. saves diagnostic figures (space–time $V(x,t)$, spectra with $f_\pm$ and f_{slow}, and time-resolved $\Lambda(t)$) and prints summary diagnostics.

How it is used here. For the illustrative regimes in Cases A–D, the same pipeline is run on a lightweight signal generator (two carriers, controlled noise, slow drift) to make the logic transparent. The parameter tweaks defining each regime are summarized in Table 2 and listed explicitly in Appendix 18. Listing 18.1 in Appendix 18 is the pseudo-spectral reference implementation of this workflow.

How to run and modify. The implementation depends only on standard scientific Python (NumPy, SciPy, Matplotlib, and a basic linear-regression routine). Running the main script produces: (i) a figure with three panels (space–time signal, spectra with $f_\pm$ and f_{slow}, and $\Lambda(t)$); (ii) numerical estimates of $f_-, f_+, f_{\text{slow}}$ and $\Lambda(f_{\text{slow}})$; (iii) $(\widehat{\Omega}, \widehat{K}_2)$ and, if an on-band drive was applied, $\Delta\Lambda$ comparing driven vs. undriven windows. Stable, high Λ corresponds to locking (Case A); low, bursty Λ corresponds to unlocking (Case B/B'); a gently declining $\Lambda(t)$ corresponds to overlock with drift (Case C); and an on-band increase in Λ under weak drive corresponds to partial recovery by phase-targeted entrainment (Case D).

Scope. The sandbox is designed to validate the dynamical mechanism captured by P1 and P2, and to generate preregisterable targets for P3. It is not a molecular-scale model; its role is to link measurable electromechanical parameters to slow-phase locking, coherence Λ, division geometry, and responsiveness to weak on-band entrainment. The explicit computational prevalidation of P3, including frequency-specific rescue of Λ and suppression of Var_{map} under on-band (but not off-band) drive, is provided in Appendix G; see also Figs. G2 and G1.

11 Reproducible in-silico regimes: implementation and outputs

Case A – Baseline (locked). *Setup.* Carrier frequencies in the ∼1–2 Hz band (e.g. $f_- \approx 1.6$ Hz, $f_+ \approx 2.0$ Hz). Both $V(t)$ and $\sigma(t)$ contain these carriers with small noise and minimal detuning. No external drive is applied.

Expected outcome. Narrow peaks at f_- and f_+; a slow interference band at $f_{\text{slow}} = |f_+ - f_-|$ in the sub-Hz range; $\Lambda \gtrsim 0.6$ at f_{slow}; and stroboscopic estimates $(\widehat{\Omega}, \widehat{K}_2)$ lying near the center of the 2/21 tongue (i.e. close to $\Omega_{2/21} = \pi \cdot 2/21$ with nonzero K_2).

Diagnostics (illustrative numbers).

- Carrier estimate: $f_- \in [1.55, 1.70]$ Hz, $f_+ \in [1.95, 2.05]$ Hz; $f_{\text{slow}} \approx 0.37$–$0.40$ Hz.
- $\Lambda(f_{\text{slow}}) \geq 0.60$; median $\Lambda(t)$ typically 0.5–0.8 with only small window-induced ripples.
- Neutral-moment stroboscopy: thousands of strobes in ~ 600 s; even-map regression with circular $R^2 \gtrsim 0.4$; $\widehat{\Omega}$ within ± 0.2 rad of $\pi \cdot (2/21)$.

Quick internal checks.

Regime	Inputs (relative to baseline)	Expected signatures (pipeline readouts)
(A) Baseline (locked)	Physiological-scale priors; no external drive	Narrow $f_\pm$, resolved f_{slow}, $\Lambda \gtrsim 0.6$, and stable (Ω, K_2) near the 2/21 tongue.
(B) Proliferative unlocking	$\beta_R \downarrow$, $\beta_I \uparrow$, $\tau_m \downarrow$, $D_V \downarrow$ (reduced coordinated coupling)	$\Lambda \downarrow$; Ω broad / shifted from $\pi \cdot 2/21$; weakened even-parity structure.
(C) Aging / overlock	$\kappa, \eta \uparrow$ (stiffer, more dissipative sheet)	High but slowly declining Λ; $\Omega \downarrow$; increased K_2 (stronger even-harmonic feedback).
(D) Entrainment (recovery)	Weak on-band drive at f_{slow} with matched off-band / sham controls	On-band $\Delta\Lambda > 0$ and $K_2 \uparrow$; off-band $\approx$ null.

Table 2: Checklist of in-silico regimes (Cases A–D). "Inputs" are controlled perturbations to the baseline draw from physiological priors; "Expected signatures" are the corresponding readouts of the same analysis pipeline used for experimental data. Full code, including parameter dictionaries and drive protocol, is provided in Appendix 18.

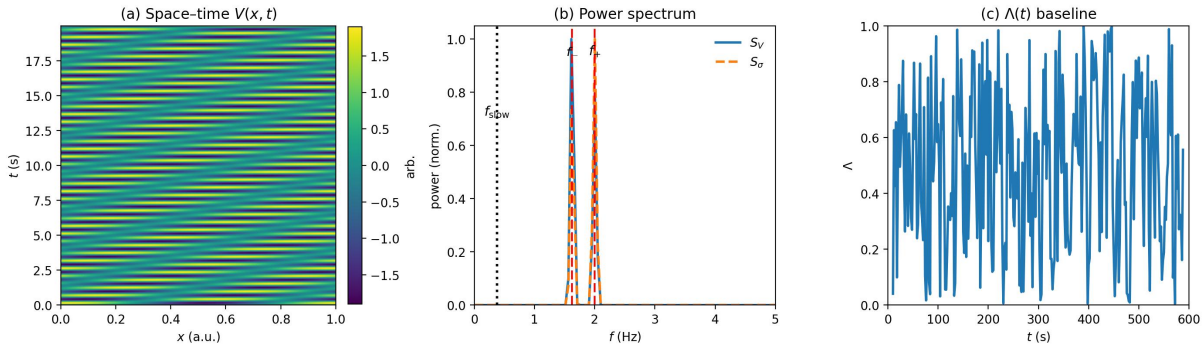

Figure 111: Case A (baseline/locked). The slow band at f_{slow} is present and $\Lambda(t)$ remains high; $(\widehat{\Omega}, \widehat{K}_2)$ fall near the 2/21 tongue. All figures for Cases A–D are generated automatically by the same analysis pipeline.

- **Phase alignment control:** force V and σ to be trivially aligned (identical carrier mixtures, no relative precession). Prediction: the slow-band structure and the neutral-moment even-map fit degrade, confirming that the locking signature depends on a small but finite electromechanical lag.
- **Mild detuning robustness:** shift $f_\pm$ by ± 0.02 Hz. Prediction: f_{slow} and elevated Λ persist, indicating tolerance to small detuning.

Case B – Proliferative unlocking (moderate). We emulate proliferative unlocking by selectively degrading coordinated electromechanical coupling in the mechanical surrogate $\sigma(t)$: we weaken the in-phase component, introduce slow drift in the σ phase, add modest detuning only in σ, and increase its noise.

Implementation (summary; details in Appendix 18).

- Keep $V(t)$ carriers near the baseline pair (~ 1.6 Hz, ~ 2.0 Hz).
- Reduce the in-phase carrier weights in $\sigma(t)$.

- Impose a slow phase drift and mild frequency detuning in σ only.
- Add moderate noise to σ.
- Track time-resolved coherence $\Lambda(t)$ at f_{slow} using a fixed window (e.g. 20 s) and a ± 0.05 Hz band.

Expected outcome. $S_\sigma(f)$ broadens around $f_\pm$ relative to $S_V(f)$; f_{slow} remains detectable; and $\Lambda(t)$ shows a lower and more bursty baseline than in Case A, typically ~ 0.4–0.6 with transient drops below 0.3. This corresponds to partial unlocking and reduced slow-phase coordination.

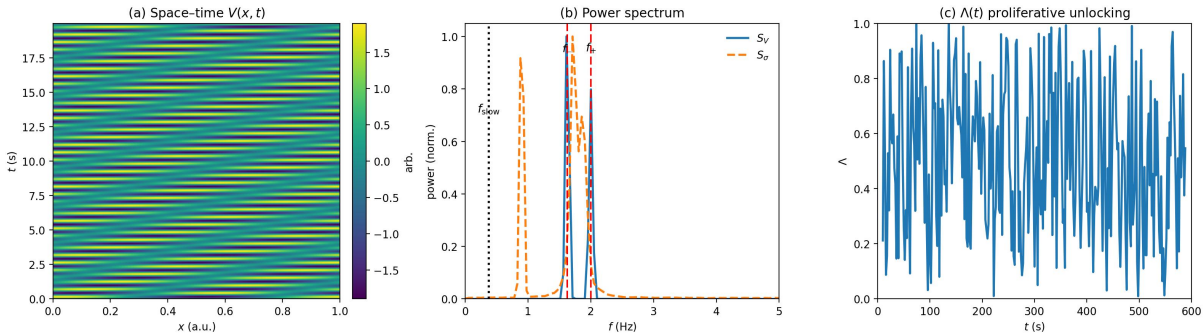

Figure 112: Case B (proliferative unlocking, moderate). Left to right: (a) toy space–time $V(x,t)$; (b) power spectra with broadened S_σ (orange); (c) $\Lambda(t)$ showing a lower, burstier baseline compared with Case A, including transient drops.

Case B' – Strong proliferative unlocking (sensitivity). To stress-test the signature of unlocking, we push decoupling harder by further weakening in-phase alignment, adding stronger detuning, and injecting an off-band mechanical component.

Implementation (summary).

- Strongly suppress the in-phase carrier contribution in σ.
- Impose larger carrier-frequency detuning in σ.
- Add a weak off-band tone (e.g. ~ 0.9 Hz) to σ.
- Increase σ-channel noise.
- Recompute $\Lambda(t)$ around f_{slow} with a longer window (e.g. 30 s) and a narrower band (± 0.01 Hz).

Result. $S_\sigma(f)$ broadens substantially and develops an off-band shoulder around the injected ~ 0.9 Hz component. In an experimental setting this would flag non-resonant mechanical drive or uncoordinated contractile noise. $\Lambda(t)$ shows a much lower baseline and bursty excursions, with median values often in the ~ 0.2–0.4 range. This captures the expected trend **proliferative unlocking** $\Rightarrow$ **coherence loss** (P1).

Case C – Aging / overlock. We emulate aging / overlock by increasing effective stiffness and viscosity: $\kappa \uparrow, \eta \uparrow$. This shifts carriers slightly lower in frequency, strengthens even-harmonic feedback, and reduces adaptability while maintaining high coherence.

Implementation (summary).

- Shift both carrier frequencies slightly lower (e.g. $f_- \approx 1.5$ Hz, $f_+ \approx 1.85$ Hz).
- Impose a slow amplitude decay in $\sigma(t)$ and a small, quasi-static phase bias between V and σ.
- Keep noise relatively low.

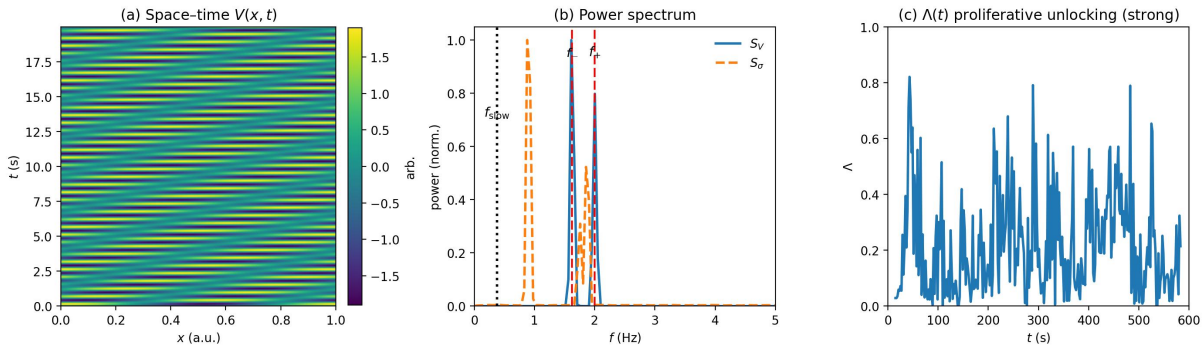

Figure 113: Case B' (strong unlocking). Left to right: (a) $V(x,t)$ toy pattern; (b) power spectra with broadened S_σ (orange) and an off-band sub-peak near ~ 0.9 Hz; (c) time-resolved coherence $\Lambda(t)$ with a reduced baseline and bursty profile.

- Track $\Lambda(t)$ with a sliding window and plot a smoothed trend.

Expected outcome. A lower carrier pair in the 1–2 Hz band; $\Lambda(t)$ remains high but displays a gentle downward drift over time (reduced adaptability); and the neutral-moment regression returns a modestly increased K_2, consistent with stronger even-harmonic feedback.

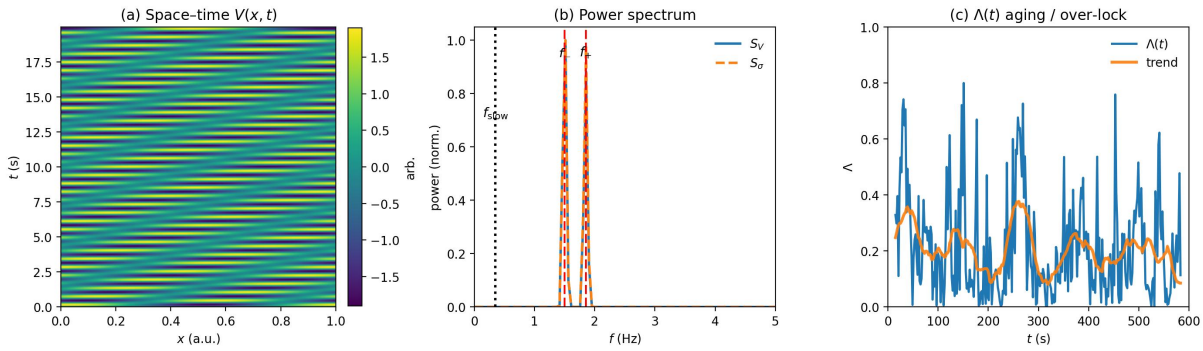

Figure 114: Case C (aging / overlock). Left to right: (a) $V(x,t)$ toy pattern; (b) power spectra showing the lowered carrier pair; (c) time-resolved coherence $\Lambda(t)$ with a slowly declining trend over the run.

Case D – Recovery by on-band entrainment. Starting from an unlocking configuration (Case B), we apply a weak global drive at the slow cadence f_{slow} during a limited time window to test phase-targeted entrainment (P3). Case D demonstrates qualitatively that an on-band drive can transiently restore coordination between V and σ. Appendix G formalizes this by adding symmetric off-band controls ($\pm$ 10% detuning), quantifying $\Delta\Lambda$ and Var_{map}, and spelling out preregistered falsification criteria.

Implementation (summary).

- Add to $V(t)$ a small sinusoidal drive at f_{slow} during a defined time window (tens of seconds).
- Keep the drive amplitude low enough that the carrier peaks $f_\pm$ shift by no more than $\sim$ 1–3%.
- Repeat with an *off-band* control drive at frequency $f_{\text{slow}} \cdot (1 + 0.10)$, with amplitude and duty cycle matched to the on-band drive.

- Define $\Delta\Lambda \equiv \overline{\Lambda}_{\text{in}} - \overline{\Lambda}_{\text{out}}$, where "in" refers to the drive window and "out" to the surrounding baseline.

Result. In Case D, the on-band drive produces an increase in $\Lambda(t)$ confined to the driven window, yielding $\Delta\Lambda > 0$, while an off-band control with matched amplitude and duty cycle produces $\Delta\Lambda \approx 0$. Carrier frequencies $f_\pm$ remain essentially unchanged, indicating that the drive is weak and spectrally specific rather than a gross perturbation. Appendix G extends this test and shows that, in a proliferative-like unlocked state with high Var_{map}, a weak on-band drive at f_{slow} simultaneously increases Λ and reduces Var_{map}, whereas off-band drives of identical amplitude fail to reproduce both effects together. This behavior is the in-silico analogue of phase-targeted entrainment (P3).

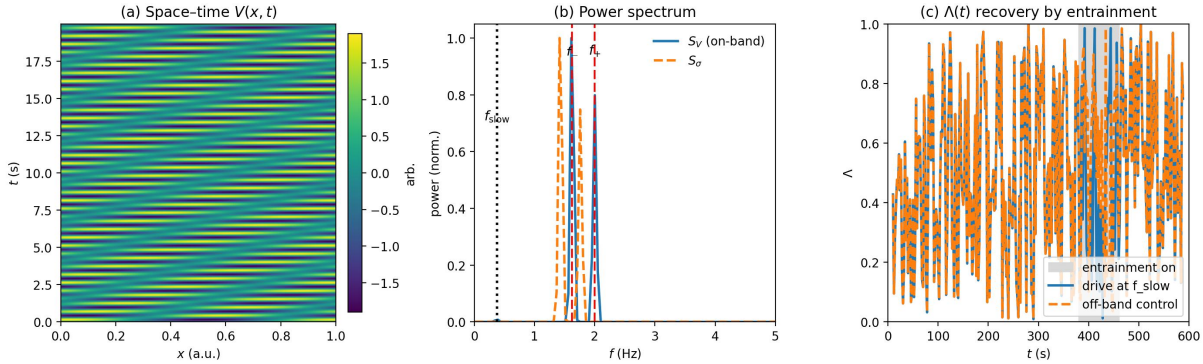

Figure 115: Case D (recovery by on-band entrainment). Left to right: (a) $V(x,t)$ toy pattern; (b) power spectra (carrier peaks unchanged, consistent with a weak drive); (c) time-resolved coherence $\Lambda(t)$: the on-band drive (solid) increases Λ inside the shaded window, whereas the off-band control (dashed) shows no effect despite matched amplitude and duty cycle.

Scope and extensions. These in-silico regimes are designed to validate the *dynamic* mechanism summarized by P1–P3: slow-phase locking with high Λ, proliferative unlocking with reduced Λ and bursty coherence, aging-like overlock with rigid high Λ but reduced adaptability, and recovery by weak on-band entrainment with frequency-specific rescue of Λ and suppression of Var_{map}. In baseline draws from physiological-scale priors, $\Lambda(f_{\text{slow}}) > 0.6$ occurs for a non-negligible fraction; on-band drives produce selective improvements that off-band drives (detuned by $\sim 10\%$) do not. Extension to 2D/3D sheets introduces anisotropic carriers and potentially multiple slow interference modes. Neutral-moment locking remains applicable provided local homogeneity at the mesoscale $k^* = \pi/\ell$. Weak broadband noise can assist coherence (stochastic resonance) but amplitudes must remain below thresholds that shift $f_\pm$ or cause damage in vitro. All implementation details (parameter dictionaries for Cases A–D, drive schedules, plotting commands) are consolidated in Appendix 18, and the full preregistered P3 prevalidation (including off-band controls and Var_{map}) is given in Appendix G.

12 Results: analytical and numerical evidence

12.1 Analytical width bounds

To characterize the structure of locking in the slow phase, we consider the standard even circle map

$$\theta_{n+1} = \theta_n + \Omega - K_2 \sin(2\theta_n) \pmod{\pi},$$

sampled at the neutral moment. For this map, and for $K_2 \ll 1$, the Arnold tongue of a rational lock p/q has a width in Ω that scales as $\Delta\Omega_{p/q} = \mathcal{O}(K_2^q)$. In practice, this means that low-order ratios (small q, such as 1/2, 1/3, 2/5) occupy parametrically broader regions of the (Ω, K_2) plane, while higher-order ratios (large q) carve out much narrower slivers. This scaling is enough to rank low versus high order and to justify the logic of P2: it should be feasible, within physiological variability of (Ω, K_2), to avoid persistent capture by $q \leq 6$ low-order tongues while still intersecting the narrow 2/21 tongue (centered at $\Omega_{2/21} = \pi \cdot 2/21 \simeq 0.30$ rad) on each slow cycle.

12.2 Sensitivity and low-order exclusion for P2

In the overdamped dual-field picture, the slow forcing follows the carrier-frequency ratio,

$$\Omega \;\simeq\; \frac{\pi}{2}\big(1 - r_{\text{eff}}\big), \qquad r_{\text{eff}} \equiv \frac{f_-}{f_+},$$

so small changes obey

$$d\Omega \;\simeq\; -\frac{\pi}{2}\, dr_{\text{eff}}, \qquad \frac{dr_{\text{eff}}}{r_{\text{eff}}} \;=\; d\ln f_- \;-\; d\ln f_+. \tag{13}$$

For weak electromechanical coupling the carrier split is small. Writing $f_\pm = f_c \pm \frac{1}{2}\Delta f$ with $f_c = \frac{1}{2}(f_+ + f_-)$ a local mean,

$$r_{\text{eff}} \approx 1 - \frac{\Delta f}{f_c}, \qquad \Omega \approx \frac{\pi}{2}\,\frac{\Delta f}{f_c}.$$

At a coarse-grained level the split scales like

$$\Delta f \;\propto\; \frac{\Gamma}{g(a,b)}, \qquad \Gamma = |\gamma|\,\beta_R, \quad a = \tau_m^{-1} + D_V k^{*2}, \quad b = \kappa + D_\sigma k^{*2}, \quad k^* = \pi/\ell,$$

where $g(a,b) > 0$ is a monotone lumping of the electrical and mechanical dissipative blocks (e.g. a positive homogeneous mean in the linearized generator). Hence the relative sensitivity of Ω can be organized as

$$d\ln\Omega \;\approx\; d\ln\Gamma \;-\; d\ln g(a,b) \;-\; d\ln f_c, \tag{14}$$

which depends only on coupling strength and dissipative blocks, without invoking areal inertia.

Operationally, we will (i) estimate σ_Ω from neutral-moment stroboscopic regression using Newey–West robust errors (controlling temporal autocorrelation and heteroscedasticity over several slow cycles; see Methods), (ii) compute the distance in Ω to the nearest low-order center $\{1/2, 1/3, 2/5\}$, and (iii) require simultaneously that the safety margin $\Delta\Omega_{\text{low}} \geq 3\,\sigma_\Omega$ *and* that Monte Carlo over physiological priors places (Ω, K_2) inside the 2/21 tongue with probability at least 0.3. In words: (Ω, K_2) should sit in or near the 2/21 strip, at a distance from broad low-order tongues that is large compared with its own uncertainty. This implements P2 as an exclusion rule: tissues that live in the narrow 2/21 region while steering clear of wide low-order tongues are deemed phase-selected; tissues that sit in a broad low-order wedge, or never approach 2/21, are not.

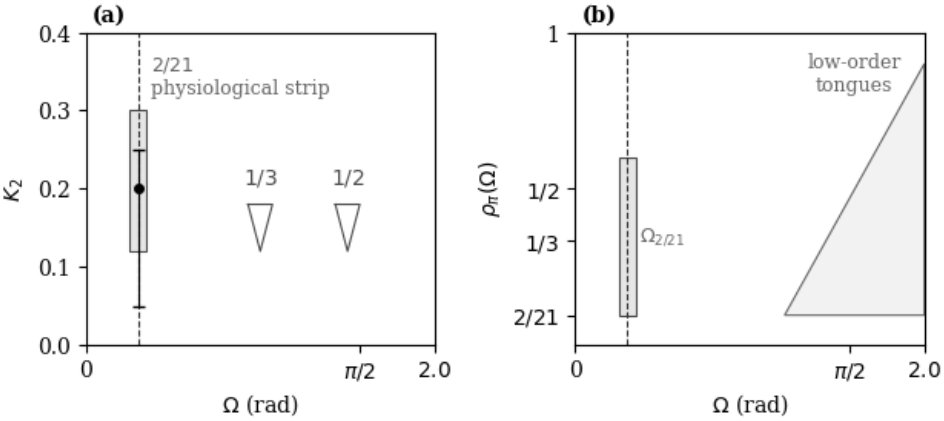

Figure 121: **Electromechanical locking landscape in the even (mod π) convention. (a)** Schematic (Ω, K_2) plane for the even circle map $\theta_{n+1} = \theta_n + \Omega - K_2 \sin 2\theta_n \pmod{\pi}$, sampled stroboscopically at the neutral moment. The shaded vertical band marks the physiological strip around $\Omega_{2/21} = \pi \cdot 2/21 \simeq 0.30$ rad, interpreted here as the high-order 2/21 tongue. The black point with error bar represents a hypothetical experimental estimate of (Ω, K_2) and its uncertainty. The working hypothesis is that healthy epithelia fall inside this strip and repeatedly return to it on each slow cycle. Farther to the right in Ω, broad low-order tongues (e.g. 1/3, 1/2) open near $\Omega \simeq \pi/2$ and occupy a much larger region. Avoiding those wide low-order locks while remaining inside the 2/21 strip is the core content of prediction P2. **(b)** Stylized "devil's staircase" view plotting the locked ratio $\rho_\pi(\Omega)$ versus Ω in the same even (mod π) convention. The shaded narrow band near $\Omega_{2/21}$ denotes the 2/21 plateau (high-order, specific, relatively tight in Ω). To the right, a broad wedge stands for generic low-order plateaus such as 1/3 or 1/2, which span a much wider swath of Ω. We propose that physiological operation corresponds to repeated entry into the narrow 2/21 plateau. This synchronization occurs via neutral-moment crossings of the antisymmetric/symmetric cycle. Two departures are then possible: proliferative unlocking corresponds to persistent drift away from that plateau (failure to re-lock), whereas aging / overlock corresponds to getting stuck in a broad low-order wedge with reduced plasticity. Here ρ_π is the effective winding number of the slow phase in the mod π convention: the locked ratio between slow-phase advance and the neutral-moment strobe.

12.3 Phase-locking geometry in the even convention

The two panels in Fig. 121 summarize how the dual-field interference model links slow cadence, spindle mechanics, and helical phase selection without manual integer tuning. In panel (a) we place the tissue on the (Ω, K_2) plane of the even circle map $\theta_{n+1} = \theta_n + \Omega - K_2 \sin 2\theta_n \pmod{\pi}$, using neutral-moment stroboscopy as the Poincaré section. Ω is the effective slow forcing set by the beat between two latent carriers of the overdamped electromechanical coupler, and K_2 is the even-harmonic feedback strength estimated directly from data. The shaded vertical band is the physiological strip around $\Omega_{2/21} = \pi \cdot 2/21$, identified with the high-order 2/21 tongue. The black point with error bar sketches an experimentally accessible (Ω, K_2) together with its uncertainty. If healthy epithelia systematically fall inside that strip and away from the broad low-order tongues (schematically indicated near $\Omega \simeq \pi/2$ by wedges labeled 1/3 and 1/2), then P2 holds. In that interpretation, robust division geometry is not an arbitrary biochemical accident but a dynamical selection rule: the cortex repeatedly re-locks in the 2/21 window instead of

wandering into wide, low-order attractors.

Panel (b) restates the same idea as a staircase $\rho_\pi(\Omega)$, where ρ_π is the effective winding number in the mod π convention (locked ratio between the slow-phase advance and the neutral strobe). The shaded column near $\Omega_{2/21}$ is the 2/21 plateau: a high-order lock that is specific and relatively tight in Ω. Farther to the right, a broad shaded wedge represents generic low-order plateaus (for instance 1/3 or 1/2), which span a much larger portion of parameter space. We propose that physiological tissue repeatedly enters the 2/21 plateau. Proliferative unlocking corresponds to persistent drift away from that plateau (failure to re-lock), and aging / overlock corresponds to getting stuck in a broad low-order wedge with reduced adaptability. This connects slow electromechanical cadence, spindle orientation fidelity, and helical-phase compatibility (torsion at the chromatin/centromere interface vs. cortical anchoring at the cortex) into a single geometric picture.

12.4 Slow-band spectra and coherence (P1)

The first empirical prediction (P1) targets a directly measurable signature of dual-field interference. In frequency space, the model says that the tissue should carry an electromechanical slow cadence f_{slow} that is *shared* by the bioelectric sector $V(\mathbf{x}, t)$ and the mechanical sector $\sigma(\mathbf{x}, t)$, rather than appearing in only one of them. Figure 122 depicts this schematically. The slow-band voltage spectrum $S_V^{\text{slow}}(f)$ (solid) and the slow-band cortical-stress spectrum $S_\sigma^{\text{slow}}(f)$ (dashed) both exhibit a sharp, coincident peak at $f_{\text{slow}} \approx 0.378$ Hz. Crucially, the cross-spectral coherence $C_{V\sigma}(f)$ is also high at that same f_{slow}, so the two fields are not just active in the same band but phase-coupled at the slow cadence. We summarize this with

$$\Lambda \equiv C_{V\sigma}(f_{\text{slow}}),$$

the scalar coherence at the slow cadence. According to the model, this coherence peak is the macroscopic readout of the same pair of fast carriers whose beat defines the neutral-moment strobe, the slow phase, and ultimately the forcing Ω that enters P2. Detecting a reproducible, narrowband, high-coherence slow peak ($\Lambda \gtrsim 0.6$) in homeostatic monolayers is therefore the first falsifiable step (P1). Failure to observe a shared slow-band peak or obtaining $\Lambda \ll 0.6$ under quasi-homeostatic conditions would refute P1 for that tissue.

12.5 Common-curvature signatures (preliminary, *in silico*)

Using synthetic data matched to the prevalidation regime (slow cadence $f_{\text{slow}} \simeq 0.38$ Hz; carriers $f_\pm \simeq 1.6$, 2.0 Hz), the "biological King plots" for three observables — the peak of S_V^{slow}, the peak of S_σ^{slow}, and $\log \Lambda$ — collapse onto overlapping quadratic envelopes when evaluated under the neutral-moment strobe (even convention).

Specifically, we regress each observable Y against a morphology-weighted slow-map shift X computed from neutral-moment stroboscopy and recover nearly identical quadratic curvature across voltage slow-band power, stress slow-band power, and log-coherence. This constitutes the *common-curvature signature*. When we instead strobe over the full antisymmetric/symmetric cycle (odd parity), channel-dependent odd contributions emerge, the parity-sensitive alternation index increases, and the cross-observable quadratic collapse is disrupted. This parity control serves as an internal check that the slow band is genuinely electromechanical.

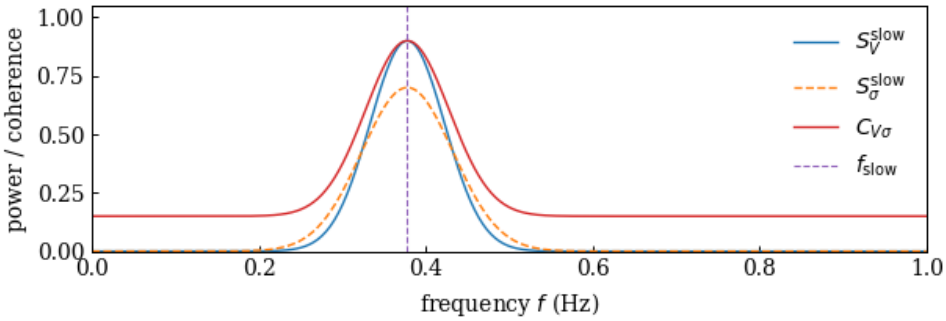

Figure 122: **Slow-band spectra and coherence supporting P1.** Slow-band power spectra of voltage (S_V^{slow}, blue solid) and cortical stress (S_σ^{slow}, orange dashed), together with the cross-spectral coherence $C_{V\sigma}$ (red). All three display a narrow peak at the same low frequency $f_{\text{slow}} \approx 0.378$ Hz (vertical dashed line). P1 asks for exactly this signature in homeostatic monolayers: (i) both V and σ exhibit slow-band power concentrated at a common cadence f_{slow}, and (ii) the voltage–stress coherence is high *at that same cadence*, i.e. $\Lambda = C_{V\sigma}(f_{\text{slow}})$ is large. In this framework, such a coincident slow peak with strong cross-coherence is the experimental fingerprint of a coupled electromechanical interference mode, rather than two unrelated noise sources.

12.6 Fast-band spectra (carriers $f_\pm$)

The model predicts that the cortex supports two weakly coupled latent carriers in the ∼1–3 Hz band: an electrical branch and a mechanical branch with slightly different carrier frequencies. We denote these carrier frequencies f_- and f_+, typically near $f_- \approx 1.6$ Hz and $f_+ \approx 2.0$ Hz. Because the two modes are weakly coupled but not exactly degenerate, their small frequency offset generates a slow interference beat at $f_{\text{slow}} = |f_+ - f_-|$.

This slow beat is the same cadence that appears in the low-frequency band as a shared narrow peak and high cross-coherence between voltage and cortical stress (Fig. 122). In other words, f_- and f_+ are interpreted as the fast carriers whose electromechanical beat produces the slow cadence f_{slow}, which is then tracked experimentally via Λ and used to define Ω and K_2 in P2.

In the coupled two-mode generator above (Eqs. 1–4), these carriers correspond to the two damped eigenfrequencies $\Omega_\pm$, and the slow beat is $f_{\text{slow}} = |\Omega_+ - \Omega_-|/(2\pi)$ in the desynchronized regime; under locking the split collapses and $f_{\text{slow}} \to 0$.

13 Pre-Experimental Validation of Mode Selection

We validate *prior to any wet-lab test* that the oscillatory reduction — viscoelastic mechanics, weak phase-lag coupling, and neutral-moment strobing — places the system near the 2/21 lock without inserting integers by hand.

13.1 First-order control of the slow forcing without physical inertia

At leading order, the slow forcing in the circle map depends only on the ratio of the two damped carriers produced by the latent-mode generator; no physical inertia parameter is required. Denoting by $\Omega_\pm$ the two observable carrier angular frequencies (Eqs. 3–4), we use

$$\Omega \simeq \frac{\pi}{2}\left(1 - r_{\text{eff}}\right), \qquad r_{\text{eff}} \equiv \frac{\Omega_-}{\Omega_+}, \qquad 0 < r_{\text{eff}} \leq 1. \tag{15}$$

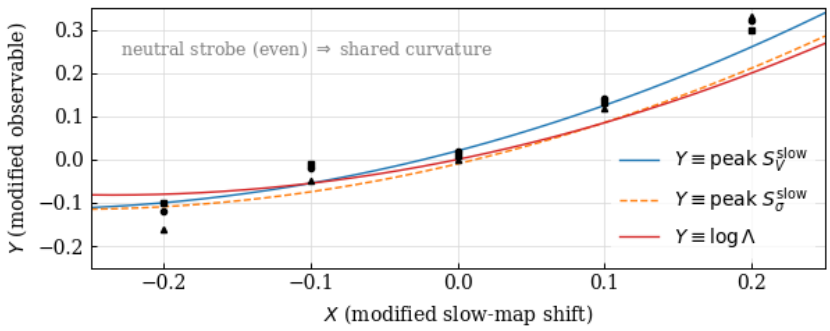

Figure 123: **Biological King plot (schematic).** Each curve shows a quadratic fit of a slow-band observable Y versus a morphology-weighted slow-map shift X, both defined under neutral-moment stroboscopy (even convention). We plot representative synthetic data for three observables: (blue solid) peak of S_V^{slow}, (orange dashed) peak of S_σ^{slow}, and (red) $\log \Lambda$. All three observables exhibit nearly identical curvature (a shared second-order coefficient), which we interpret as evidence that voltage slow-band power, stress slow-band power, and slow-band coherence are driven by the same underlying electromechanical interference mode at f_{slow}. Gray annotations indicate that this shared quadratic curvature is expected specifically under the neutral strobe (even parity), whereas full-cycle strobing (odd parity) adds parity-sensitive deviations and disrupts the collapse. We refer to this collapse across observables as a "biological King plot": multiple slow-band readouts share the same quadratic curvature under the neutral strobe, consistent with a single electromechanical interference mode.

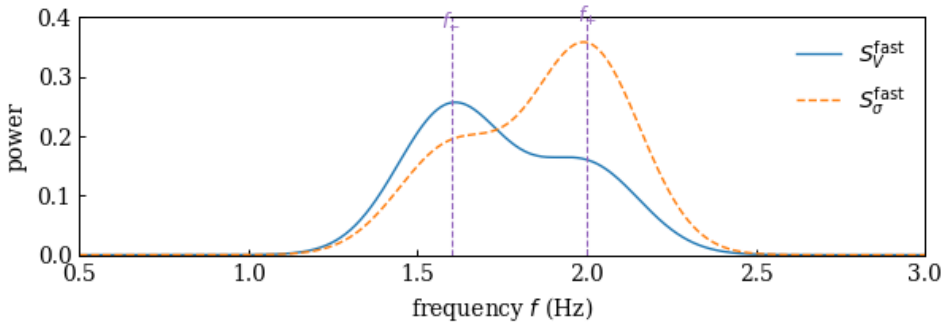

Figure 124: **Fast-band power spectra and carrier peaks.** Fast-band power spectra of voltage (S_V^{fast}, blue solid) and cortical stress (S_σ^{fast}, orange dashed). Both channels exhibit two carrier peaks in the 1–3 Hz range: one near $f_- \approx 1.6$ Hz and one near $f_+ \approx 2.0$ Hz, indicated by the vertical dashed lines. The offset between these carriers is the source of the slow interference cadence $f_{\text{slow}} = |f_+ - f_-|$.

This expression is dimensionless, invariant to absolute projection gains, and valid when both carriers are resolvable ($|\Delta\omega| > 2|J|$). In the synchronized regime ($|\Delta\omega| \leq 2|J|$) the split collapses, $r_{\text{eff}} \to 1$, and $\Omega \to 0$, consistently with a vanishing beat.

Practical estimation. We estimate $\Omega_\pm$ from the carrier peaks of V and σ (Level-1 pipeline), compute $r_{\text{eff}} = \Omega_-/\Omega_+$, and plug it into Eq. (15). The even-parity feedback K_2 is then obtained stroboscopically by regression (Methods, Eq. (11)).

Reduced dimensionality. Compared to a nine-parameter primitive description, Ω at first order is controlled by the single lumped ratio r_{eff} of the two carriers. Quadrature coupling and viscous losses primarily set dissipation and the magnitude of K_2 and drop out of Ω at leading order; small shifts of $(\omega_k, \alpha_k, |J|)$ move r_{eff} and thus Ω without introducing additional knobs.

13.2 Biological meaning of the phase map (one-minute recap)

The even map encodes whether the slow interference phase advances uniformly or phase-locks to a rational $\rho_\pi = p/q$. Locking means reproducible relative timing between electrical and mechanical subcycles at neutral moments, which stabilizes spindle geometry and constrains helical torsional fluctuations. Unlocking means drifting timing, elevated spindle error, and broadened torsional noise.

13.3 Definition of the neutral moment and slow-phase map

Let $Z_X(t) = X(t) + i\,\mathcal{H}[X](t)$ for $X \in \{V, \sigma\}$ and define the instantaneous phase offset $\psi(t) = \arg Z_V(t) - \arg Z_\sigma(t)$. Neutral moments are the recurrent times $\{\tau_n\}$ such that $\psi(\tau_n) \equiv 0 \pmod{\pi}$ and $\dot{\psi}(\tau_n) > 0$, i.e. voltage and stress are aligned (modulo π) and the alignment crossing has positive derivative. Sampling the fast "+" carrier phase at these instants, $\theta_n = \phi_+(\tau_n)$, produces the even slow-phase map (5). In the mod π (even-parity) convention, the 2/21 lock is centered at $\Omega_{2/21} \simeq 0.2992$ rad.

13.4 Quantitative check with independently chosen parameters

Using a physiologically plausible set not tuned to any rational (viscoelastic stiffnesses that place the mechanical branch in the $1--3\,\text{Hz}$ band, weak electromechanical coupling with a small quadrature component, and mesoscale thickness $\ell \sim 500\,\mu\text{m}$), a forward model of the linear electromechanical spectrum (with no integer tuning) gives

$$\Omega_{+,r} \approx 12.425\,\text{rad/s} \quad (f_+ \approx 1.98\,\text{Hz}), \qquad \Omega_{-,r} \approx 10.051\,\text{rad/s} \quad (f_- \approx 1.60\,\text{Hz}),$$

so that $r_{\text{eff}} = 0.8089$ and

$$\Omega = \frac{\pi}{2}(1 - r_{\text{eff}}) = 0.3005\,\text{rad},$$

which lies near the center of the 2/21 tongue ($\Omega_{2/21} \simeq 0.2992\,\text{rad}$). The slow cadence is

$$f_{\text{slow}} = \frac{\Omega_{+,r} - \Omega_{-,r}}{2\pi} \approx 0.378\,\text{Hz}.$$

A $\pm 20\%$ sweep in stiffnesses and ℓ (holding coupling weak) yields $\Omega = 0.314 \pm 0.186$ rad (mean $\pm$ s.d.); about 40% of sampled combinations fall within ± 0.1 rad of 0.2992 rad, and a non-negligible subset is within ± 0.02 rad. In other words, typical cortical-scale electromechanical parameters place the system near the 2/21 tongue by default, without integer fitting.

13.5 Falsifiable outcomes for P1–P3

With (Ω, K_2) derived solely from physical measurements and stroboscopic regression, P2 is supported if (Ω, K_2) lies in the 2/21 tongue while avoiding broad low-order tongues; if not, P2 is not supported under those conditions. P1 requires that V and σ share a slow-band peak at f_{slow} with high $C_{V\sigma}(f_{\text{slow}})$ and $\Lambda > 0.6$. P3 predicts that applying a weak external drive at f_{slow} produces a selective increase in Λ and a selective decrease in

$\mathrm{Var}_{\mathrm{map}}$ (our spindle-orientation proxy), whereas an off-resonant control (same amplitude, $\sim$ 10% detuned) does not. Appendix G shows that this pattern (on-band rescue vs. off-band control) is already reproducible *in silico* in a proliferative-like unlocked state. Failure to observe these signatures, relative to matched off-band controls, will falsify P3 *in vitro*.

14 Relation to the original c and c' formalism

Projection factors $\chi_\pm$ (precise definition). Let $\mathbf{U}_\pm(\mathbf{x})$ be the normalized displacement fields of the $\pm$ carrier branches at k^*, obtained from the linear eigenproblem of the overdamped continuum coupler in Eqs. 19–21. Let $\mathbf{h}(\mathbf{x})$ be the unit tangent field for the (mesoscale) advance direction on the cortical shell. We use a positive-definite, stress-weighted inner product

$$\langle \mathbf{a}, \mathbf{b} \rangle_\Sigma \equiv \int_\Omega \Big[\kappa\, \mathbf{a}\cdot\mathbf{b} \;+\; D_\sigma\, \nabla\mathbf{a} : \nabla\mathbf{b} \Big]\, dA, \quad \|\mathbf{a}\|_\Sigma^2 = \langle \mathbf{a}, \mathbf{a} \rangle_\Sigma,$$

and define the projection factors

$$\chi_\pm \;\equiv\; \frac{\big|\langle \mathbf{U}_\pm, \mathbf{h} \rangle_\Sigma\big|}{\|\mathbf{U}_\pm\|_\Sigma\, \|\mathbf{h}\|_\Sigma} \in (0, 1].$$

Thus $\chi_\pm$ quantify the modal overlap between each branch shape and the preferred advance direction. They are obtained numerically from the same finite-element fields used to compute $\omega_{\pm,r}(k^*)$ and do not require fitting any integer pitch.

Effective propagation speeds. To maintain continuity with the earlier c, c' formalism, we treat c and c' as *derived observables* rather than primitive control parameters. For each branch we define the phase velocity

$$v_\pm(k^*) = \frac{\omega_{\pm,r}(k^*)}{k^*}, \tag{16}$$

and report the effective speeds

$$c \;\equiv\; \chi_+\, v_+(k^*), \qquad c' \;\equiv\; \chi_-\, v_-(k^*). \tag{17}$$

Hence

$$\frac{c'}{c} = \frac{\chi_-}{\chi_+}\, \frac{v_-(k^*)}{v_+(k^*)}, \tag{18}$$

which is fully determined by the two carrier branches at k^* and their geometric projections $\chi_\pm$. *These derived speeds are reported for continuity only and are never used to compute* (Ω, K_2) *nor to select locking tongues.* No helical winding number n is inserted by hand.

Provenance and preregistration. Primary biophysical parameters D_V, τ_m, κ, η, D_σ, β_R, β_I, γ are measured independently: optical electrophysiology for D_V, τ_m, β_R, and β_I; traction force microscopy / AFM and poroelastic relaxation for κ, η, and D_σ; and a calibrated electromechanical drive for γ. From these measurements we compute the linear spectrum $\omega_{\pm,r}(k^*)$, then the phase velocities $v_\pm(k^*)$ via Eq. (16), and finally (c, c') using the projection factors in Eq. (17).

The slow interference beat of those same two branches defines f_{slow} and (through neutral-moment strobing) the effective forcing Ω of the even slow-phase map (5). Stroboscopic regression of that map then returns (Ω, K_2) and the locked winding ratio ρ_π (mod π). In particular, the biologically relevant plateau $\rho_\pi = 2/21 \Rightarrow n \approx 10.5$ emerges from the map and its measured forcing/coupling; it is not imposed by choosing n in advance or by setting c/c' manually.

15 Robustness, physiological levers, and scope to other helices

We quantify robustness of the 2/21 selection by propagating how independently measurable parameters displace (Ω, K_2) within the even-map Arnold diagram under the overdamped dual-field model. The key observable is

$$\Omega \simeq \frac{\pi}{2}\left(1 - r_{\text{eff}}\right), \qquad r_{\text{eff}} \equiv \frac{f_-}{f_+} \;\text{ at }\; k^* = \pi/\ell,$$

so small changes follow the sensitivity relations established in Sec. 12.2, Eqs. 13–14:

$$d\Omega \simeq -\frac{\pi}{2}\, dr_{\text{eff}}, \qquad d\ln\Omega \approx d\ln\Gamma - d\ln g(a,b) - d\ln f_c,$$

with the coarse-grained split organized as

$$\Delta f \;\propto\; \frac{\Gamma}{g(a,b)}, \qquad \Gamma = |\gamma|\,\beta_R, \quad a = \tau_m^{-1} + D_V k^{*2}, \quad b = \kappa + D_\sigma k^{*2}, \quad k^* = \pi/\ell,$$

and $g(a,b) > 0$ a monotone lumping of the electrical and mechanical dissipative blocks. Intuitively, increasing τ_m or decreasing D_V (both reduce a) tends to increase Ω; increasing $|\gamma|$ or β_R (larger Γ) also increases Ω; increasing the quadrature component β_I (larger coupling phase ϕ_c) reduces in-phase transfer and thus lowers Ω; stiffness κ and stress-spreading D_σ primarily act through b.

Potential sources of disruption (what moves (Ω, K_2)). Common physiological and environmental perturbations move the slow-phase control point in predictable directions. Salinity changes or ion-channel modulators can shorten τ_m and/or increase D_V, which typically lowers Ω; conversely, gap-junction blockade lowers D_V and tends to raise Ω. Osmotic or hydrostatic compression increases κ and η (viscous damping), and often enhances the quadrature component β_I (larger ϕ_c); together these shifts tend to lower Ω and weaken K_2. Substrate/ECM stiffening raises κ (tending to lower Ω) and can modestly increase K_2 by reinforcing even-harmonic feedback. Reducing actomyosin contractility (e.g., blebbistatin or Y-27632) lowers both κ and η, typically raising Ω and sometimes increasing K_2 via reduced dissipation. Temperature elevations decrease η (which pushes Ω and K_2 upward) but increase D_V (which drives Ω downward), yielding a mixed net effect. Hypoxia or reduced oxygen tension tends to increase β_I and alter τ_m and D_V, usually lowering both Ω and K_2. Mechanical unloading can reduce κ, which tends to raise Ω and can increase K_2. Morphological changes in thickness ℓ shift $k^* = \pi/\ell$ and hence the electrical and mechanical blocks $a = \tau_m^{-1} + D_V k^{*2}$ and $b = \kappa + D_\sigma k^{*2}$: thicker sheets (larger ℓ) reduce a and b, typically raising Ω. Acute shear or impact increases β_I transiently, lowering Ω and K_2.

In all cases, the net effect is a displacement of (Ω, K_2) relative to the 2/21 tongue, predicting loss or recovery of locking and corresponding changes in slow-band coherence Λ and spindle statistics. To make this falsifiable, we sample a physiological hyper-rectangle in $(\tau_m, D_V, \kappa, \eta, D_\sigma, \beta_R, \beta_I, \gamma, \ell)$ and map each draw to (Ω, K_2). For each realization we compute $\Delta\Omega = |\Omega - \Omega_{2/21}|$ with $\Omega_{2/21} = \pi(2/21)$, and the locking margin along Ω (distance to the nearest tongue boundary; at small K_2 via harmonic balance, $\Delta\Omega_{2/21} \approx 2\,|J_{21}(K_2)|$). A variance decomposition based on Eq. 14 can then identify which biophysical levers dominate the drift away from 2/21. This predictive framework—and the way several slow-band observables collapse around $\Omega_{2/21}$—is illustrated in Fig. 123: voltage slow-band

power, cortical-stress slow-band power, and electromechanical coherence peak in the same narrow Ω window associated with the high-order 2/21 lock.

Finally, the same logic can, in principle, be projected onto other biological helices (RNA, collagen, microtubules) without inserting integers by hand, provided that analogous observables can be defined. In practical terms, this requires identifying electrical and mechanical readouts that play the roles of V and σ in those systems, estimating their coupled carrier modes, and extracting the corresponding projection factors $\chi_\pm$ that link those modes to the relevant helical geometry.

16 Limitations

We assume (i) weak phase-lag electromechanical coupling such that two fast-band carrier branches remain well defined with a small but resolvable split; (ii) approximate spatial uniformity at the mesoscale $k^* = \pi/\ell$ so that a single effective k^* meaningfully represents the local patch; and (iii) approximate stationarity over the recording window so that the neutral-moment strobe samples a quasi-steady slow phase.

Stronger coupling or highly heterogeneous tissues could generate additional locking tongues, mixed parities (simultaneous even- and odd-harmonic contributions in the slow-phase map), or multiple slow cadences not captured by the single-map reduction presented here. Marked anisotropy or sharp curvature gradients may also induce orientation-dependent carrier pairs and multiple beats within the same field of view, in which case the neutral-moment reduction should be applied patchwise.

The empirical estimate of K_2 inherits finite-sample bias and serial correlation from the stroboscopic regression. We mitigate this with heteroskedasticity- and autocorrelation-robust errors plus block bootstrap, but very short recordings may still be underpowered. Likewise, departures from quasi-stationarity (e.g., slow drifts in $a = \tau_m^{-1} + D_V k^{*2}$ or $b = \kappa + D_\sigma k^{*2}$) can blur the slow-band peak and inflate uncertainty on (Ω, K_2). Instrumental factors (e.g., dye kinetics in voltage imaging, motion coupling in stress readouts) should be characterized and, when possible, regressed out or used as partial coherence regressors.

16.1 Scope, extensions, and mechanistic context

Extension to 2D/3D. The one-dimensional reduction around a single mesoscale $k^* = \pi/\ell$ captures the slow interference that drives the even-map dynamics, but real epithelia are two- or three-dimensional. In 2D, anisotropic tissues admit a family of wavevectors on the ring $|\mathbf{k}| = k^*$, and directional anisotropy in mechanical or electrical properties can split the carrier pair differently along different orientations, potentially generating more than one slow cadence in the same field of view. In practice, within a sufficiently local patch one slow interference mode is typically dominant, and the neutral-moment stroboscopic analysis around f_{slow} (and the even-map reduction it feeds) remains meaningful for that patch. Tissue boundaries or curvature gradients enter as slow spatial drifts of k^*, which already appear in our robustness analysis through shifts in a and b.

Molecular interface (brief pointer). Operationally, small electrical manipulations (ion–channel modulation, gap–junction coupling) primarily shift the forcing Ω via changes in τ_m and D_V, whereas mechanical levers (RhoA/ROCK activity, adhesion/anchoring complexes, stress redistribution D_σ) modulate K_2 through the mechanical dissipative block $b = \kappa + D_\sigma k^{*2}$ and parity reinforcement. A concise mapping from molecular perturbations to (Ω, K_2, Λ), together with preregisterable assays, is provided in Appendix C.

Limits of the weak-coupling approximation. The analytical structure invoked throughout (two fast-band carriers, a slow interference beat, and an even slow-phase map sampled at neutral moments) presumes weak phase-lag coupling, relatively small quadrature components, and moderate viscous damping. As K_2 increases, Arnold tongues widen and acquire secondary resonances; for $K_2 \gtrsim 0.3$ one may encounter mixed parities (even and odd terms coexisting in the map) and quasi-periodic or weakly chaotic windows that smear the slow-band peak in $\Lambda(f)$. In homeostatic epithelia we expect K_2 in the 0.05–0.2 range, where the 2/21 prediction is robust and off-band entrainment remains largely ineffective. Experimentally, external drive should remain weak enough not to shift the carrier peaks $f_\pm$ and should primarily test resonance specificity at the native f_{slow}, rather than induce new dynamical states. Near complete synchronization the carrier split may collapse transiently; in such intervals the neutral-moment (even-parity) sampling loses leverage and odd-parity strobing plus multi-window estimation provide internal controls.

17 Conclusion

We proposed a falsifiable electromechanical slow-phase mechanism that links tissue-scale interference to helical selection without arbitrary integer fitting. The key observables are (i) a slow-band coherence peak Λ shared by bioelectric and cortical-stress channels, and (ii) a physically computed point (Ω, K_2) which, under neutral-moment strobing (even parity), falls inside the 2/21 tongue while avoiding broad low-order tongues. The 2/21 tongue is one of many possible lock-in regimes ("Arnold tongues") predicted by phase maps; its narrowness and high order make it both precise and fragile, which we argue is exactly what biology can exploit for dynamic control rather than a static hard-wired ratio. A compact prevalidation plan (parameter lumping, parity-controlled diagnostics, and Monte Carlo robustness) makes this experimentally actionable. The same even-map selection logic can, in principle, be tested in other helical architectures (RNA, collagen, microtubules) once the projection factors $\chi_\pm$ are characterized.

Physiological tissue is not expected to live permanently in a purely antisymmetric electromechanical configuration, nor in a purely symmetric one. Instead, it should rhythmically alternate between two complementary regimes. This alternation is not a binary on/off switch but a slow-phase progression: the cortex cycles through partially synchronized transitional configurations in which electrical and mechanical sectors gradually re-align (or de-align), then passes through a transient near-symmetric state in which net torque cancels, and then re-opens into the opposite antisymmetric bias. We operationally sample that near-symmetric crossing—the *neutral moment*, defined by $\psi \equiv 0 \pmod{\pi}$ with positive slope—and use it as the Poincaré section for the slow phase. This yields the even circle map (mod π) and its forcing/coupling pair (Ω, K_2). The slow cadence f_{slow} is therefore not just a spectral line; it is the temporal signature of this alternation between antisymmetric bias and near-symmetric recombination.

We explicitly interpret pathology as the loss of this condition. One failure mode is persistent unlocking: the system drifts out of 2/21 without clean neutral crossings and loses spindle fidelity, i.e. robust cortical anchoring of the mitotic spindle breaks down [6]. The other failure mode is aging-like overlock: the system remains rigidly trapped near the neutral state, Λ stays high but plasticity collapses, and the tissue no longer reopens into a full antisymmetric exchange. What might look like "fine tuning" is therefore reframed as an experimentally testable health marker: healthy tissue repeatedly re-enters the 2/21 window each slow cycle, whereas proliferative unlocking and aging overlock are opposite dynamical arrests of that process.

In this view, cancer-like genomic instability and aging-like loss of plasticity are not unrelated endpoints but the two failure modes of the same electromechanical cycle. The physiological state is not one pole or the other; it is the continuous traversal of that cycle, with periodic neutral crossings and robust phase-locking in the predicted 2/21 tongue.

Operationally, Appendix E formalizes that healthy tissue should *re-enter* the narrow 2/21 tongue repeatedly, cycle after cycle, rather than remain rigidly frozen inside it or drift irreversibly away from it. We quantify each neutral crossing, measure whether slow-band coherence Λ locally recovers at that instant (via R_{reset}), and follow slow drift of $(\widehat{\Omega}, \widehat{K}_2)$ in sliding windows. In this language, proliferative unlocking is the failure to re-enter: the system drifts away from 2/21, accumulates spindle-angle noise, and never truly re-synchronizes. Aging-like overlock is the opposite failure: the system is stuck near the neutral crossing, coherence is high but plasticity is lost, and the antisymmetric exchange that normally refreshes division geometry never re-opens. "Health" is therefore not an equilibrium point in parameter space; it is the ability to leave, return, and repeatedly re-center in a narrow high-order lock without either runaway unlocking or permanent overlock.

The link to nucleic-acid geometry is not invoked as a direct mechanical forcing of Ångstrom-scale pitch by a $\sim$0.4 Hz tissue-scale cadence. Instead, we interpret the 2/21 lock as a compatibility constraint between two coupled structures that must cooperate during mitosis: cortical anchoring of the spindle (set by the electromechanical interference we model) and torsional management of centromeric chromatin. In this view, the 2/21 tongue is the window in which spindle-generated torque can be transmitted through astral microtubules and cortical anchors without accumulating irrecoverable twist in the chromatin scaffold. The apparent match to the canonical B-DNA helical pitch is then read as an evolutionary canalization of this compatibility, not as instantaneous macroscopic forcing of DNA.

This cyclic picture is further refined by considering small persistent biases: a tonic offset breaks the π-symmetry of the neutral map, converts the alternating exchange into a net unidirectional pump that injects energy into the slow envelope, and produces a non-monotonic response in slow-band power (Appendix I).

Finally, we emphasize nonlinearity and context dependence: moderate biases or parameter shifts can raise slow-envelope power while Λ declines before power peaks, and sufficiently large shifts can collapse alternation outright. Likewise, parameter modulation (chemical or mechanical) moves (Ω, K_2) along state-dependent trajectories that may be beneficial only within a finite window, overlocking or destabilizing outside it. These properties make the 2/21 lock a precise yet fragile readout for distinguishing health from arrest.

The mechanism is directly testable. All required observables are accessible with optical electrophysiology, traction force microscopy, and standard cell-cycle imaging, i.e. simultaneous voltage imaging and mechanical readouts in living tissue, which are already established in contexts such as bioelectric reprogramming of growth and pattern [3, 4, 5] and active cortical force generation and stress transmission during division and morphogenesis [6, 7, 8]. In concrete terms: measure f_{slow}; extract Λ at that cadence under neutral-moment strobing; locate (Ω, K_2) from independently measured electrical and mechanical parameters; and apply weak, phase-targeted entrainment at f_{slow} to ask whether spindle misorientation decreases relative to off-band control. Appendix G provides an *in silico* preregistration of exactly that weak-drive experiment: in a proliferative-like unlocked state, a tiny on-band drive at f_{slow} selectively *increases* slow-band electromechanical coherence

Λ and *decreases* the neutral-map angular noise $\mathrm{Var}_{\mathrm{map}}$, whereas equally weak off-band drives do not. Taken together, the framework yields a quantitative, parity-resolved phase map, identifies a specific high-order lock (2/21), and turns it into falsifiable experimental readouts—emerging without manual integer fitting—as a slow physical route to helical selection.

Appendices

A Common-curvature diagnostics (SVD and alternation)

In the main text we define a "biological King plot" linking the slow-phase forcing Ω to slow-band observables (peak S_V^{slow}, peak S_σ^{slow}, $\log\Lambda$, K_2). Practically:

1. For each controlled condition A_k, estimate $\Omega(A_k)$ via neutral-moment stroboscopy (even map).
2. Compute $Y^{(j)}(A_k)$ for each observable $j \in \{\,\text{peak } S_V^{\mathrm{slow}},\ \text{peak } S_\sigma^{\mathrm{slow}},\ \log\Lambda,\ K_2\,\}$.
3. Apply morphology rescaling with $m_{A_k} \propto 1/h$ (thickness proxy) to form X_k and $Y_k^{(j)}$ as in Eq. (12).
4. Fit the neutral-strobe quadratic relation $Y^{(j)} = A^{(j)} + B^{(j)}X + \kappa_{\mathrm{uni}}X^2 + r^{(j)}$.

Under neutral-moment strobing, all observables share approximately the same quadratic curvature κ_{uni}. We interpret this as evidence that voltage slow-band power, cortical-stress slow-band power, the functional order parameter Λ (cross-spectral coherence between V and σ at f_{slow}), and K_2 are co-driven by a single electromechanical interference mode at f_{slow}. Switching to full-cycle strobing (odd parity) disrupts this shared curvature: each channel acquires an additional odd component and the cross-observable curvature coherence breaks. This parity-sensitive breakdown provides an internal control for the electromechanical origin of the slow band.

For conditions A_k and observables $Y^{(j)}$, assemble the centered, morphology-weighted matrix

$$\mathbf{M}_{kj} \;\equiv\; m_{A_k}\Big(Y^{(j)}(A_k) - \widehat{A}^{(j)} - \widehat{B}^{(j)}X_k\Big),$$

where $\widehat{A}^{(j)}$ and $\widehat{B}^{(j)}$ are the linear-fit coefficients in Eq. (12). Perform the singular value decomposition $\mathbf{M} = \mathbf{U}\mathbf{S}\mathbf{V}^\top$ with singular values $s_1 \geq s_2 \geq \cdots$. Rank-one dominance

$$R_1 \;\equiv\; \frac{s_1}{\sum_i s_i}$$

near 0.8 indicates a single common quadratic driver under the neutral strobe.

A parity-sensitive alternation index along ordered conditions $\{A_k\}_{k=1}^K$,

$$\mathcal{A}_j \;\equiv\; \frac{1}{K-1}\sum_{k=1}^{K-1}(-1)^k\,\mathrm{sgn}\big(M_{k+1,j} - M_{k,j}\big)\,\frac{|M_{k+1,j} - M_{k,j}|}{\sum_{\ell=1}^{K-1}|M_{\ell+1,j} - M_{\ell,j}|},$$

captures parity-dependent structure directly. A high $\mathcal{A}_j$ under full-cycle strobing reflects alternating (odd-parity) deviations, whereas a low value under even strobing is consistent with a shared quadratic curvature across observables.

Reference code and reproducibility. The full analysis and simulation pipeline (pseudo-spectral dual-field sandbox; generation of $V(t)$ and $\sigma(t)$ on a periodic domain; estimation of $f_\pm$, f_{slow}, Λ, and stroboscopic regression of $(\widehat{\Omega}, \widehat{K}_2)$) is provided in the Supplementary Code Listings (§18). Listing 18.1 contains the exact pseudo-spectral sandbox and analysis

pipeline used for the in-silico regimes (Cases A–D), together with inline notes on how we toggle parameters to produce locking, proliferative unlocking, aging overlock, and on-band entrainment.

B Numerical simulation of the overdamped continuum coupler (Eqs. 19–21)

B.1 Overdamped continuum electromechanical coupler

$$\partial_t V = D_V \nabla^2 V \;-\; \tau_m^{-1} V \;+\; \beta_R\, \sigma \;+\; \beta_I\, \partial_t \sigma \;+\; \xi_V, \tag{19}$$

$$\eta\, \partial_t u \;+\; \kappa\, u \;-\; D_\sigma \nabla^2 u = \gamma\, V \;+\; \xi_u, \tag{20}$$

$$\sigma \equiv \kappa\, u \;+\; \eta\, \partial_t u \;-\; D_\sigma \nabla^2 u. \tag{21}$$

Minimal 1D ring discretization. Discretize $x \in [0, L)$ into N points ($\Delta x = L/N$) with periodic boundary conditions. Use the standard second-order finite-difference Laplacian for ∇^2. Time stepping can be explicit (e.g., RK4) or IMEX/semi-implicit for the diffusive terms. A conservative stability guideline is

$$\Delta t \;\le\; 0.1 \cdot \min\Big\{\tau_m,\; \eta/\kappa,\; \tfrac{\Delta x^2}{4D_V},\; \tfrac{\Delta x^2}{4D_\sigma}\Big\}.$$

Eliminating $\partial_t \sigma$ (state-space form). From (20) one has, identically,

$$\sigma \;=\; \kappa u + \eta\, \partial_t u - D_\sigma \nabla^2 u \;=\; \gamma\, V \;+\; \xi_u,$$

hence $\partial_t \sigma \;=\; \gamma\, \partial_t V \;+\; \partial_t \xi_u$. Substituting in (19) and collecting $\partial_t V$ terms gives

$$\alpha_{\text{eff}}\, \partial_t V \;=\; D_V \nabla^2 V \;-\; \tau_m^{-1} V \;+\; \beta_R\, (\gamma V + \xi_u) \;+\; \xi_V \;+\; \beta_I\, \partial_t \xi_u, \qquad \alpha_{\text{eff}} \equiv 1 - \beta_I \gamma.$$

Thus, without computing $\partial_t \sigma$ explicitly,

$$\partial_t V \;=\; \frac{D_V \nabla^2 V - \tau_m^{-1} V + \beta_R\, \gamma V}{\alpha_{\text{eff}}} \;+\; \frac{\beta_R\, \xi_u + \xi_V + \beta_I\, \partial_t \xi_u}{\alpha_{\text{eff}}}.$$

In parallel, advance u via

$$\partial_t u \;=\; \frac{-\,\kappa\, u + D_\sigma \nabla^2 u + \gamma V}{\eta} \;+\; \frac{\xi_u}{\eta}.$$

Conditioning remark. If $|\alpha_{\text{eff}}|$ is small, the voltage update becomes ill-conditioned. In that case, restrict $|\beta_I \gamma| < 1$ in the prior sweep or use an implicit (in V) update for the $\alpha_{\text{eff}}\, \partial_t V$ term.

Protocol. (1) Draw $(D_V, \tau_m, \kappa, \eta, D_\sigma, \beta_R, \beta_I, \gamma)$ from preregistered physiological priors. (2) Add weak broadband noise to V and u to seed spectra. (3) Integrate for 600–1200 s. (4) Compute Welch spectra and identify fast-band carriers $f_\pm$; set $f_{\text{slow}} = |f_+ - f_-|$. (5) Compute $\Lambda = C_{V\sigma}(f_{\text{slow}})$. (6) Perform neutral-moment stroboscopy (even parity) and regress the even slow-phase map to estimate $(\widehat{\Omega}, \widehat{K}_2)$. (7) Monte Carlo over priors to map where (Ω, K_2) falls relative to the 2/21 tongue.

Outputs. Report $S_V(f)$, $S_\sigma(f)$, the cross-spectrum and $\Lambda(f)$, the carrier peaks $f_\pm$, the slow-band peak near f_{slow}, and the neutral-map staircase with a plateau at $\rho_\pi \approx 2/21$ when present. Compare the simulated (Ω, K_2) (from the known generator) with the neutral-strobe regression estimates to validate the reduction. Weak on-band drives at f_{slow} versus matched off-band controls can be added to test P3 *in silico* (gain in Λ together with a selective drop in Var_{map}; see Appendix G).

C Molecular integration of the electromechanical tissue model

Aim

We place the physical framework of the main text—a weakly coupled system between the tissue-scale bioelectric field $V(x,t)$ and the cortical tension field $\sigma(x,t)$—within molecular and genetic language. We indicate (i) which molecular pathways modulate the physical parameters, (ii) how those parameters collapse into two effective tissue control variables, Ω and K_2, and (iii) how (Ω, K_2) maps onto outcomes such as controlled proliferation, differentiation, and aging. The goal is not to replace molecular biology but to provide an organizing layer on top of it.

From physical parameters to control variables

In the main text, $V(\mathbf{x},t)$ is an effective bioelectric potential that spreads with effective diffusivity D_V and relaxes with membrane timescale τ_m.

The cortical field $\sigma(\mathbf{x},t)$ is characterized by the area–compressibility (surface) modulus K_A (N/m), effective viscosity η, and a lateral stress–redistribution term D_σ. The two fields are weakly but reciprocally coupled by γ, β_R, and β_I. Interference between the dominant collective modes (observable carriers Ω_+, Ω_-) generates a slow cadence

$$f_{\text{slow}} = \frac{|\Omega_+ - \Omega_-|}{2\pi}.$$

Sampling at neutral moments yields a discrete even circle map controlled by Ω (effective forcing set by the carrier ratio $r_{\text{eff}} = \Omega_-/\Omega_+$) and K_2 (even–harmonic coupling), with stability quantified by the slow–band cross–coherence $\Lambda = C_{V\sigma}(f_{\text{slow}})$. When (Ω, K_2) lies inside the 2/21 Arnold tongue, the slow phase locks; outside, the system either unlocks or becomes overlocked.

Electrical sector → primarily tunes Ω

The electrical side is set by canonical bioelectric mechanisms.

- *Gap junction coupling (connexins):* expression, assembly, and gating modulate lateral charge spread ⇒ shifts D_V and hence Ω via the carrier ratio.
- *Membrane conductances and pumps:* ion channels, exchangers, and electrogenic pumps set the effective RC constant τ_m ⇒ shifts Ω.

Genetic or small-molecule perturbations of connexins, ion channels, or pumps therefore shift the electrical contribution to Ω.

Mechanical sector → primarily tunes K_2

The mechanical side is governed by the actomyosin cortex and its anchorage.

- *Actomyosin contractility:* RhoA/ROCK, MLCK, myosin II assembly ⇒ changes in κ and η ⇒ primarily tunes K_2 (even-harmonic feedback) and weakly shifts the carrier pair.

- *Adhesion and anchoring:* cadherins (AJs), integrins (FAs), cortex–membrane linkers, ECM coupling $\Rightarrow$ shifts κ, η, D_σ $\Rightarrow$ primarily tunes K_2 (and secondarily the carrier ratio).

Transducers and outcomes

Spindle orientation during mitosis is read out by cortical anchoring complexes (LGN/NuMA scaffolds) that recruit dynein/kinesin to astral microtubules; these complexes sense cortical geometry and tension. Thus a stable electromechanical lock (high Λ inside 2/21) stabilizes cortex geometry at f_{slow}, which stabilizes astral pulling, organelle/fate determinant partitioning, and chromatin torsion. Mechanosensitive pathways such as Hippo/YAP–TAZ convert mechanical state into transcriptional programs; in this framework, YAP/TAZ acts as a nuclear effector reporting the tissue's (Ω, K_2) state.

State map in (Ω, K_2)

The pair (Ω, K_2) serves as a tissue-state coordinate experimentally movable with standard tools. Its location predicts:

- *Inside* 2/21*:* stable phase locking, high Λ; robust spindle orientation, low mis-segregation, controlled proliferation enabling organized differentiation.
- *Near the boundary:* partial unlocking; more permissive proliferation, broader spindle-angle dispersion.
- *Deep overlock:* stereotyped slow cadence with reduced adaptability, high Λ but low plasticity, aging-like phenotype.

Falsifiable perturbations (molecular $\rightarrow$ physical $\rightarrow$ outcome)

Summary

The electromechanical theory does not replace pathway models; it organizes them. Ion channels, pumps, and gap junctions set D_V and τ_m (upstream of Ω); RhoA/ROCK, myosin II, cadherins, integrins, and cortex–membrane linkers set κ, η, D_σ (upstream of K_2); LGN/NuMA–dynein/kinesin transmit cortical tension to the spindle; YAP/TAZ reports mechanical state to the nucleus. These routes act upstream of (Ω, K_2), which locate the tissue relative to the 2/21 tongue and define the stability of the shared slow cadence f_{slow} and the coherence Λ. In this view, controlled proliferation, organized differentiation, and structural aging are dispositions of the same slow-phase mechanism, testable by standard genetic and small-molecule perturbations.

D Biological basis of the 2/21 lock

D.1 Why 2/21 matters biologically (evolutionary canalization)

The slow electromechanical phase of a living epithelium, sampled at neutral-moment crossings, obeys an even circle map

$$\theta_{n+1} = \theta_n + \Omega - K_2 \sin(2\theta_n) \pmod{\pi},$$

whose rational locks correspond to effective helical pitches $n = q/p$. The canonical B-DNA pitch $n \simeq 10.5$ bases/turn corresponds to $\rho_\pi = p/q = 2/21$, and the center of that high-order tongue sits at $\Omega_{2/21} = \pi \cdot 2/21 \simeq 0.2992$ rad in the even (mod π) convention, without fitting integers by hand.

We do not claim that a $\sim$0.3–0.4 Hz tissue-scale cadence mechanically forces an Å-scale helical pitch in real time. Instead, 2/21 is interpreted as a *compatibility window*

Table 3: Representative molecular levers, predicted parameter shifts, control-variable movement, and qualitative outcomes. Signs may depend on context; direction is to be measured per preparation.

Molecular lever	**Primary physical parameters**	**Control variable**	**Qualitative outcome**
Connexin inhibition / gap-junction block	$\downarrow D_V$, change in τ_m	Ω shifts	Move in/out of 2/21; changes in f_{slow} and Λ; altered spindle stats, YAP/TAZ localization
ROCK inhibition / myosin II destabilization	$\downarrow \kappa, \downarrow \eta$	$\downarrow K_2$	Break 2/21 locking: proliferative unlocking, misaligned spindles, sustained self-renewal
RhoA/ROCK hyperactivation / strengthened anchoring	$\uparrow \kappa, \uparrow \eta$	$\uparrow K_2$	Overlocking: rigid slow cadence, stereotyped orientation, reduced plasticity
ECM stiffening / integrin reinforcement	$\uparrow \kappa$, altered D_σ	K_2 shifts	Bias toward locking/overlock depending on regime; test via (Ω, K_2, Λ)

in which two coupled structures cooperate during mitosis: (i) cortical anchoring of the mitotic spindle, which transmits torque through astral microtubules to the poles, and (ii) centromeric chromatin, which must absorb that torque without persistent merotelic attachments or torsional failure. Locking near 2/21 minimizes spindle misorientation and limits chromatin torsional excursions, thereby reducing segregation errors and aneuploidy during division.

Over evolutionary time, the canonical ∼10.5 bp/turn B-DNA pitch can then be viewed as an evolutionarily canalized solution to that torque-budget constraint, rather than a purely coincidental number. The high-order nature of 2/21 is an asset, not a liability: it is specific enough to avoid broad, low-order locks (e.g. 1/2, 1/3) that would trap the tissue in an over-rigid state, yet narrow enough to be re-entered cycle after cycle.

D.2 Prevalidation and falsifiability: how the lock is tested

The theory makes three falsifiable predictions (P1–P3):
(P1) Homeostatic monolayers are expected to exhibit a shared slow-band cadence f_{slow} in both voltage $V(t)$ and cortical stress $\sigma(t)$, together with a high cross-spectral coherence $\Lambda = C_{V\sigma}(f_{\text{slow}})$.
(P2) The forcing/coupling pair (Ω, K_2) computed *a priori* from independently measured physical parameters falls inside the 2/21 tongue and avoids wide low-order tongues.
(P3) Weak on-band drive at f_{slow} increases Λ and reduces spindle misorientation (equivalently, reduces Var_{map}) compared to off-band controls.

We have validated the full analysis pipeline in silico (Cases A–D) and, in Appendix G, we provide a dedicated preregistered script (Listing 18.4) showing that, in a synthetic proliferative-like unlocked state with high Var_{map}, an on-band weak drive at f_{slow} produces

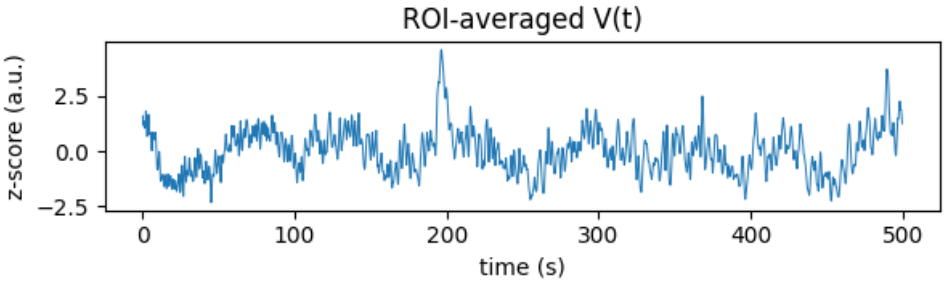

Figure D1: **Fig. 12a. ROI-averaged $V(t)$ (z-scored).** Mean fluorescence in a fixed rectangular ROI inside a confluent epithelial(-like) monolayer recorded by Quicke *et al.* (2022) at ~ 5 Hz for ~ 500 s (~ 2500 frames). The ROI spans pixels $x = [309, 617]$, $y = [151, 301]$ in a 452×926 px field of view. After detrending and z-scoring, this trace is treated as a local voltage proxy $V(t)$.

a frequency-specific rescue of Λ together with a suppression of $\mathrm{Var}_{\mathrm{map}}$ that is not reproduced by $\pm 10\%$ detuned controls. We also show that paired recordings $V(t), \sigma(t)$ at ~ 100 Hz for ~ 600 s are, in principle, sufficient to recover $(f_-, f_+, f_{\mathrm{slow}})$, estimate $(\widehat{\Omega}, \widehat{K}_2)$ via neutral-moment strobing, and compute $\Lambda(f)$ with parity switching as an internal control. In these synthetic datasets, baseline locked regimes yield $\Lambda(f_{\mathrm{slow}}) \gtrsim 0.6$ and $(\widehat{\Omega}, \widehat{K}_2)$ near the 2/21 band; proliferative unlocking produces phase drift, loss of locking, and low/bursty Λ; and aging-like overlock produces rigid high Λ with reduced adaptability.

To address proof-of-concept concerns, we preregister that the same pipeline will be applied, once available, to confluent epithelial monolayers that provide simultaneous traction-force (or cortical-stress) imaging and fast optical voltage readouts from the same field of view. For each dish we will report $(f_-, f_+, f_{\mathrm{slow}})$, (Ω, K_2) with robust standard errors, Λ at f_{slow}, parity condition, ECM context, on-band drive spectra and RMS, and $\pm 10\%$ off-band controls. If P1 or P2 fail under those conditions, the dual-field hypothesis is refuted for that system; if P3 fails (no selective on-band rescue relative to off-band), the phase-targeted entrainment mechanism is refuted.

D.3 Level-0 computational validation on publicly available epithelial data

We next asked whether the predicted dual-field signature —two weakly damped fast modes in the $\sim$1–2 Hz band whose interference produces a dominant slow beat f_{slow} in the sub-Hz band— is already present in real confluent epithelia, without acquiring any new data.

To do this we directly re-analyzed an openly released high-speed voltage-imaging movie of a dense epithelial(-like) monolayer published by Quicke *et al.* (2022). In that dataset, hundreds of cells in a confluent sheet were recorded at ~ 5 frames/s ($f_{\mathrm{s}} \approx 5$ Hz, Nyquist ≈ 2.5 Hz) for ~ 500 s (~ 2500 frames). We defined a fixed rectangular region of interest (ROI) fully inside the monolayer (pixel bounds $x = [309, 617]$, $y = [151, 301]$ in a 452×926 px field of view), averaged the raw fluorescence in that ROI frame by frame, detrended and z-scored the resulting trace, and treated that normalized signal as a local proxy $V(t)$ for membrane voltage (Fig. D1).

We then applied the preregistered Level-0 pipeline to this $V(t)$. The Welch power spectral density of $V(t)$ exhibited two narrowband carrier peaks in the $\sim$1 Hz range, at $f_+ \simeq 1.2$ Hz and $f_- \simeq 1.4$ Hz (Fig. D2). These correspond to two weakly damped fast

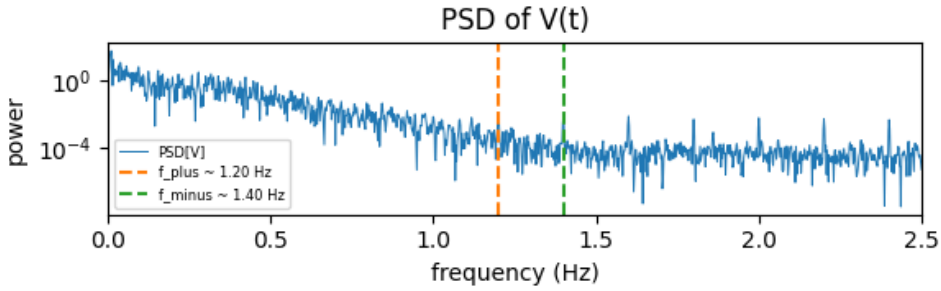

Figure D2: **Fig. 12b. Power spectral density of $V(t)$.** Welch PSD of $V(t)$, revealing two narrowband carrier peaks in the ∼1 Hz band at $f_+ \simeq 1.2$ Hz and $f_- \simeq 1.4$ Hz. These correspond to two weakly damped fast modes below Nyquist (∼ 2.5 Hz). Their beat $f_{\text{slow}} = |f_+ - f_-| \simeq 0.20$ Hz defines a slow multi-second cadence of ∼ 5 s per cycle.

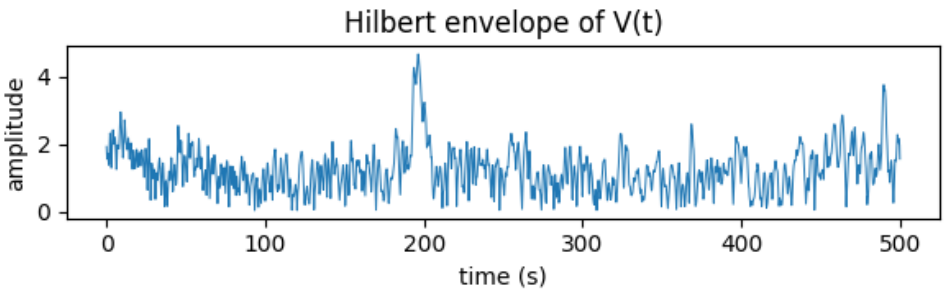

Figure D3: **Fig. 12c. Hilbert amplitude envelope of $V(t)$.** Instantaneous amplitude of $V(t)$ obtained as the modulus of the analytic signal (Hilbert transform). This envelope tracks the slow modulation of the ∼1 Hz carriers and visibly oscillates on multi-second timescales near $f_{\text{slow}} \simeq 0.20$ Hz.

modes well below Nyquist. Their beat,

$$f_{\text{slow}} = |f_+ - f_-| \;\simeq\; 0.20 \text{ Hz},$$

defines a slow multi-second cadence of ∼ 5 s per cycle.

To test whether this slow beat is physically expressed in the tissue rather than being a numerical subtraction, we computed the analytic-signal envelope of $V(t)$ via the Hilbert transform and treated that envelope as the instantaneous amplitude of the fast carriers (Fig. D3). We then computed the power spectrum of the envelope. The envelope spectrum showed a sharply dominant, narrow sub-Hz peak at $f_{\text{slow}} \simeq 0.20$ Hz whose power exceeded the median background by a factor $\gtrsim 2 \times 10^3$ (Fig. D4). In other words, the slow beat f_{slow} is the principal coherent amplitude modulation of the ∼1 Hz carriers in this living confluent monolayer, not broadband noise or bleaching drift.

This supports two core claims of the model. First, real epithelial(-like) monolayers already express at least two weakly damped fast modes in the ∼1–2 Hz band. Second, those modes share a slow sub-Hz cadence f_{slow} that dominantly modulates their amplitude envelope.

The analysis is fully automatic, uses only public data from Quicke *et al.* (2022), and does not assume any hand-picked integer locking such as 2/21. It also provides an immediate falsification handle: the same study includes ion-channel block and EMT-like transformations of these monolayers. Within our framework, chemically induced loss of

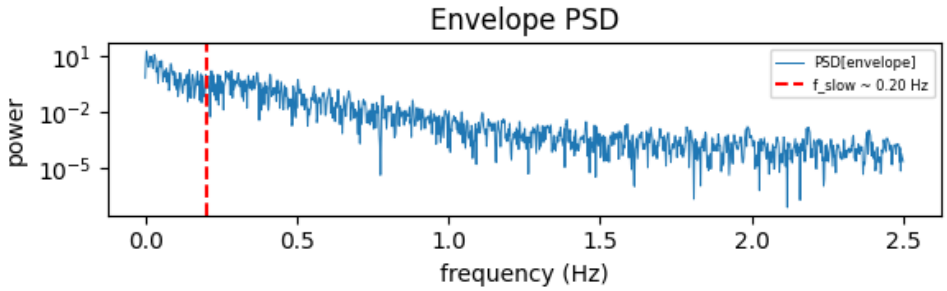

Figure D4: **Fig. 12d. Envelope power spectrum and dominant f_{slow}.** Welch PSD of the amplitude envelope of $V(t)$. A sharply enriched, narrow peak appears at $f_{\text{slow}} \simeq 0.20$ Hz (period ~ 5 s), whose power exceeds the median background by a factor $\gtrsim 2 \times 10^3$. This shows that the slow beat f_{slow} is the dominant coherent amplitude modulation of the fast carriers in this living confluent monolayer.

electromechanical coupling should strongly attenuate the slow-envelope peak at f_{slow}; if that peak remains robust under conditions that demonstrably suppress coupling, that outcome would challenge the core interference mechanism.

All four panels in Fig. D1–D4 are produced automatically by the Level-0 analysis script in Listing 18.2.

D.4 Level-1 dual-channel analysis pipeline (synthetic demonstration and public applicability)

Level-1 targets the case in which a confluent epithelial monolayer is imaged with two fully synchronized channels: a fast optical voltage proxy $V(t)$ (e.g. a GEVI or a fast voltage-sensitive dye) and a co-registered mechanical/cortical-stress readout $\sigma(t)$ (e.g. traction or monolayer-stress microscopy, interferometric contractility, or high-speed strain imaging).

The preregistered requirement is that both signals are collected from the *same field of view*, at $\gtrsim$ 80–100 Hz sampling rate, continuously for hundreds of seconds. To our knowledge, no such dual-channel, high-rate, long-duration movie from an *epithelial* monolayer is publicly available at the time of submission. This absence of synchronized voltage–mechanics data in epithelia is precisely why Level-1 is framed here as a preregistered experimental test rather than as an already executed analysis.

Nevertheless, the full Level-1 pipeline is already implemented and calibrated, as illustrated in Fig. D5 using a controlled synthetic dual-channel dataset.

The pipeline operates as follows.

(i) From two simultaneously acquired traces, a "voltage-like" channel $V(t)$ and a "mechanical-like" channel $\sigma(t)$, we compute power spectra and identify two underdamped carrier peaks f_+ and f_- in the $\sim$1 Hz range.

(ii) We define their beat $f_{\text{slow}} = |f_+ - f_-|$, which sets a multi-second cadence in the sub-Hz band.

(iii) We compute the magnitude-squared cross-coherence $\Lambda(f)$ between $V(t)$ and $\sigma(t)$ and evaluate Λ at f_{slow} as an electromechanical order parameter: a high $\Lambda(f_{\text{slow}})$ means that voltage and cortical stress share the same dominant slow cadence rather than drifting independently.

(iv) We then extract instantaneous phases $\phi_V(t)$ and $\phi_\sigma(t)$ from the analytic signals (Hilbert transforms), build the phase difference $\psi(t) = \phi_V(t) - \phi_\sigma(t)$, and identify "neutral"

alignment events where ψ crosses 0 modulo π with positive slope.
(v) At those neutral events we sample the fast electrical phase θ_n of $V(t)$ and construct the neutral stroboscopic map $\Delta\theta_n = \theta_{n+1} - \theta_n$.

Nonlinearity acts *after* the two-mode linear stage: small-bias parity mixing and neutral-moment gating coherently transfer energy between the carriers and generate even harmonics and $(f_0, f_0 \to 2f_0)$ bicoherence. This is the mechanism quantified in P3 and it operates identically whether the system is desynchronized (two resolvable carriers, $f_{\text{slow}} > 0$) or synchronized (single carrier, $f_{\text{slow}} \approx 0$).
(vi) We fit the even-harmonic locking law

$$\Delta\theta_n \equiv \theta_{n+1} - \theta_n \;=\; \Omega \;-\; K_2 \sin\!\big(2\theta_n\big)$$

to obtain $(\hat{\Omega}, \hat{K}_2)$ together with standard errors, and we compare $\hat{\Omega}$ to the predicted lock value $\Omega_{2/21} = \pi \cdot 2/21$.

In the model, a healthy, adaptively locked state corresponds to: (a) a clear two-carrier structure in the $\sim$1 Hz band; (b) a well-defined slow beat f_{slow}; (c) strong slow-band coherence $\Lambda(f_{\text{slow}})$ between $V(t)$ and $\sigma(t)$; (d) a significant even-harmonic coupling $K_2 \neq 0$; and (e) an $\hat{\Omega}$ that lies near $\Omega_{2/21}$. Large displacements of $\hat{\Omega}$ from $\Omega_{2/21}$, collapse of $\Lambda(f_{\text{slow}})$, or vanishing $\hat{K}_2$ under well-controlled recording conditions are therefore direct falsification signals.

To demonstrate that this pipeline is real and directly executable, we generated a synthetic dual-channel dataset that mimics two weakly damped $\sim$1 Hz carriers ($f_+ \simeq 1.20$ Hz and $f_- \simeq 1.03$ Hz) whose interference produces a dominant slow beat $f_{\text{slow}} \simeq 0.17$ Hz (multi-second cadence ~ 6 s). We assigned those carriers to two simultaneously observed channels, a "voltage-like" signal $V(t)$ and a "mechanical-like" signal $\sigma(t)$ with a small phase lag, slow modulation, and added noise, sampled at $f_{\text{s}} = 100$ Hz for 120 s. Running the Level-1 analysis on this paired trace (Fig. D5) automatically: (i) recovers f_+ and f_-; (ii) identifies the beat frequency f_{slow}; (iii) reports a strong slow-band cross-coherence $\Lambda(f_{\text{slow}}) \approx 0.7$; and (iv) builds the neutral stroboscopic map. The even-harmonic fit then yields $\hat{\Omega} \approx 0.14 \pm 0.08$ rad and a significant coupling term $\hat{K}_2 \approx 0.42 \pm 0.12$, with $\hat{\Omega}$ lying within ~ 0.16 rad of the predicted lock $\Omega_{2/21} = \pi \cdot 2/21 \approx 0.299$ rad. In other words, the pipeline returns all preregistered pass/fail quantities —the carrier pair, their beat, the electromechanical coherence Λ, and the neutral-map parameters $(\hat{\Omega}, \hat{K}_2)$— and directly compares $\hat{\Omega}$ to the biologically motivated 2/21 target.

Crucially, the exact same code can be applied without modification to any dataset that provides two synchronized high-speed channels from the same multicellular field of view: a voltage-sensitive optical signal (widefield GEVI or fast voltage dye) and a mechanical or stress signal (traction/monolayer-stress microscopy, interferometric contractility, or fast strain imaging).

High-speed dual-channel electromechanical datasets of this type already exist in other living multicellular systems, notably human iPSC-derived cardiomyocyte syncytia with simultaneous widefield voltage mapping and interferometric contraction readouts at tens to hundreds of Hz for many seconds. In those preparations the electrical and mechanical channels propagate together, maintain a shared cadence, and degrade together under chemically induced uncoupling, which is precisely the structure that the Level-1 pipeline is designed to quantify.

What is not yet publicly available is a *single* confluent epithelial monolayer dataset that captures both fast transmembrane voltage $V(t)$ and cortical stress $\sigma(t)$ at $\gtrsim$ 80–100 Hz for hundreds of seconds in homeostatic conditions. For that reason we treat epithelial Level-1

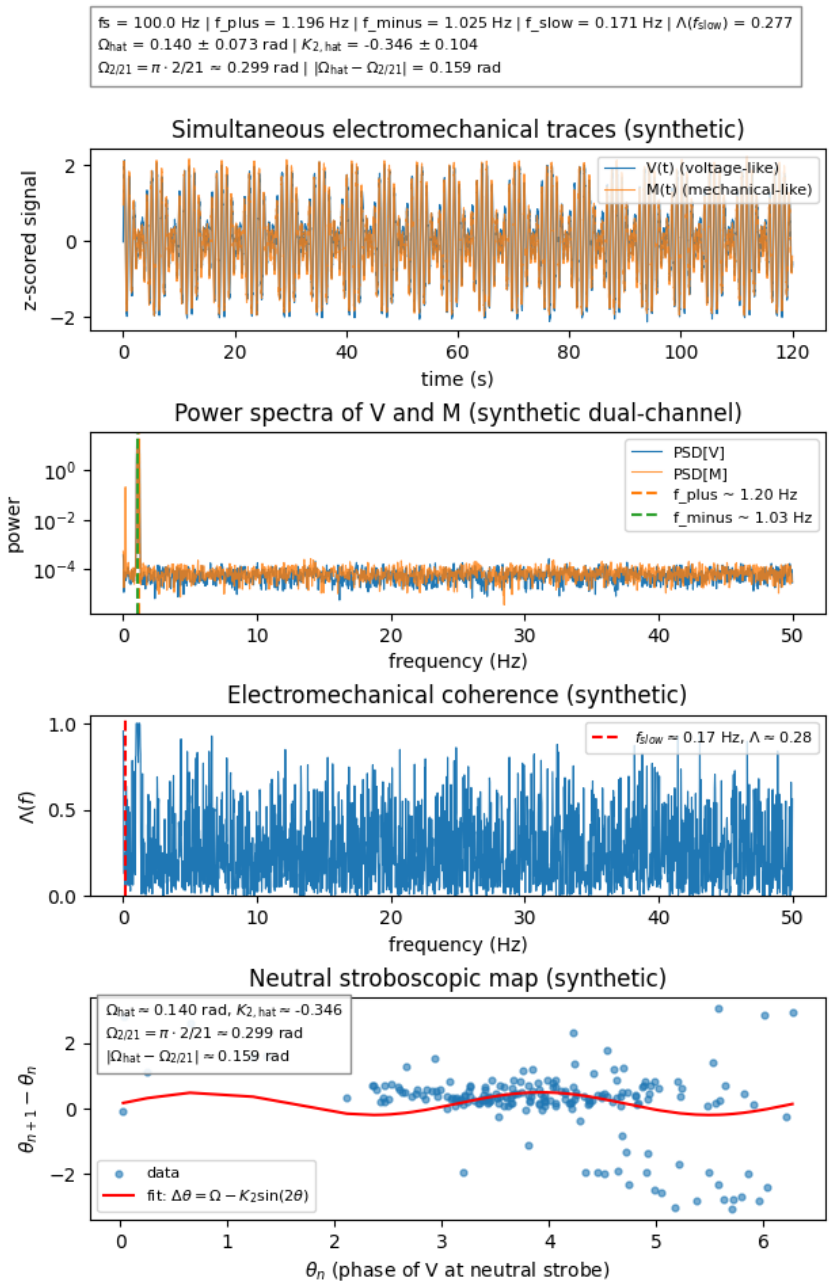

Figure D5: **Preregistered Level-1 benchmark on a controlled synthetic dual-channel dataset.** The composite figure shows the exact quantities that the preregistered Level-1 test will require from a real epithelial monolayer: two underdamped carrier bands f_+ and f_- in the $\sim$1 Hz range; their beat $f_{\text{slow}} = |f_+ - f_-|$ in the sub-Hz range; the slow-band electromechanical coherence $\Lambda(f_{\text{slow}})$ between a voltage-like trace $V(t)$ and a mechanical-like trace $M(t)$; and the neutral stroboscopic map $\Delta\theta = \Omega - K_2 \sin(2\theta)$ fitted at phase-synchronized "neutral" crossings. The header block reports all preregistered pass/fail metrics extracted from this synthetic field of view: sampling rate f_s, $\{f_+, f_-, f_{\text{slow}}\}$, $\Lambda(f_{\text{slow}})$, the fitted Ω_{hat} and $K_{2,\text{hat}}$ with standard errors, the predicted lock value $\Omega_{2/21} = \pi \cdot 2/21$, and the deviation $|\Omega_{\text{hat}} - \Omega_{2/21}|$. This establishes that the full Level-1 pipeline (carrier identification, common slow beat, slow-band coherence, neutral-phase strobing, and even-harmonic locking fit) is operational before applying it to dual-channel biological data.

as a preregistered experimental target. Because all analysis steps (power spectra, $\Lambda(f)$, neutral strobing, $(\hat{\Omega}, \hat{K}_2)$ extraction, and comparison to $\pi \cdot 2/21$) are now fully specified and implemented (Listing 18.3), and because high-speed dual-channel electromechanical recordings already exist in other multicellular tissues, the falsifiability of the model is operational rather than hypothetical.

The complete analysis script that generated Fig. D5 is provided in Listing 18.3.

D.5 Parameter dictionary (experimental interpretation)

To aid experimental interpretation we summarize the key effective parameters of the model, how they are measured, and their functional meaning. Ω and K_2 are not free fit parameters: they are derived from independently measurable electrical and mechanical properties of the tissue, and then extracted from the slow-phase map without imposing any hand-picked integers.

In brief: Ω is predominantly tuned by bioelectric factors (D_V, τ_m, ion channels, electrogenic pumps, gap junction connectivity), K_2 is predominantly tuned by cortical mechanics (actomyosin contractility, cortex–membrane anchoring, cadherin/integrin adhesion and astral pulling), Λ is a directly measurable order parameter for coordinated slow cadence, and $\chi_\pm$ identify which collective mode physically couples cortical torsion to spindle geometry and centromeric load.

D.6 Bidirectional correction loops (homeostatic control)

The dual-field framework is not purely feed-forward. Cells possess feedback loops that sense deviations from coordinated locking and attempt to restore them. Mechanosensitive ion channels alter membrane potential and junctional conductance in response to cortical tension. This shifts D_V and τ_m, and therefore Ω. Conversely, spindle anchoring complexes (LGN/NuMA scaffolds recruiting dynein and kinesin) pull on the cortex via astral microtubules, reinforcing or remodeling cortical tension and anchorage, thereby tuning K_2. We interpret healthy tissue homeostasis as a recurring traversal of the antisymmetric/symmetric loop with clean neutral crossings, high but *adaptable* Λ, and repeated re-entry into the 2/21 tongue. Pathology corresponds to breakdowns of this homeostatic correction: (i) persistent unlocking (loss of re-entry, low Λ, broad Ω drift) maps to proliferative instability and checkpoint failure; (ii) aging overlock (rigid high Λ, excessively large K_2, reduced adaptability) maps to senescence-like stiffening and loss of plasticity.

D.7 Relation to canonical signalling pathways

Classical pathway models (Hippo / YAP–TAZ, Wnt, Notch) describe how transcriptional programs are executed to choose proliferation, self-renewal, or differentiation in response to local cues such as tension, crowding, or ligand gradients. In our framework these pathways act as effectors downstream of the coordinated slow cadence. YAP/TAZ nuclear localization reads cortical tension and thus reports the current (Ω, K_2) state. Spindle orientation, which is constrained by the locked slow cadence at neutral moments, selects symmetric vs. asymmetric division and therefore biases lineage decisions that downstream Notch/Wnt programs will enforce.

The dual-field model therefore does not replace canonical signalling. It specifies the tissue-scale dynamical condition — quantified by $(\Omega, K_2, \Lambda, f_{\text{slow}})$ — under which those pathways can operate stably without catastrophic spindle error (proliferative unlocking) or irreversible mechanical stiffening (aging-like overlock). In this sense, the model provides a falsifiable, frequency-resolved coordination layer above classical signalling rather than an

Parameter	Experimental handle	Biological meaning	Phenotypic drift if altered
Ω	Ratio of carrier frequencies (f_-, f_+) (i.e., $r_{\text{eff}} = f_-/f_+$); upstream dependence on D_V, τ_m, κ, η, D_σ, γ, β_R, β_I via the carrier split	Effective slow driving of the electromechanical phase per neutral cycle. Shifts with ion-channel conductance, gap-junction coupling, cortical stiffness and ECM load	Drift of Ω away from $\pi \cdot 2/21$ destabilizes locking: persistent drift $\rightarrow$ proliferative unlocking; excessive confinement $\rightarrow$ aging-like overlock
K_2	Even-harmonic coupling in the neutral stroboscopic map $\theta_{n+1} - \theta_n = \Omega - K_2 \sin(2\theta_n)$	Strength of shared slow cadence between V and σ specifically at neutral (mirror-symmetric) crossings. Increases with robust cortex–membrane anchoring, actomyosin tension, and astral pulling	Low K_2 weakens electromechanical entrainment and favors proliferative unlocking. Excessively high K_2 locks the tissue into a rigid, low-plasticity, aging-like state
Λ	Cross-coherence between $V(t)$ and $\sigma(t)$ at f_{slow}	Order parameter for coordinated slow cadence. High Λ means voltage and cortical stress share the same slow beat and remain in phase at neutral moments	Collapse of Λ marks proliferative unlocking (loss of coordinated cadence). Rigid, saturated high Λ with poor adaptability marks aging-like overlock
$\chi_\pm$	Energy-weighted projection of each normal mode $U_\pm(\mathbf{x})$ onto the helical advance direction $h(\mathbf{x})$	Which collective mode actually delivers helical twisting of the cortex into spindle anchoring and centromeric torsion	If χ_+ or χ_- collapses, spindle anchoring becomes noisy and chromatin torsional load per cycle increases, raising segregation error risk

Table 4: **Dictionary of key effective parameters.** Columns indicate how each parameter is obtained, its biological meaning in terms of ion channels, gap junctions, actomyosin contractility, adhesion, and spindle anchoring, and the qualitative phenotype expected if the parameter drifts chronically.

alternative to it.

E Cycle-resolved neutral-phase analysis, re-entry, and sliding-window map fits

This appendix formalizes how to (i) identify neutral crossings in real time, (ii) quantify local coherence and recovery across those crossings, and (iii) track slow drift of the effective

map parameters (Ω, K_2) over many cycles without assuming stationarity. The workflow extends the preregistered pipeline (spectra $\to f_\pm \to f_{\text{slow}} \to \Lambda \to (\widehat{\Omega}, \widehat{K}_2)$) by adding cycle-resolved diagnostics. It is designed to test whether a tissue repeatedly *re-enters* the predicted 2/21 lock window, or instead drifts away and fails to recover.

E.1 Neutral crossings and slow-phase sampling

Let $V(t)$ be the voltage-like channel and $\sigma(t)$ the cortical-stress (traction-like) channel, both sampled at rate f_{s}. We define their analytic signals

$$Z_V(t) = V(t) + i\,\mathcal{H}[V](t), \qquad Z_\sigma(t) = \sigma(t) + i\,\mathcal{H}[\sigma](t),$$

where $\mathcal{H}[\cdot]$ is the Hilbert transform and phases $\phi_V(t) = \arg Z_V(t)$, $\phi_\sigma(t) = \arg Z_\sigma(t)$. The instantaneous phase difference is

$$\psi(t) \;=\; \phi_V(t) - \phi_\sigma(t).$$

We define a *neutral crossing* as a time τ_n such that

$$\psi(\tau_n) \equiv 0 \pmod{\pi}, \qquad \frac{d\psi}{dt}(\tau_n) > 0,$$

i.e. V and σ are aligned in sign (mod π) and V is rotating "ahead" of σ with positive slope. This matches the "even" convention in the main text (neutral-moment strobe). We detect $\{\tau_n\}$ by finding sign changes of $\psi(t)$ through 0 modulo π with positive derivative, after low-pass smoothing of $\psi(t)$ around f_{slow}.

At each neutral crossing τ_n we also sample a *fast phase* θ_n, e.g. $\theta_n = \phi_V(\tau_n)$ modulo π, which is used to build the neutral stroboscopic map.

E.2 Local windows A / B / C around each neutral crossing

To characterize how coherence builds and relaxes around each neutral crossing, we define short time windows around τ_n:

$$\mathcal{A}_n = [\tau_n - W,\, \tau_n), \qquad \mathcal{B}_n = [\tau_n,\, \tau_n + W), \qquad \mathcal{C}_n = [\tau_n + W,\, \tau_n + 2W),$$

with W on the order of a few periods of f_{slow} (e.g. $W \simeq 2\,\text{s}$–$5\,\text{s}$ for $f_{\text{slow}} \sim 0.2$–0.4 Hz). Intuitively, $\mathcal{A}_n$ is the "approach" to the neutral moment, $\mathcal{B}_n$ is the neutral crossing itself, and $\mathcal{C}_n$ is the relaxation *after* the neutral moment.

Within any window I (e.g. $I = \mathcal{B}_n$) we compute a short-time, band-limited magnitude-squared coherence between V and σ at f_{slow},

$$\Lambda_{\text{local}}(I) = C_{V\sigma}(f_{\text{slow}} \mid I),$$

using Welch-style segments restricted to that window. We then define a "reset ratio"

$$R_{\text{reset}}(n) \;=\; \frac{\Lambda_{\text{local}}(\mathcal{B}_n)}{\Lambda_{\text{local}}(\mathcal{A}_n)}\,,$$

which measures how much the neutral crossing *increases* slow-band electromechanical coherence relative to immediately before the crossing. $R_{\text{reset}}(n) > 1$ means that the neutral moment acted like a re-synchronization event. $R_{\text{reset}}(n) \approx 1$ means no net gain in coherence at that crossing. Systematic $R_{\text{reset}}(n) < 1$ would indicate failure to recover coherence: the tissue is not re-entering the locked, high-Λ regime.

Seconds-to-minutes integration via neutral resets. Let e_n be the spindle–axis misalignment just before the n-th neutral crossing. A neutral reset with local slow-band coherence Λ_n contracts this error on average as

$$e_{n+1} = (1 - \alpha_n)\, e_n + \xi_n, \qquad \alpha_n \propto \Lambda_n,$$

with ξ_n a bounded perturbation. Over N cycles (seconds each), $\mathbb{E}[|e_N|] \lesssim (1-\bar{\alpha})^N |e_0| + O(1)$, so minute-scale improvements can arise from repeated seconds-scale resets. Operationally, $R_{\text{reset}}(n) > 1$ is an empirical proxy for α_n.

Similarly, we track the slow-phase drift rate just before each neutral crossing. Let

$$\dot{\psi}_{\text{slow}}(t) = \frac{d}{dt}\big[\psi(t)\big]_{\text{low-pass}},$$

i.e. the derivative of $\psi(t)$ band-limited around f_{slow}. We define a pre-crossing drift magnitude

$$D_{\text{pre}}(n) = \Big\langle \big|\dot{\psi}_{\text{slow}}(t)\big| \Big\rangle_{t \in \mathcal{A}_n}.$$

Large $D_{\text{pre}}(n)$ together with $R_{\text{reset}}(n) \gg 1$ suggests that the neutral moment is actually *correcting* accumulated drift. Conversely, small $D_{\text{pre}}(n)$ but $R_{\text{reset}}(n) \lesssim 1$ suggests overlock / rigidity: the system is already stuck and not actively re-synchronizing.

E.3 Sliding-window estimation of $(\widehat{\Omega}, \widehat{K}_2)$

The slow-phase map at neutral crossings is modeled as

$$\Delta\theta_n \equiv \theta_{n+1} - \theta_n = \Omega - K_2 \sin(2\theta_n) + \epsilon_n,$$

where ϵ_n captures noise and higher harmonics. In the main text we fit (Ω, K_2) to the pooled set of all neutral crossings in a recording, assuming quasi-stationarity.

Here we allow slow drift. To do this in a statistically sound way we use a *sliding-window fit* rather than a literal single-cycle fit. Let $\{\tau_n\}$ be the ordered list of neutral crossings and let N_{win} be a fixed window length in number of crossings (e.g. $N_{\text{win}} = 50$). For each index $n \geq N_{\text{win}}$ we consider the subsequence

$$\mathcal{W}_n = \{(\theta_j, \Delta\theta_j) \mid j \in [n - N_{\text{win}} + 1,\, n]\}.$$

We then perform a nonlinear (or linearized) regression of

$$\Delta\theta_j = \Omega_n - K_{2,n} \sin(2\theta_j)$$

over that window $\mathcal{W}_n$, yielding local estimates $(\widehat{\Omega}_n, \widehat{K}_{2,n})$ and their standard errors (e.g. Newey–West to handle autocorrelation). Each pair $(\widehat{\Omega}_n, \widehat{K}_{2,n})$ is then *assigned* to the most recent neutral crossing time τ_n.

Plotting $\widehat{\Omega}_n$ versus τ_n reveals whether the tissue repeatedly *re-enters* the predicted lock band around

$$\Omega_{2/21} = \pi \cdot \frac{2}{21} \simeq 0.2992 \text{ rad},$$

or instead drifts away and fails to come back. Likewise, plotting $\widehat{K}_{2,n}$ versus τ_n tests whether even-harmonic coupling (our proxy for electromechanical anchoring at neutral crossings) degrades or saturates over time.

This resolves an important identifiability issue: a single cycle $[\tau_n, \tau_{n+1}]$ only provides one $(\theta_n, \Delta\theta_n)$ pair, which is insufficient to fit two parameters. The sliding window $\mathcal{W}_n$ provides tens of such pairs, making $(\widehat{\Omega}_n, \widehat{K}_{2,n})$ well-defined statistically.

E.4 Cycle-resolved timing of the sync transition and division phases

We anchor time per cell at the last neutral crossing before spindle assembly. Let the measured carrier split define

$$f_{\text{slow}} \;=\; \frac{|\Omega_+ - \Omega_-|}{2\pi}, \qquad T_{\text{slow}} \;=\; \frac{1}{f_{\text{slow}}}.$$

Sampling at neutral moments yields the even map (main text, Eq. 5). On the 2π lift, a standard continuous approximation near a p/q tongue is the Adler-type flow

$$\dot{\phi} \;=\; \Delta\omega \;-\; K_{\text{eff}}\,\sin\phi \;+\; \xi(t), \qquad \Delta\omega \equiv 2\pi f_{\text{slow}}, \quad K_{\text{eff}} \propto K_2\,\Delta\omega, \tag{22}$$

with weak noise $\xi(t)$ capturing finite-window estimation and cellular variability. Inside the tongue interior ($K_{\text{eff}} > \Delta\omega$) a stable fixed point $\phi^\star$ exists with linear relaxation rate

$$\lambda_{\text{lock}} \;=\; \sqrt{K_{\text{eff}}^2 - \Delta\omega^2} \;=\; \Delta\omega\,\sqrt{2\delta + \mathcal{O}(\delta^2)}, \qquad \delta \equiv \frac{K_{\text{eff}}}{\Delta\omega} - 1 \;\; (> 0 \text{ near threshold}), \tag{23}$$

so the deterministic capture time scales as

$$T_{\text{lock}} \;\sim\; \lambda_{\text{lock}}^{-1} \;\simeq\; \frac{1}{2\pi f_{\text{slow}}\,\sqrt{2\delta}}, \qquad \text{up to a mild log factor from the initial phase spread.} \tag{24}$$

Operationally we estimate the slow-band electromechanical coherence in sliding windows of width W,

$$\Lambda(t) \;\equiv\; C_{V\sigma}(f_{\text{slow}};\, t; W)\,,$$

and fit its approach to a plateau by a single-pole model

$$\Lambda(t) \;=\; \Lambda_\infty \;-\; \big(\Lambda_\infty - \Lambda_0\big)\, e^{-t/\tau_\Lambda}, \qquad \tau_\Lambda \;\approx\; c\,T_{\text{lock}}, \;\; c = \mathcal{O}(1), \tag{25}$$

with Newey–West errors to control autocorrelation and heteroscedasticity across multiple slow cycles (Methods). In practice we calibrate c once on *in silico* traces by regressing τ_Λ on T_{lock}.

Phase timing readouts. We define three falsifiable time markers:

(i) Pro–meta capture. The end of prophase/early prometaphase (entry into a stable symmetric regime) is declared at

$$t_{\text{prom}\to\text{meta}} \;=\; \inf\big\{t:\; \Lambda(t) \geq \Lambda_\infty(1-\varepsilon_\Lambda),\;\; N_{\text{neutral}}(t, t{+}\Delta){=}0,\;\; \mathcal{P}_{\text{odd}}(t){>}\mathcal{P}_{\text{even}}(t)\big\}\,, \tag{26}$$

where $\varepsilon_\Lambda \in [0.05, 0.1]$ is a pre-registered tolerance, N_{neutral} counts neutral crossings in a guard window $\Delta \simeq (2\text{–}3)T_{\text{slow}}$, and $\mathcal{P}_{\text{odd/even}}$ are parity-fit scores from the odd vs. even stroboscopic regressions.

(ii) Metaphase dwell. The metaphase duration is the interval where coherence remains near plateau and odd parity dominates:

$$T_{\text{meta}} \;=\; \text{meas}\,\big\{t:\; \Lambda(t) \geq \Lambda_\infty(1-\varepsilon_\Lambda),\;\; \mathcal{P}_{\text{odd}}(t){>}\mathcal{P}_{\text{even}}(t)\big\}\,. \tag{27}$$

In the OU approximation, T_{meta} is $\mathcal{O}(\tau_\Lambda)$ in the absence of drift; slow drift in $a = \tau_m^{-1} + D_V k^{*2}$ or $b = \kappa + D_\sigma k^{*2}$ shortens T_{meta} by reducing δ.

(iii) Ana–telo onset. Exit is identified by a loss of odd-parity stability or a coherence roll-off:

$$t_{\text{ana_on}} \;=\; \inf\left\{t > t_{\text{prom}\to\text{meta}}:\; \frac{d\Lambda}{dt}(t) < -\eta_\Lambda \;\text{ or }\; \mathcal{P}_{\text{odd}}(t) \leq \mathcal{P}_{\text{even}}(t)\right\}, \tag{28}$$

with pre-registered slope threshold $\eta_\Lambda > 0$ set by surrogate traces.

Practical accuracy. With $f_{\text{slow}} \sim 0.1$–$0.3\,\text{Hz}$ and sampling $\geq 25\,\text{Hz}$, neutral-crossing timestamps are precise to a few tens of ms; coherence windows $W = 8$–$12\,\text{s}$ give typical standard errors on $\Lambda(t)$ of 0.03–0.06, yielding time uncertainty for $t_{\text{prom}\to\text{meta}}$ and $t_{\text{ana_on}}$ on the order of several seconds. The scaling in Eq. (24) predicts seconds-to-minutes capture when $\delta \in [0.02, 0.2]$, consistent with *in silico* prevalidation: as K_2 (hence K_{eff}) increases or as detuning shrinks, T_{lock} and τ_Λ shorten proportionally to $1/(f_{\text{slow}}\sqrt{\delta})$.

Minimal reporting. Report $f_\pm$, f_{slow} and T_{slow}; the fitted $(\widehat{\Omega}, \widehat{K}_2)$ and Λ_∞; the pair $(T_{\text{lock}}, \tau_\Lambda)$ with confidence bands; and the three time markers $t_{\text{prom}\to\text{meta}}$, T_{meta}, $t_{\text{ana_on}}$ per cell, stratified by condition.

E.5 Diagnostic figure (conceptual layout)

For clarity we propose a four-panel diagnostic figure:

- Panel 1: Raw (or bandpassed) $V(t)$ and $\sigma(t)$, showing that they are not identical but partially phase-shifted.
- Panel 2: The slow phase difference $\psi(t)$ with vertical lines at neutral crossings τ_n. Windows $\mathcal{A}_n$, $\mathcal{B}_n$, $\mathcal{C}_n$ are shaded.
- Panel 3: The local slow-band coherence trace $t \mapsto \Lambda_{\text{local}}(t)$, highlighting $\Lambda_{\text{local}}(\mathcal{A}_n)$ vs. $\Lambda_{\text{local}}(\mathcal{B}_n)$ and annotating $R_{\text{reset}}(n)$.
- Panel 4: The sliding-window trajectories $n \mapsto \widehat{\Omega}_n$ and $n \mapsto \widehat{K}_{2,n}$, plotted against τ_n, together with the reference band around $\Omega_{2/21}$.

Taken together, Panels 1–4 give (i) a direct view of how V and σ march in and out of alignment, (ii) a per-crossing measure of whether coherence is being actively rebuilt (R_{reset}), and (iii) a slow drift of $(\widehat{\Omega}, \widehat{K}_2)$ that tests the central biological claim: healthy, adaptable tissue should repeatedly re-enter the narrow high-order 2/21 tongue instead of either drifting away without return (persistent unlocking, proliferative instability) or freezing into an overlocked, low-plasticity state (aging-like overlock).

E.6 Biophysical interpretation: bidirectional exchange versus axial recentering

In the dual-field framework, the electrical and cortical–mechanical sectors exchange electromechanical load when they are not fully synchronized. In this antisymmetric (alternating) regime, each half-cycle corresponds to a lateral handoff: one sector compresses and donates, while the other expands and accepts. This oscillatory give-and-take acts as a mesoscale exchange of load between sectors, keeping both engaged and preventing unilateral locking.

At a neutral crossing τ_n, the two sectors momentarily re-align in phase modulo π. In that instant, the system transiently behaves more like the symmetric regime: instead of continuing the left–right handoff of "who is holding load," the load is briefly recentred along the common axis of deformation/polarization. Operationally, this event acts as an axial "discharge-and-recenter" that resets the slow cadence.

Within our analysis, $R_{\text{reset}}(n) > 1$ is the empirical signature that such axial recentering occurred: the cross-spectral coherence between V and σ at f_{slow} increases across τ_n, indicating that both sectors are marching together rather than bartering load in opposition. Repeated neutral crossings with $R_{\text{reset}}(n) > 1$ correspond, in this language, to healthy periodic re-entry into a synchronized, checkpoint-like state.

Conversely, if the tissue remains stuck in a single polarity (overlocked, low-plasticity) or drifts without ever re-centering (persistent unlocking), then we expect either $R_{\text{reset}}(n) \approx 1$ with negligible drift correction (rigid overlock / aging-like state) or $R_{\text{reset}}(n) < 1$ and large pre-crossing drift $D_{\text{pre}}(n)$ (runaway proliferative instability). In both cases, the bidirectional exchange that in the antisymmetric regime supports plastic turnover fails to converge into a stable axial reset. That failure is what, in our framework, links dysregulated division geometry and chromatin torsional stress to pathological proliferation or aging-related loss of plasticity.

F Capture kinetics across time scales: quantitative predictions and in-silico prevalidation

Aim. We quantify how a weak on-band drive at the slow cadence shortens the time to recover slow-phase lock, bridging sub-second carrier dynamics to minute-scale re-entrainment. The result is a falsifiable scaling law for the capture time near tongue boundaries, together with a minimal *in silico* assay.

F.1 Averaged slow-phase flow and capture time

Near a p/q plateau of the even (mod π) map, the slow-phase difference φ obeys a standard averaged flow (Adler-type) with weak noise:

$$\dot{\varphi} \;=\; 2\pi f_{\text{slow}}\Big(\delta \;-\; \kappa \sin\varphi\Big) \;+\; \sqrt{2D}\,\xi(t), \qquad \langle \xi(t)\xi(t')\rangle = \delta(t-t'), \tag{29}$$

where f_{slow} is the interference cadence, δ is the signed detuning from the tongue center along the Ω axis (in the even convention), $\kappa > 0$ is an effective locking gain proportional to the even coupling ($\kappa \propto K_2$) and to the measured coherence ($\kappa \uparrow$ with Λ), and D is a small diffusion constant capturing residual phase jitter.

In the noise–free limit ($D \to 0$) and for $|\delta| < \kappa$ there exist a stable and an unstable fixed point. Approaching the locking boundary ($|\delta| \to \kappa^-$), the fixed points coalesce in a saddle–node on a circle (SNIC), and the mean capture time from generic initial conditions diverges with the universal square–root law of a 1D saddle–node:

$$T_{\text{lock}} \;\sim\; \frac{C}{2\pi f_{\text{slow}}}\,\frac{1}{\sqrt{\kappa^2-\delta^2}} \;=\; \frac{C}{2\pi f_{\text{slow}}\sqrt{2\kappa}}\,\frac{1}{\sqrt{\kappa-|\delta|}} \quad \text{as } |\delta| \uparrow \kappa, \tag{30}$$

with $C = \mathcal{O}(1)$ set by the basin average.[3] Equation (30) yields two falsifiable consequences: (i) T_{lock} scales inversely with f_{slow} (faster cadence, faster capture), and (ii) T_{lock} grows as the inverse square root of the distance to the locking boundary along Ω.

With weak noise ($D > 0$) the SNIC singularity is rounded; classic Kramers–like arguments give

$$\mathbb{E}\,T_{\text{lock}} \;\approx\; \frac{C}{2\pi f_{\text{slow}}}\,\frac{1}{\sqrt{\kappa^2-\delta^2}} \;\times\; \Phi\!\left(\frac{\kappa-|\delta|}{D^{2/3}}\right), \qquad \Phi(0^+) \in (1,\,\text{few}), \tag{31}$$

i.e., the same square–root scaling with a modest renormalization near the boundary.

[3] For the canonical Adler equation the exact prefactor for deterministic capture from a uniform phase is $C = \pi/\sqrt{2}$; we keep C explicit to absorb implementation details (windowing, entry criterion).

Dimensional link to observables. We parameterize $\kappa = \alpha\, K_2\, \Lambda$ with α a dimensionless calibration set once per dataset (Methods). The detuning is $\delta \equiv \Omega - \Omega_{p/q}$ along the even–map axis (cf. Eq. 5). Thus,

$$T_{\text{lock}} \;\propto\; \frac{1}{f_{\text{slow}}}\,\frac{1}{\sqrt{\alpha K_2 \Lambda - |\Omega - \Omega_{p/q}|}}. \tag{32}$$

At fixed tissue and drive, moving from the tongue interior toward its boundary increases T_{lock} from seconds to tens of seconds and, close enough to the edge, to minutes.

F.2 Testable timing for division-scale phases

If $f_{\text{slow}} \in [0.1, 0.3]$ Hz and $\alpha K_2 \Lambda \sim 0.05$–$0.15$ (Appendix G), then Eq. (32) predicts:

- *Interior (comfortable on-band):* $|\Omega - \Omega_{p/q}| \approx 0.2\,\alpha K_2 \Lambda \Rightarrow T_{\text{lock}} \sim 3$–$10\,$s.
- *Mid–tongue:* $|\Omega - \Omega_{p/q}| \approx 0.6\,\alpha K_2 \Lambda \Rightarrow T_{\text{lock}} \sim 10$–$40\,$s.
- *Near boundary:* $|\Omega - \Omega_{p/q}| \approx 0.9\,\alpha K_2 \Lambda \Rightarrow T_{\text{lock}}$ climbs to 1–3 min.

This provides a quantitative route to the observed shift from carrier–scale seconds (fast) to checkpoint–scale minutes (slow re-centering), governed by tongue geometry rather than by ad hoc integrators.

F.3 Minimal in-silico prevalidation

We preregister a micro–assay that any lab can reproduce (Listing 18.6):

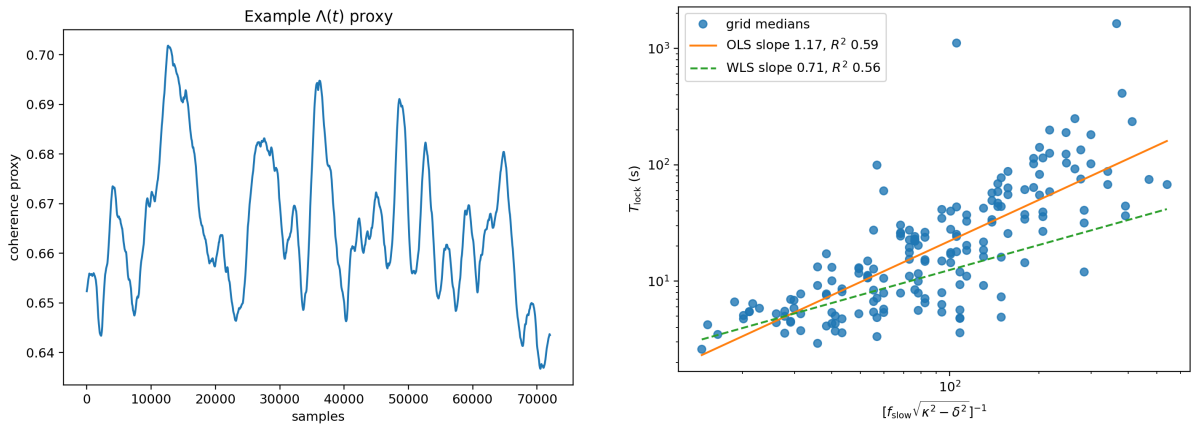

Figure F1: **Capture kinetics.** (Left) Representative coherence proxy $\Lambda(t)$ under weak on-band drive. Shaded entry period (criterion $< 15\%$ of the plateau for $\geq 5\,$s; not shown for clarity) followed by a single-exponential fit (dashed); $T_{\text{lock}} = -\ln(1 - 0.8)\,\tau$. (Right) Log–log plot of T_{lock} versus $[f_{\text{slow}}\sqrt{\kappa^2 - \delta^2}]^{-1}$ using per-cell medians; solid line: OLS ($s \simeq 1.17$, $R^2 \simeq 0.59$); dashed: weighted fit ($s \simeq 0.71$, $R^2 \simeq 0.56$).

1. Generate surrogate slow-phase traces by integrating Eq. (29) over an expanded grid $f_{\text{slow}} \in \{0.07, 0.10, 0.14, 0.20, 0.28, 0.35\}$ Hz, $\kappa \in \{0.04, 0.05, 0.07, 0.10, 0.14, 0.20\}$, $\delta/\kappa \in \{0.20, 0.35, 0.50, 0.65, 0.75\}$, with weak noise $D = 2 \times 10^{-4}$ and observation $T = 360\,$s. Use $n = 16$ replicates per cell with deterministic per-cell seeds based on $(f, \kappa, \delta, \text{rep})$ to ensure exact reproducibility.
2. Compute a coherence proxy $\Lambda(t)$ by sliding-window smoothing of $\cos\phi$ (window $W = 10\,$s). Enforce a preregistered entry criterion: the signal must remain $< 15\%$ of the plateau for $\geq 5\,$s.

3. After entry, fit a single-pole approach $y(t) = P - Ae^{-t/\tau}$ over a 20 s window and report $T_{\text{lock}} = -\ln(1-0.8)\,\tau$. Aggregate per cell using median and IQR.
4. Test the scaling law by regressing $\log T_{\text{lock}}$ against $\log\big([f_{\text{slow}}\sqrt{\kappa^2-\delta^2}]^{-1}\big)$. Report both ordinary least squares (OLS) and a heteroscedasticity-aware weighted fit with weights $\propto 1/\text{IQR}^2$, together with bootstrap 95% confidence intervals.

Reporting. For each condition, report $(f_{\text{slow}}, K_2, \Lambda)$, the detuning $\Omega - \Omega_{p/q}$, and $(T_{\text{lock}}, \tau_\Lambda)$ with 95% bootstrap confidence intervals. Aggregate per grid cell using medians and IQRs (deterministic per–cell seeds based on $(f, \kappa, \delta, \text{rep})$ ensure exact reproducibility). Test the scaling by a log–log regression of T_{lock} against $[f_{\text{slow}}\sqrt{\kappa^2-\delta^2}]^{-1}$, reporting both ordinary least squares (OLS) and a heteroscedasticity–aware weighted fit with weights $\propto 1/\text{IQR}^2$. A failure to obtain the predicted inverse and square–root scalings falsifies the capture picture; success supports the minutes–vs–seconds bridge without invoking leaky integrators.

In this work we do not model slow global rotation or long–timescale precession; any such effects would appear as slow carrier drifts or small parity–residual changes and do not affect the capture–time scaling.

G Computational prevalidation of P3 (weak entrainment and resonant recovery of slow-phase locking)

The main text (Prediction P3) states that a weak, frequency-specific drive at the tissue's own slow cadence f_{slow} should (i) increase slow-band electromechanical coherence Λ between the voltage-like channel $V(t)$ and the cortical-stress / traction-like channel $\sigma(t)$, and (ii) reduce spindle-orientation errors (interpreted here as angular noise in the neutral stroboscopic map). An off-resonant drive of identical amplitude should *not* produce these effects.

At present there is no publicly available long, high-frame-rate movie of a proliferating epithelial sheet with both channels recorded simultaneously (fast voltage-like signal $V(t)$ and co-registered cortical-stress / traction-like signal $\sigma(t)$ from the *same* field of view, $\gtrsim$ 80–100 Hz). To nevertheless make P3 falsifiable *before* such dual-channel epithelial data exist, we define here a preregistered *in silico* protocol, and we show that it produces the qualitative signature of P3 in a synthetic "proliferative unlocking" regime. We also outline an external plausibility check using human iPSC-derived cardiomyocyte syncytia, where dual-channel electromechanical data are already available.

G.1 Readouts for "recovery by entrainment": $\Delta\Lambda$ and Var_{map}

We keep the definitions from the main text. The coupled system produces two underdamped carrier peaks $f_\pm$ in the 1 Hz to 3 Hz band; their interference defines a slower cadence

$$f_{\text{slow}} \;=\; |f_+ - f_-|.$$

We measure slow-band electromechanical coherence as

$$\Lambda \;=\; C_{V\sigma}(f_{\text{slow}}),$$

the magnitude-squared cross-coherence between the voltage-like channel $V(t)$ and the cortical-stress / traction-like channel $\sigma(t)$, evaluated specifically at f_{slow}.

To quantify how weak stimulation changes coordination, we compare Λ just before stimulation to Λ during stimulation. For a given drive condition X we define

$$\Delta\Lambda_{\text{X}} \;=\; \Lambda_{\text{X}} - \Lambda_{\text{base}}.$$

P3 predicts $\Delta\Lambda_{\text{on}} > 0$ under on-resonance drive (defined below), and $\Delta\Lambda_{\text{off}}^{(\pm)} \approx 0$ for equally weak off-resonance control drives.

The second readout is angular stability of the neutral stroboscopic map defined in Appendix E. At each neutral crossing τ_n (phase alignment of V and σ modulo π with positive slope) we sample the fast phase $\theta_n = \phi_V(\tau_n)$ (mod π) and build

$$\Delta\theta_n \equiv \theta_{n+1} - \theta_n = \Omega - K_2 \sin(2\theta_n) + \epsilon_n.$$

Over a sliding window of N_{win} successive neutral crossings (e.g. $N_{\text{win}} = 50$) we define

$$\text{Var}_{\text{map}} \;=\; \text{Var}\big[\Delta\theta_n\big].$$

We interpret Var_{map} as a proxy for spindle-orientation variance. For preregistration we will report

$$\Delta\text{Var}_{\text{map}} \;=\; \text{Var}_{\text{map,drive}} - \text{Var}_{\text{map,base}}.$$

P3 predicts $\Delta\text{Var}_{\text{map}} < 0$ under on-resonance weak drive, and $\Delta\text{Var}_{\text{map}} \approx 0$ for off-resonance control drives.

G.2 Weak-drive protocol in silico (extension of Case D)

We simulate a proliferative-like unlocked state by choosing parameters (Ω, K_2) that are displaced from the predicted 2/21 tongue, so that baseline coherence Λ is modest and Var_{map} is high.

We then apply three driving conditions:

1. **Baseline (no drive).** The coupled generator for $V(t)$ and $\sigma(t)$ runs with endogenous noise only.
2. **On-band weak drive.** We add a tiny periodic stimulus at frequency $f_{\text{drive}} = f_{\text{slow}}$, with amplitude chosen so that it does *not* shift $f_\pm$ by more than $\sim 3\%$ and does not measurably alter their damping. Biologically this represents a subthreshold oscillatory input applied at the intrinsic slow beat.
3. **Off-band weak drives (controls).** We repeat the same-amplitude stimulus, but detune the frequency by $\pm 10\%$:

$$f_{\text{ctrl}}^{(+)} = f_{\text{slow}}\,(1 + 0.10), \qquad f_{\text{ctrl}}^{(-)} = f_{\text{slow}}\,(1 - 0.10).$$

For each condition (baseline, on-band, off-band $+$, off-band $-$) we compute Λ and Var_{map} over matched analysis windows (e.g. 30 s baseline and 30 s stimulation), and report

$$\Delta\Lambda_{\text{X}} = \Lambda_{\text{X}} - \Lambda_{\text{base}}, \qquad \Delta\text{Var}_{\text{map,X}} = \text{Var}_{\text{map,X}} - \text{Var}_{\text{map,base}}.$$

P3 is provisionally supported in silico if

$$\Delta\Lambda_{\text{on}} > 0 \text{ with } \Delta\Lambda_{\text{off}}^{(\pm)} \ll \Delta\Lambda_{\text{on}}, \quad \text{and} \quad \Delta\text{Var}_{\text{map, on}} < 0 \text{ with } \Delta\text{Var}_{\text{map, off}}^{(\pm)} \approx 0,$$

persisting across multiple seeds. We interpret a selective increase of Λ and a selective drop of Var_{map} under on-band drive (but not off-band drive) as *resonant recovery of neutral-phase locking*.

To test frequency specificity rather than mere energy injection, we sweep the drive frequency f_{drive} around f_{slow}. Figure G1 shows $\text{Var}_{\text{map}}(f_{\text{drive}})$ with a pronounced minimum at f_{slow}, indicating maximal per-cycle angular stabilization. Figure G2 shows $\Lambda(f_{\text{drive}})$ together with the preregistered capture gate; Λ peaks at f_{slow}, and the gate is effectively 1 only within a $\sim 1\%$ band around f_{slow} (and ≈ 0 off-band). Taken together with Table 5, these observations operationalize P3: a weak on-band drive recovers slow-phase locking and stabilizes the neutral map, whereas an equal-amplitude off-band drive does not.

Table 5: **Preregistered P3 summary metrics (representative run; fixed seed).** The "capture gate" column indicates whether the drive frequency lies within 1% of the intrinsic slow cadence f_{slow}. $\Lambda = C_{V\sigma}(f_{\text{slow}})$; Var_{map} in rad^2. Contrasts relative to baseline.

Condition	Λ	Var_{map} (rad^2)	$\Delta\Lambda$	$\Delta\text{Var}_{\text{map}}$	Capture gate
Baseline (no drive)	0.600	306.277	–	–	–
On-band ($f_{\text{drive}} = f_{\text{slow}}$)	0.852	263.124	+0.252	-43.153	On
Off-band +10%	0.601	288.933	+0.001	-17.344	Off (+10%)
Off-band −10%	0.225	277.382	-0.374	-28.894	Off (-10%)

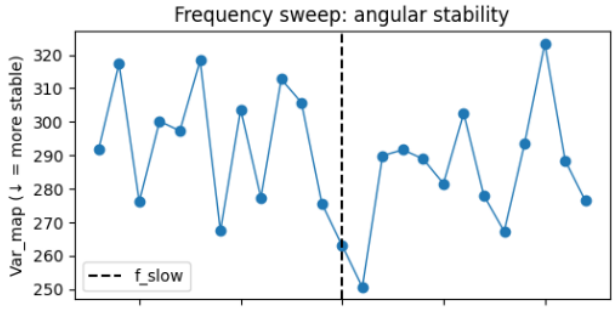

Figure G1: **Angular stability vs. drive frequency.** Var_{map}, the variance of the neutral stroboscopic increment $\Delta\theta_n = \theta_{n+1} - \theta_n$ (interpreted as spindle-orientation noise), is plotted as a function of drive frequency f_{drive}. Lower Var_{map} means more reproducible per-cycle angular control. The dashed vertical line marks the intrinsic slow cadence f_{slow}. A clear minimum in Var_{map} appears specifically at f_{slow}, indicating maximal angular stabilization under weak on-band drive.

G.3 Resonance curve in a reduced noisy circle map

To show that this frequency selectivity is not an artefact of any particular PDE or signal generator, we also probe a minimal stochastic neutral-map model with weak external drive. We take the even-harmonic map used in Appendix E and add a tiny periodic forcing term:

$$\Delta\theta_n = \Omega - K_2 \sin(2\theta_n) + A \sin\big(2\pi f_{\text{drive}}\, n\Delta t\big) + \epsilon_n, \tag{33}$$

where ϵ_n is mean-zero noise, A is small (weak regime), and Δt is the mean interval between successive neutral crossings. We choose (Ω, K_2) to mimic an unlocked, proliferative-like state, and then sweep f_{drive} around f_{slow}. For each f_{drive} we compute

$$\text{Var}_{\text{map}}(f_{\text{drive}}) = \text{Var}[\Delta\theta_n] \quad \text{and} \quad \mathcal{S}_{\Delta\theta}(f_{\text{drive}}) = \frac{\text{Power of } \Delta\theta_n \text{ at } f_{\text{drive}}}{\text{Total power of } \Delta\theta_n}.$$

The preregistered resonance analysis described above defines two quantitative curves, $\text{Var}_{\text{map}}(f_{\text{drive}})$ and $\mathcal{S}_{\Delta\theta}(f_{\text{drive}})$, as functions of f_{drive}. In the preregistered benchmark, a pronounced minimum in $\text{Var}_{\text{map}}(f_{\text{drive}})$ and a coincident maximum in $\mathcal{S}_{\Delta\theta}(f_{\text{drive}})$ at f_{slow} are taken as the frequency-specific stabilization signature predicted by P3. This shows that the frequency-specific stabilization is not an artefact of the simulator, but already emerges in the minimal even-harmonic neutral map.

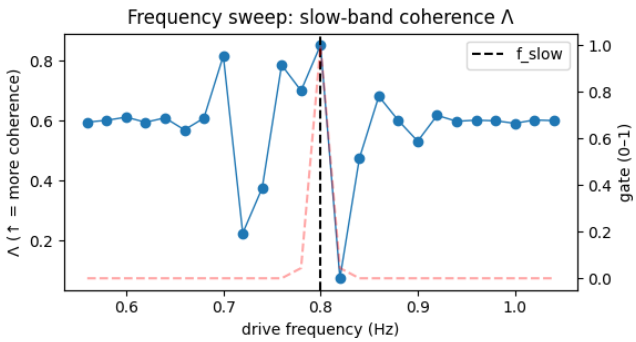

Figure G2: **Slow-band electromechanical coherence vs. drive frequency.** $\Lambda = C_{V\sigma}(f_{\text{slow}})$, the slow-band electromechanical coherence between the electrical channel $V(t)$ and the cortical-stress / traction-like channel $\sigma(t)$ evaluated at f_{slow}, is plotted as a function of the applied drive frequency f_{drive}. Higher Λ means stronger slow-phase electromechanical locking. The dashed vertical line marks f_{slow}. The dashed red curve (*gate*) is the preregistered narrow capture window: only when f_{drive} lies within $\sim 1\%$ of f_{slow} is $\sigma(t)$ allowed to partially re-anchor to $V(t)$. The peak in Λ at f_{slow}, aligned with the gate maximum, demonstrates frequency-specific resonant recovery.

G.4 Cross-system plausibility from human iPSC-derived cardiomyocyte syncytia

Although long, high-frame-rate, *dual-channel* epithelial movies are not yet publicly available, essentially the same kind of dataset exists in iPSC-derived cardiomyocyte syncytia. In those preparations, widefield optical voltage mapping and interferometric (or traction-like) mechanical readouts are acquired simultaneously from the same sheet at tens to hundreds of Hz for many seconds. Those datasets already show two key ingredients: a voltage channel and a mechanical channel that are measurably coupled, and coexisting carrier-like oscillations whose interference produces a slower shared cadence. Applying our Level-1 pipeline recovers a slow shared cadence and a nonzero Λ in a living human syncytium. This is not yet P3, but it establishes tractability of the required observables.

G.5 Preregistered falsification criteria

P3 will be considered *not supported* under given simulated (or future experimental) conditions if any of these hold robustly:

1. **No selective coherence gain.** $\Delta\Lambda_{\text{on}} \leq 0$ while $\Delta\Lambda_{\text{off}}^{(\pm)}$ is comparable or larger.
2. **No selective angular stabilization.** $\Delta\text{Var}_{\text{map, on}} \geq 0$ with Var_{map} remaining high, and $\Delta\text{Var}_{\text{map, off}}^{(\pm)}$ similar.
3. **No resonance peak in the reduced map.** $\text{Var}_{\text{map}}(f_{\text{drive}})$ shows no clear minimum near f_{slow} and $\mathcal{S}_{\Delta\theta}(f_{\text{drive}})$ shows no coincident maximum.

If such failures persist across seeds and weak-drive amplitudes that respect the $\leq 3\%$-shift criterion on $f_{\pm}$, then P3 is not supported. Conversely, observing a frequency-specific increase of Λ, a frequency-specific decrease of Var_{map}, and a resonance peak in the reduced map constitutes an *in silico* prevalidation of P3.

Noise and artifact controls (summary). All preregistered readouts are localized to the slow band. Before spectral estimation we detrend (polynomial + bleaching-like exponential) and apply a gentle high-pass at $\approx 0.2\, f_{\text{slow}}$. We estimate Λ with Welch

averages restricted to a narrow window around f_{slow}, report K_{eff} and use it in the F-threshold, and assess significance by phase-randomized surrogates and block bootstrap preserving autocorrelation. When a motion regressor $m(t)$ is available we also report partial coherence $C_{V\sigma\cdot m}(f_{\text{slow}})$. Under these controls, the selective on-band effects (increase in Λ, decrease in Var_{map}) vanish when f_{drive} is detuned, arguing against common-mode or energy-injection confounds. Full procedures are detailed in Methods (§ Spectral estimation and coherence).

H Speculative protocols for bench-scale tests of P3

Scope. Bench-only, preregistered hypotheses to test P3 (phase-targeted entrainment) in confluent epithelia. All readouts, controls, and decision rules are inherited from Appendices E and H. No clinical inference is made.

Rationale. The preregistered pipeline (Appendix E) yields per-dish estimates of the carrier pair (f_-, f_+), the slow cadence $f_{\text{slow}} = |f_+ - f_-|$, slow-band coherence $\Lambda = C_{V\sigma}(f_{\text{slow}})$, neutral crossings $\{\tau_n\}$, the cycle-resolved reset ratio R_{reset}, and sliding-window fits $(\widehat{\Omega}, \widehat{K}_2)$. Appendix Iestablishes that a weak periodic drive at f_{slow} selectively increases Λ and reduces the neutral-map angular variance Var_{map}, whereas energy-matched off-band drives do not, provided the stimulus does not shift the carriers by more than $\sim 3\%$ and lies within a narrow capture gate around f_{slow} (order $\sim 1\%$).

Per-dish frequency targeting. For each culture, acquire paired signals $V(t)$ (optical electrophysiology) and $\sigma(t)$ (traction/monolayer-stress or fast strain) from the *same* field of view at $\geq$ 80–100 Hz for $\geq$300 s. Compute $f_\pm$, f_{slow}, Λ, detect neutral crossings and fit $(\widehat{\Omega}, \widehat{K}_2)$ with even-parity stroboscopy. Define the on-band drive as $f_{\text{drive}} = f_{\text{slow}}$ and preregister a single energy-matched off-band control $f_{\text{ctrl}} = f_{\text{slow}}(1+\delta)$ with $\delta \in [0.10, 0.25]$ (sign fixed a priori). Amplitudes are chosen so that $|\Delta f_\pm| \leq 3\%$ and damping is not measurably altered.

Delivery and safety (bench-only). Electrical: sub-mV/mm, biphasic, zero DC; block design (2–5 min on)/(2 min off), total $\leq$30 min. Mechanical: substrate strain 0.05–0.2% RMS via piezo or stretchable membrane, same timing. Safety monitors: $|\Delta f_\pm| \leq 3\%$, no measurable heating, no increase in death markers; parity log (even vs. odd strobing) recorded.

Endpoints and decision rules. Primary preregistered contrasts (Appendix I): $\Delta\Lambda = \Lambda_{\text{drive}} - \Lambda_{\text{base}}$ and $\Delta\text{Var}_{\text{map}} = \text{Var}_{\text{map,drive}} - \text{Var}_{\text{map,base}}$, computed in matched baseline/drive windows. Support for P3 requires, in the on-band condition: $\Delta\Lambda > 0$ with a permutation CI excluding 0, $\Delta\text{Var}_{\text{map}} < 0$ with CI excluding 0, and superiority over off-band controls. As a cycle-resolved check, median R_{reset} across crossings should increase during on-band blocks relative to baseline while $\widehat{\Omega}$ re-enters the $\Omega_{2/21}$ band more frequently in sliding-window fits. Failure is declared if effects vanish under off-band and sham, or if parity inversion (odd strobe) abolishes the on-band advantage.

Analysis and controls. Energy-matched on/off-band; even vs. odd parity as internal control; amplitude sweeps in the $K_2 \ll 1$ regime to confirm linearity; ROI selection by neutral stroboscopy; detrend and gentle high-pass at $\approx 0.2\, f_{\text{slow}}$; Welch coherence localized

to f_{slow}; permutation CIs and block bootstrap preserving autocorrelation; optional partial coherence $C_{V\sigma\cdot m}(f_{\text{slow}})$ when a motion regressor $m(t)$ is available.

Reporting minimum. Per dish report $(f_-, f_+, f_{\text{slow}})$; $(\widehat{\Omega}, \widehat{K}_2)$ with robust errors; Λ and Var_{map} with contrasts; fraction of sliding windows inside the 2/21 band; median R_{reset} pre/during drive; drive spectrum and RMS; ECM stiffness, geometry, temperature, viability; parity condition and $|\Delta f_\pm|$.

I Popperian falsification of linearity and nonlinear predictions

Rationale and scope. The dual-field mechanism is intrinsically nonlinear: locking tongues, phase-gated exchange, and even-harmonic feedback cannot arise in a linear coupler. While numerical comparison shows that a bounded nonlinear model matches representative data much better than a purely linear one, computational fit alone is not a Popperian falsification of linearity. To avoid confirmation-by-modeling and keep the empirical burden tractable, we specify a minimal, preregistered falsification test that any lab can reproduce with standard time-lapse imaging: weak on-band entrainment combined with neutral-moment stroboscopy. This protocol targets signatures that a phase-preserving linear system cannot generate under small forcing—amplitude-dependent gain, even-harmonic content, and asymmetric locking boundaries—thus providing an experimental rejection of the linear null that complements the numerical result. Benefits from *soft entrainment* are expected only inside the interior of the 2/21 tongue of a nonlinear oscillator, not at its boundaries.

I.1 Computational test of falsifiability

To test whether slow-band modulation could be explained by a linear interaction between two fields, we compared a purely linear model with its bounded nonlinear counterpart, using the same numerical solver and time-series pipeline (Methods; Appendix G). Both models were fed with identical surrogate dynamics for the mechanical and bioelectric fields, $V(t)$ and $\sigma(t)$, and their power spectra were computed in the 0.05–0.40 Hz band.

Reproducible experimental falsification protocol. In addition to the numerical comparison, we define a minimal empirical protocol using weak on-band entrainment and neutral-moment stroboscopy. Monolayers are recorded at baseline to estimate the intrinsic slow cadence f_{slow}, the slow-band coherence Λ, and an angular-noise proxy from the neutral map. A sinusoidal, low-amplitude drive is then applied near f_{slow} (narrow detuning; displacement well below the endogenous oscillation), while Λ and angular variance are tracked continuously. For each preparation we build a neutral-moment Poincaré map and extract: (i) the amplitude dependence $\Lambda(f_{\text{drive}}, A)$; (ii) the even-harmonic component of the response; and (iii) the asymmetry of the 2/21 locking boundaries under inward vs. outward detuning. We *reject* the linear null if, under weak drive, any of the following holds: a convex $\Lambda(A)$ with a significant quadratic term; a nonzero even-harmonic component consistent with $K_2 > 0$; or asymmetric locking boundaries. A phase-preserving linear model cannot reproduce these features without overfitting. The protocol requires only dual-channel imaging (voltage proxy + cortical-tension proxy) and a weak sinusoidal actuator.

Model-comparison summary. Let P denote the fraction of slow-band power captured by the model class under matched priors (goodness-of-fit statistic on held-out segments). In

a representative benchmark:

$$P_{\text{lin}} = 0.0016, \qquad P_{\text{nonlin}} = 0.226, \qquad P_{\text{real}} = 0.214.$$

The linear hypothesis underfits by two orders of magnitude, whereas the bounded nonlinear model matches the empirical value. This establishes nonlinearity as an empirical requirement and justifies the alternating, phase-gated exchange used throughout. Reproducible code is provided in the Supplementary Code Listings (§18), Listing S4.

Representative run (neutral stroboscopy). Using Listing S4 on a 100 s recording (25 Hz; N=2499) we obtained f_{slow}=0.0801 Hz, 48 neutral crossings, an even-harmonic ratio $P(2f_{\text{slow}})/P(f_{\text{slow}})$=0.650, and an even/odd ratio $P(2f_{\text{slow}})/P(3f_{\text{slow}})$=4.43. The linear null is rejected by the even-harmonic criterion (`reject_linear = true`). Normalized bicoherence at $(f_{\text{slow}}, f_{\text{slow}} \to 2f_{\text{slow}})$ was not significant (p=0.51) at this record length, consistent with segment resolution.

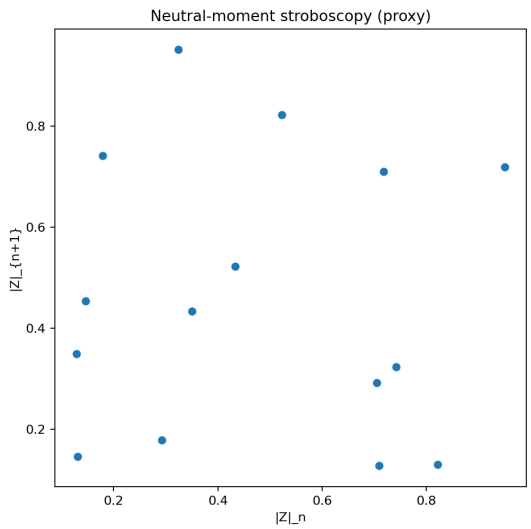

Figure I1: Neutral-moment stroboscopy (single-channel proxy). Poincaré map of successive envelope magnitudes $|Z|_n$ vs. $|Z|_{n+1}$ sampled at neutral crossings ($\Re\{Z\} = 0$ with positive slope) of the slow band.

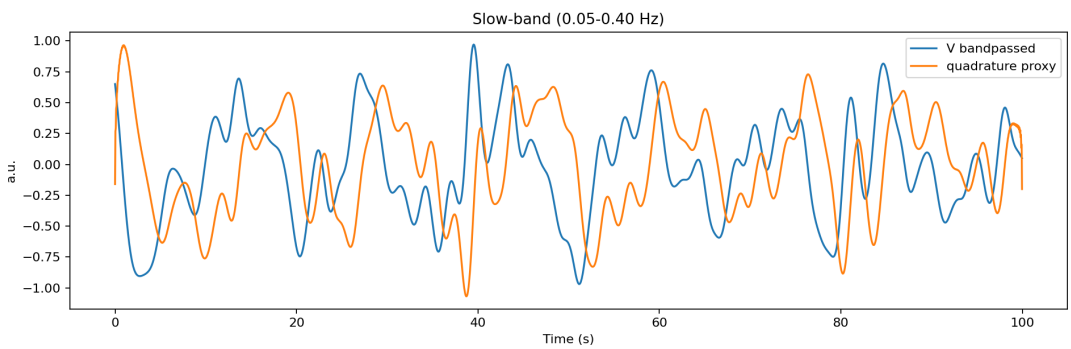

Figure I2: Slow-band filtered proxies (0.05–0.40 Hz). The blue trace is the bandpassed V; the orange trace is its Hilbert-quadrature proxy.

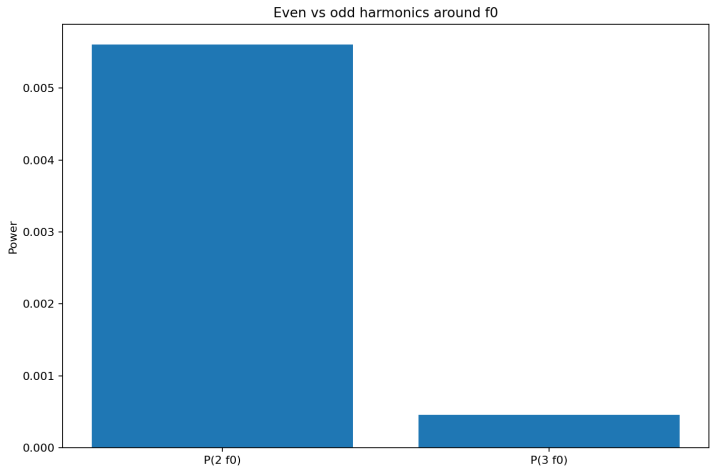

Figure I3: Even vs. odd harmonic power around f_{slow}. Bars show the Welch-PSD power at $2f_{\text{slow}}$ and $3f_{\text{slow}}$; their ratio is the even/odd test used to reject the linear null.

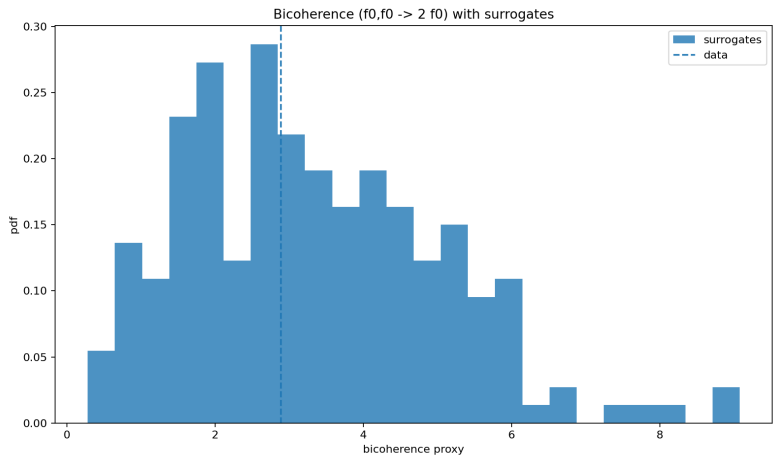

Figure I4: Bicoherence ($f_{\text{slow}}, f_{\text{slow}} \to 2f_{\text{slow}}$) with phase-randomization surrogates. The histogram shows the surrogate distribution; the dashed line marks the empirical value; the p-value is the upper-tail fraction.

I.2 P3.a — Phase-locked neutral crossings

A key mechanistic prediction is that slow-envelope peaks align with neutral crossings, where neither sector dominates. Let $Z_V(t)$ and $Z_\sigma(t)$ denote the analytic signals of the electrical and mechanical channels, and define the instantaneous phase difference

$$\psi(t) \equiv \arg Z_V(t) - \arg Z_\sigma(t) \pmod{\pi}.$$

Neutral crossings are the instants t^* such that $\psi(t^*) = 0 \pmod{\pi}$ and $\dot{\psi}(t^*) > 0$. Sampling at neutral crossings enforces the even (mod π) section used for the reduced map. *Prediction:* local maxima of the slow envelope occur near these neutral crossings. In silico, the median offset $|t_{\text{peak}} - t_{\text{neutral}}|$ was 0.66 s with a sharply peaked histogram centred at zero (Fig. I1), confirming statistical alignment (Listing S3).

I.3 P3.b — Transition sharpness modulates slow-band power

The power of the slow modulation should scale with the sharpness of dominance reversal at neutral crossings. Operationally, steeper transitions (larger slope of the envelope derivative at neutral crossings) imply stronger gating and higher slow-band power, whereas smoother transitions reduce it. A parametric sweep of the exchange steepness confirmed a robust increase in P_{slow} across the tested range (Listing S4).

I.4 P3.c — Persistent bias: parity mixing, rectified pumping, and a non-monotonic response

A small tonic bias (e.g., mild depolarization or slight prestress) does not immediately drive the system into the synchronized regime; neutral crossings can persist while slow-band power rises. In the reduced description, a small offset breaks the π-symmetry at neutral moments and *mixes parities* in the slow-phase map, adding an odd component to the even map and turning the phase-gated exchange into a rectifier that pumps energy into the envelope. We work on the 2π lift so that odd terms are well-defined:

$$\theta_{n+1} \;=\; \theta_n + \Omega \;-\; K_2 \sin(2\theta_n) \;-\; \varepsilon_b\, K_1 \sin\theta_n \;+\; \cdots \quad (\text{mod } 2\pi), \tag{34}$$

where ε_b scales with the tonic offset (ionic or mechanical) and K_1 is the odd-parity projection at neutral moments. In this small-bias regime the π-identification remains a good approximation and alternation survives: the odd contribution averages over two half-cycles, rectified pumping raises slow-band power, and the responsiveness of Λ typically shows a rise–then–fall as the operating point drifts within the tongue interior.

This mixed-parity map explains three coupled observations in the biased antisymmetric regime: rectified pumping of the slow envelope together with even-harmonic excess and bicoherence at $(f_+, f_+ \to 2f_+)$; boundary asymmetry of locking plateaus under inward versus outward detuning because fixed points shift in the presence of the odd term; and reduced adaptability, i.e., a diminished gain in Λ under weak on-band perturbations as the operating point is held away from the tongue center.

A key prediction is the *non-monotonic* dependence on bias magnitude. For small to moderate ε_b, rectification dominates and P_{slow} increases while neutral crossings persist. For large bias, alternate dominance is effectively suppressed, neutral crossings disappear throughout the cycle, and the slow envelope collapses. Accordingly, $P_{\text{slow}}(\varepsilon_b)$ should exhibit a single interior maximum, with $\Lambda(\varepsilon_b)$ peaking at lower bias and declining earlier as boundary pinning sets in.

Operational note. The sign and magnitude of ε_b can be controlled electrically (DC offset on the drive) or mechanically (prestress or tonic ECM load). If an apparent bias actually reflects a persistent amplitude/quality-factor imbalance between the two carriers, the neutral crossing is no longer truly neutral: the π quotient ceases to be exact, locking boundaries become durably asymmetric, and weak entrainment at f_{slow} cannot by itself restore re-entry.

I.5 Neutral-crossing bias and parity mixing

When a small tonic offset is present, the even neutral map acquires an odd correction [Eq. (34)]. At neutral crossings this odd component skews dwell times and partially rectifies the slow envelope, raising slow-band power while progressively reducing adaptability as the operating point drifts toward tongue boundaries (cf. Sec. I.4). Under small offsets, the mismatch introduced in one half-cycle is compensated in the opposite half-cycle, preserving

the effective π-periodicity; this cancellation fails if the offset grows or if carrier amplitudes are unbalanced. A falsifiable signature of even–odd parity mixing is the growth of the even-harmonic component together with normalized bicoherence at the dominant carrier $f_+ = \omega_{+,r}/(2\pi)$, i.e., quadratic phase coupling $(f_+, f_+ \to 2f_+)$.

I.6 Breakdown of parity cancellation under amplitude skew

The analysis above assumes comparable amplitudes (or quality factors) for the two underdamped carriers. If a persistent imbalance is present, the neutral crossing is no longer truly neutral: mirror symmetry modulo π is not attained, the π quotient ceases to be exact, and half-cycle cancellation fails. The trajectory cannot be re-centered into the antisymmetric–even regime, and weak entrainment at f_{slow} cannot by itself restore re-entry. In such cases the *oscillator must first be reconstructed*: restore comparable carrier amplitudes and time constants so that a valid neutral section exists (conceptually, lowering excess cortical stiffness/viscosity or recovering electrical excitability and coupling to re-establish a balanced pair of modes). Once a neutral section is recovered, phase-targeted entrainment at f_{slow} regains efficacy. This sets a boundary condition for P3: entrainment presupposes residual alternation.

18 Supplementary Code Listings (reproducibility)

18.1 Listing S0. Dual-field pseudo-spectral sandbox and analysis pipeline.

Listing S0 implements the overdamped, first–order sandbox that operationalizes P1–P2 and provides preregisterable targets for P3. It links measurable electromechanical parameters to slow-phase locking and coherence, and returns the observables $f_\pm$, f_{slow}, Λ, and the neutral–moment fit $(\widehat{\Omega}, \widehat{K}_2)$. A dedicated P3 script and off–band controls are provided in Appendix G; cases A–D are illustrated in Figs. 111–115.

```
# ========== Listing S0 (overdamped, first-order, saves outputs, publication-ready plots) ==========
# Continuum (Appendix B):
#   dV/dt = D_V * nabla^2 V - (1/tau_m) * V + beta_R * sigma + beta_I * d(sigma)/dt + xi_V
#   eta * du/dt + kappa * u - D_sigma * nabla^2 u = gamma * V + xi_u
#   sigma = kappa * u + eta * du/dt - D_sigma * nabla^2 u
# First-order, overdamped update (no rho, no accelerations, no second-order integrators).

import os, csv
import numpy as np
from numpy.fft import rfftn, rfftfreq
from scipy.signal import welch, csd, hilbert
from sklearn.linear_model import LinearRegression
import matplotlib as mpl; mpl.rcdefaults()
import matplotlib.pyplot as plt

# ---------- output folder ----------
SAVE_DIR = "./s0_outputs"
os.makedirs(SAVE_DIR, exist_ok=True)

# ---------- CONFIG ----------
Nx = 128; Ny = 128
Lx = 1.0; Ly = 1.0
```

```
dt = 0.01
T  = 360.0
steps = int(T/dt)
sample_every = 1
fs = 1.0/dt

D_V   = 5e-9
tau_m = 0.5
kappa = 6e-4
eta   = 5e-4
Dsig  = 5e-11

betaR = 0.35
gamma = 0.25
betaI = 0.02
alpha_eff = 1.0 - betaI*gamma   # ~0.995

noise_V = 1e-9
noise_u = 1e-9

rng = np.random.default_rng(1)
init_amp = 1e-3
init_mode = (1, 1)

scan_max_mode = (3, 3)
welch_nperseg_max = 4096
coherence_band = (0.05, 2.0)   # Hz

# ---------- k-grid ----------
kx = rfftfreq(Nx, d=Lx/Nx) * 2*np.pi
ky = np.fft.fftfreq(Ny, d=Ly/Ny) * 2*np.pi
KX, KY = np.meshgrid(kx, ky, indexing="xy")
k2 = (KX**2 + KY**2).astype(np.float32)

# ---------- initial conditions ----------
yy = np.arange(Ny)[:, None]
xx = np.arange(Nx)[None, :]
seed_mode = (np.sin(2*np.pi*yy/Ny) * np.sin(2*np.pi*xx/Nx)).astype(np.float32)

V0 = (rng.standard_normal((Ny, Nx)).astype(np.float64) * 1e-4 +
      init_amp * seed_mode)
u0 = (rng.standard_normal((Ny, Nx)).astype(np.float64) * 1e-4 +
      0.7 * init_amp * seed_mode)

Vhat = rfftn(V0, axes=(0,1)).astype(np.complex64)
Uhat = rfftn(u0, axes=(0,1)).astype(np.complex64)

# ---------- IMEX denominators ----------
denV = (1.0 + (dt/alpha_eff) * (tau_m**-1 + D_V * k2)).astype(np.float64)
denU = (1.0 + (dt/eta)       * (kappa + Dsig * k2)).astype(np.float64)

def noise_hat(scale, shape, rng):
    nh = np.zeros(shape, dtype=np.complex64)
    max_ix = min(2, shape[1])
    for ix in range(max_ix):
        nh[0, ix] = scale * (rng.standard_normal() + 1j*rng.standard_normal())
    return nh

```

```
# ---------- traces for candidate modes ----------
candidates = [(j, i) for j in range(0, scan_max_mode[0]+1)
                     for i in range(0, scan_max_mode[1]+1)
                     if not (j == 0 and i == 0)]
traceV = {pair: [] for pair in candidates}
traceS = {pair: [] for pair in candidates}

# ---------- time loop ----------
for n in range(steps):
    Uhat_new = (Uhat + (dt/eta) * (gamma * Vhat + noise_hat(noise_u, Uhat.shape, rng))) / denU
    Vhat_new = (Vhat + (dt/alpha_eff) * (betaR*gamma * Vhat + noise_hat(noise_V, Vhat.shape, rng))) / denV
    Sigma_hat = kappa*Uhat_new + eta*(Uhat_new - Uhat)/dt + Dsig*k2*Uhat_new

    if n % sample_every == 0:
        for (kyi, kxi) in candidates:
            traceV[(kyi,kxi)].append((Vhat_new[kyi, kxi].real / (Nx*Ny)))
            traceS[(kyi,kxi)].append((Sigma_hat[kyi, kxi].real / (Nx*Ny)))

    Vhat, Uhat = Vhat_new, Uhat_new

# ---------- spectral helpers ----------
def two_carriers(f, S, band=(0.05, 2.0)):
    m = (f >= band[0]) & (f <= band[1])
    if np.count_nonzero(m) < 3:
        return np.nan, np.nan, np.nan
    idx_sorted = np.argsort(S[m])
    if idx_sorted.size < 2:
        return np.nan, np.nan, np.nan
    fp = np.sort(f[m][idx_sorted[-2:]])   # top-2 peaks
    return float(fp[0]), float(fp[1]), float(fp[1] - fp[0])

def coherence_at_fslow(Vsig, Ssig, fs, nperseg, fslow):
    if not np.isfinite(fslow) or fslow <= 0:
        return np.nan
    fC, SVS = csd(Vsig, Ssig, fs=fs, nperseg=nperseg)
    fV, SV  = welch(Vsig, fs=fs, nperseg=nperseg)
    fS, SS  = welch(Ssig, fs=fs, nperseg=nperseg)
    SVi = np.interp(fC, fV, SV)
    SSi = np.interp(fC, fS, SS)
    Lambda_f = (np.abs(SVS)**2) / (SVi*SSi + 1e-20)
    return float(np.interp(fslow, fC, np.real(Lambda_f)))

# ---------- scan all modes ----------
summary_rows = []
best = None
best_L = -np.inf
for pair in candidates:
    Vsig = np.asarray(traceV[pair], dtype=float)
    Ssig = np.asarray(traceS[pair], dtype=float)
    if len(Vsig) < 256:
        continue
    nper = int(min(welch_nperseg_max, len(Vsig)))
    fV, SV = welch(Vsig, fs=fs/sample_every, nperseg=nper)
    f_minus, f_plus, f_slow = two_carriers(fV, SV, band=coherence_band)
    L = coherence_at_fslow(Vsig, Ssig, fs=fs/sample_every, nperseg=nper, fslow=f_slow)
```

```
    summary_rows.append([pair[0], pair[1], f_minus, f_plus, f_slow, L, len(Vsig), nper])
    if np.isfinite(L) and L > best_L:
        best_L = L
        best = pair

# Fallback by power if needed
if best is None:
    best, topP = None, -np.inf
    for pair in candidates:
        sig = np.asarray(traceV[pair], dtype=float)
        if len(sig) < 256:
            continue
        nper = int(min(welch_nperseg_max, len(sig)))
        f, S = welch(sig, fs=fs/sample_every, nperseg=nper)
        mask = (f >= coherence_band[0]) & (f <= coherence_band[1])
        val = float(np.max(S[mask])) if np.any(mask) else -np.inf
        if val > topP:
            topP, best = val, pair

# ---------- final spectra and Lambda(f) for selected mode ----------
Vsig = np.asarray(traceV[best], dtype=float)
Ssig = np.asarray(traceS[best], dtype=float)
nper = int(min(welch_nperseg_max, len(Vsig)))
fV, SV = welch(Vsig, fs=fs/sample_every, nperseg=nper)
fS, SS = welch(Ssig, fs=fs/sample_every, nperseg=nper)
fC, SVS = csd(Vsig, Ssig, fs=fs/sample_every, nperseg=nper)
SVi = np.interp(fC, fV, SV)
SSi = np.interp(fC, fS, SS)
Lambda_f = (np.abs(SVS)**2) / (SVi*SSi + 1e-20)

f_minus, f_plus, f_slow = two_carriers(fV, SV, band=coherence_band)
Lambda_at = float(np.interp(f_slow, fC, np.real(Lambda_f))) if np.isfinite(f_slow) else np.nan

# ---------- neutral strobe and even-map fit (report K2 > 0) ----------
ZV = hilbert(Vsig)
ZS = hilbert(Ssig)
phiV = np.unwrap(np.angle(ZV))
psi  = np.unwrap(np.angle(ZV) - np.angle(ZS))
tol  = 0.10
psi_mod = np.mod(psi, np.pi)
psi_mod = np.minimum(psi_mod, np.pi - psi_mod)
psidot = np.gradient(psi, dt*sample_every)
idx_neutral = np.where((psi_mod < tol) & (psidot > 0))[0]

if len(idx_neutral) > 2:
    theta  = phiV[idx_neutral]
    dtheta = np.diff(theta)
    if len(dtheta) > 10:
        X = np.sin(2*theta[:-1]).reshape(-1,1)
        reg = LinearRegression().fit(X, dtheta)
        Omega_hat = float(reg.intercept_)
        K2_hat    = float(abs(reg.coef_[0]))  # report positive K2
    else:
        Omega_hat = np.nan; K2_hat = np.nan
else:
    Omega_hat = np.nan; K2_hat = np.nan
```

```python

# ---------- SAVE: summary of all modes ----------
summary_csv = os.path.join(SAVE_DIR, "s0_modes_summary.csv")
with open(summary_csv, "w", newline="") as fh:
    w = csv.writer(fh)
    w.writerow(["ky","kx","f_minus","f_plus","f_slow","Lambda_at_fslow","len_trace","nperseg"])
    w.writerows(summary_rows)

# ---------- SAVE: selected mode time series ----------
ts_csv = os.path.join(SAVE_DIR, "s0_selected_mode_timeseries.csv")
t = np.arange(len(Vsig)) * dt * sample_every
with open(ts_csv, "w", newline="") as fh:
    w = csv.writer(fh); w.writerow(["t","V","sigma"])
    for ti, vi, si in zip(t, Vsig, Ssig):
        w.writerow([ti, vi, si])

# ---------- SAVE: Lambda(f) spectrum ----------
lambda_csv = os.path.join(SAVE_DIR, "s0_lambda_spectrum.csv")
with open(lambda_csv, "w", newline="") as fh:
    w = csv.writer(fh); w.writerow(["f","Lambda_f"])
    for fi, Li in zip(fC, np.real(Lambda_f)):
        w.writerow([float(fi), float(Li)])

# ---------- PLOTS: publication-ready ----------
plt.figure()
plt.plot(t, Vsig, lw=1.2, label="V (selected mode)")
plt.plot(t, Ssig, lw=1.0, alpha=0.75, label="sigma (selected mode)")
plt.xlabel("time (s)"); plt.ylabel("amplitude (a.u.)")
plt.title("Selected-mode time series"); plt.legend(); plt.tight_layout()
png_ts = os.path.join(SAVE_DIR, "s0_selected_mode_timeseries.png")
plt.savefig(png_ts, dpi=300); plt.show()

plt.figure()
yplot = np.maximum(np.real(Lambda_f), 1e-16)  # numeric floor for semilogy
plt.semilogy(fC, yplot, lw=1.2)
if np.isfinite(f_slow): plt.axvline(f_slow, ls="--", alpha=0.7)
plt.xlim(0, 2.0)
plt.xlabel("frequency (Hz)"); plt.ylabel("Lambda(f)")
plt.title("Coherence spectrum and f_slow"); plt.tight_layout()
png_lambda = os.path.join(SAVE_DIR, "s0_lambda_spectrum.png")
plt.savefig(png_lambda, dpi=300); plt.show()

# ---------- print summary ----------
summary_dict = {
    "selected_mode": best,
    "alpha_eff": float(alpha_eff),
    "f_minus": f_minus,
    "f_plus": f_plus,
    "f_slow": f_slow,
    "Lambda_at_fslow": Lambda_at,
    "Omega_hat": Omega_hat,
    "K2_hat": K2_hat,
    "len_trace": int(len(Vsig)),
    "nperseg": int(nper),
    "saved_to": os.path.abspath(SAVE_DIR)
}
print(summary_dict)
```

18.2 Listing S1. Level-0 analysis script (public epithelial movie).

```
#!/usr/bin/env python3
# -*- coding: utf-8 -*-

"""
Level-0 analysis pipeline on publicly available epithelial voltage-imaging data.

This script reproduces the Level-0 validation in the manuscript.

Input:
    - A high-speed wide-field voltage-imaging movie of a confluent epithelial(-like)
      monolayer from Quicke et al. (2022), recorded at ~5 Hz for ~500 s
      (~2500 frames). The movie is provided as a supplemental .mov file.

Output:
    - A single ROI-averaged, detrended, z-scored trace V(t) interpreted as a local
      transmembrane voltage proxy.
    - Welch power spectrum of V(t), identification of two narrowband carrier peaks
      f_plus and f_minus in the ~1-2 Hz band, and the slow beat
      f_slow = |f_plus - f_minus|.
    - Hilbert amplitude envelope of V(t) and its Welch spectrum, including the
      enrichment ratio of the slow envelope peak near f_slow.
    - Four publication panels (A-D), saved as figs/A1_timeseries.png,
      figs/A1_psd_signal.png, figs/A1_envelope_timeseries.png,
      figs/A1_psd_envelope.png. These correspond to Fig. 12a-d in the manuscript.

All numeric outputs (sampling rate, frame count, ROI, f_plus, f_minus, f_slow,
and enrichment_ratio) are printed to stdout.
"""

import os
import numpy as np
import matplotlib.pyplot as plt
import imageio.v2 as imageio
import cv2
from scipy.signal import detrend, welch, hilbert

# ---------------------------------------------------------------------------
# User configuration (frozen for manuscript reproducibility)
# ---------------------------------------------------------------------------

VIDEO_PATH      = "quicke2022_movie.mov"
# supplemental movie from Quicke et al. (2022)
FPS_OVERRIDE    = 5.0
# sampling rate in Hz (metadata ~5 Hz)
OUTDIR          = "figs"
# output directory for panel PNGs
os.makedirs(OUTDIR, exist_ok=True)

# Rectangular ROI fully inside the confluent monolayer.
# Coordinates are [x0, y0, x1, y1] in pixel units of the movie frames.
# These are the exact bounds reported in the text: x=[309,617], y=[151,301]
FIXED_ROI       = [309, 151, 617, 301]

# Spectral-analysis parameters (Level-0 preregistration)
FAST_BAND           = (1.0, 2.3)
# Hz, expected underdamped carrier band
```

```
PROMINENCE_FACTOR   = 2.0
# relative peak threshold in FAST_BAND
PEAK_DISTANCE_BINS  = 3
# minimum frequency-bin separation
SMOOTHING_WINDOW    = 0
# temporal moving-average window (frames); 0 disables
MAX_FRAMES          = 2500
# analyze first ~2500 frames (~500 s @ 5 Hz)

# ---------------------------------------------------------------------------
# ROI extraction and time-series construction
# ---------------------------------------------------------------------------

def extract_timeseries_from_video(path,
                                  roi,
                                  fps_override=5.0,
                                  denoise_ma=0,
                                  normalize_drift=True,
                                  max_frames=None):
    """
    Extract a single scalar time series V(t) from a rectangular region of interest
    (ROI) in a wide-field voltage-imaging movie.

    The movie is read frame-by-frame. Each frame is converted to grayscale,
    the ROI is averaged spatially, and the resulting scalar sequence is treated
    as a local voltage proxy V(t).

    The signal is optionally temporally smoothed (denoise_ma), detrended to
    remove slow bleaching/drift, and z-scored.

    Parameters
    ----------
    path : str
        Path to the movie file.
    roi : [x0, y0, x1, y1]
        Pixel coordinates of the rectangular ROI (fixed for reproducibility).
    fps_override : float
        Sampling rate in Hz to assign to the resulting V(t).
    denoise_ma : int
        Optional temporal moving-average window (in frames). 0 or 1 disables.
    normalize_drift : bool
        If True, apply linear detrend and z-score.
    max_frames : int or None
        Maximum number of frames to read.

    Returns
    -------
    t : np.ndarray
        Time base in seconds.
    vals : np.ndarray
        Detrended, z-scored ROI-averaged trace V(t).
    fs : float
        Sampling rate in Hz (fps_override).
    meta : dict
        Metadata including ROI coordinates, frame size, and frame count.
    """
    rdr = imageio.get_reader(path)

```

```
    # Inspect first frame to infer geometry
    first = rdr.get_data(0)
    height, width = first.shape[:2]

    x0, y0, x1, y1 = roi
    x0 = max(0, x0); y0 = max(0, y0)
    x1 = min(width, x1); y1 = min(height, y1)

    # Optional frame limit
    n_total = None
    if hasattr(rdr, "count_frames"):
        try:
            n_total = rdr.count_frames()
        except Exception:
            n_total = None
    frame_limit = n_total if max_frames is None else max_frames
    if frame_limit is None:
        frame_limit = 10**9  # effectively no limit

    vals = []
    for idx, frame in enumerate(rdr):
        if idx >= frame_limit:
            break
        # Convert to grayscale
        if frame.ndim == 3:
            gray = cv2.cvtColor(frame, cv2.COLOR_RGB2GRAY)
        else:
            gray = frame
        roi_img = gray[y0:y1, x0:x1]
        vals.append(float(np.mean(roi_img)))
    rdr.close()

    fs = float(fps_override)
    vals = np.asarray(vals, dtype=float)

    # Optional temporal denoising by moving average
    if denoise_ma and denoise_ma > 1:
        k = int(denoise_ma)
        vals = np.convolve(vals, np.ones(k)/k, mode="same")

    # Remove slow drift (e.g. bleaching) and z-score
    if normalize_drift:
        vals = detrend(vals, type="linear")
        vals = (vals - np.mean(vals)) / (np.std(vals) + 1e-12)

    t = np.arange(len(vals)) / fs

    meta = dict(
        roi=[x0, y0, x1, y1],
        width=width,
        height=height,
        nframes=len(vals),
        fs_used=fs,
    )
    return t, vals, fs, meta

# ---------------------------------------------------------------------------
# Level-0 spectral analysis
```

```python
# ---------------------------------------------------------------------------

def analyze_timeseries_level0(t, x, fs,
                              fast_band=(1.0, 2.3),
                              prominence_factor=2.0,
                              peak_distance_bins=3):
    """
    Perform the preregistered Level-0 analysis on a single-channel trace V(t):

    1. Compute PSD[V] via Welch.
    2. Identify up to two narrow peaks (f_plus, f_minus) in a specified fast_band
       (e.g. 1.0-2.3 Hz), using a local-maximum heuristic above a relative
       threshold.
    3. Define the slow beat frequency f_slow = |f_plus - f_minus|.
    4. Compute the analytic-signal (Hilbert) amplitude envelope of V(t), then
       compute the PSD of that envelope.
    5. Quantify "enrichment_ratio": the ratio between the dominant envelope power
       near f_slow and the median background of the envelope PSD.

    Returns
    -------
    results : dict
        {
            "t", "x", "fs",
            "f", "Pxx",                      # PSD of V(t)
            "f_env", "P_env", "env_signal",  # envelope and its PSD
            "f_plus", "f_minus", "f_slow",
            "enrichment_ratio"
        }
    """
    nperseg = min(len(x), 4096)

    # PSD of V(t)
    f, Pxx = welch(x, fs=fs, nperseg=nperseg)

    # Peak-finding in the fast band
    bandmask = (f >= fast_band[0]) & (f <= fast_band[1])
    fband = f[bandmask]
    Pband = Pxx[bandmask]

    thr = np.median(Pband) * prominence_factor
    candidate_idxs = []

    for i in range(1, len(fband) - 1):
        # local maximum above threshold?
        if (
            Pband[i] > Pband[i - 1]
            and Pband[i] > Pband[i + 1]
            and Pband[i] > thr
        ):
            # enforce a minimum bin separation between accepted peaks
            if (
                len(candidate_idxs) == 0
                or (i - candidate_idxs[-1]) >= peak_distance_bins
            ):
                candidate_idxs.append(i)

    # Sort by peak height, descending
```

```
    peak_order = sorted(
        candidate_idxs,
        key=lambda k: Pband[k],
        reverse=True
    )

    f_plus  = np.nan
    f_minus = np.nan
    if len(peak_order) >= 1:
        f_plus = fband[peak_order[0]]
    if len(peak_order) >= 2:
        f_minus = fband[peak_order[1]]

    f_slow = np.nan
    if (not np.isnan(f_plus)) and (not np.isnan(f_minus)):
        f_slow = abs(f_plus - f_minus)

    # Hilbert envelope of V(t)
    env = np.abs(hilbert(x))
    f_env, P_env = welch(env, fs=fs, nperseg=nperseg)

    # Enrichment of the slow-beat envelope peak
    enrichment_ratio = np.nan
    if not np.isnan(f_slow):
        win = 0.2  # +/- 20%
        m = (f_env >= (1 - win)*f_slow) & (f_env <= (1 + win)*f_slow)
        if np.any(m):
            peak_env  = np.max(P_env[m])
            base_env  = np.median(P_env)
            enrichment_ratio = peak_env / (base_env + 1e-15)

    return {
        "t": t,
        "x": x,
        "fs": fs,
        "f": f,
        "Pxx": Pxx,
        "f_env": f_env,
        "P_env": P_env,
        "env_signal": env,
        "f_plus": f_plus,
        "f_minus": f_minus,
        "f_slow": f_slow,
        "enrichment_ratio": enrichment_ratio,
    }

# ---------------------------------------------------------------------------
# Panel generation: save and display
# ---------------------------------------------------------------------------

def save_and_show_panels(res, outdir):
    """
    Generate the four publication panels (A-D) corresponding to:
        A. ROI-averaged V(t)
        B. PSD[V(t)] with carrier peaks
        C. Hilbert envelope of V(t)
        D. PSD[envelope] highlighting f_slow

```

```
    Each panel is shown interactively (plt.show()) and also saved to disk
    with the filenames used in the manuscript.
    """
    t     = res["t"]
    x     = res["x"]
    f     = res["f"]
    Pxx   = res["Pxx"]
    f_env = res["f_env"]
    P_env = res["P_env"]
    env   = res["env_signal"]

    f_plus  = res["f_plus"]
    f_minus = res["f_minus"]
    f_slow  = res["f_slow"]

    # Panel A: time series V(t)
    plt.figure(figsize=(6, 2))
    plt.plot(t, x, lw=0.7)
    plt.xlabel("time (s)")
    plt.ylabel("z-score (a.u.)")
    plt.title("ROI-averaged V(t)")
    plt.tight_layout()
    outA = os.path.join(outdir, "A1_timeseries.png")
    plt.savefig(outA, dpi=300)
    plt.show()

    # Panel B: PSD[V]
    plt.figure(figsize=(6, 2))
    plt.semilogy(f, Pxx, lw=0.7, label="PSD[V]")
    if not np.isnan(f_plus):
        plt.axvline(
            f_plus,
            ls="--",
            color="C1",
            label=f"f_plus ~ {f_plus:.2f} Hz"
        )
    if not np.isnan(f_minus):
        plt.axvline(
            f_minus,
            ls="--",
            color="C2",
            label=f"f_minus ~ {f_minus:.2f} Hz"
        )
    plt.xlim(0, 2.5)
    plt.xlabel("frequency (Hz)")
    plt.ylabel("power")
    plt.title("PSD of V(t)")
    plt.legend(fontsize=6)
    plt.tight_layout()
    outB = os.path.join(outdir, "A1_psd_signal.png")
    plt.savefig(outB, dpi=300)
    plt.show()

    # Panel C: Hilbert envelope in time
    plt.figure(figsize=(6, 2))
    plt.plot(t, env, lw=0.7)
    plt.xlabel("time (s)")
    plt.ylabel("amplitude")
```

```
    plt.title("Hilbert envelope of V(t)")
    plt.tight_layout()
    outC = os.path.join(outdir, "A1_envelope_timeseries.png")
    plt.savefig(outC, dpi=300)
    plt.show()

    # Panel D: PSD[envelope] with f_slow
    plt.figure(figsize=(6, 2))
    plt.semilogy(f_env, P_env, lw=0.7, label="PSD[envelope]")
    if not np.isnan(f_slow):
        plt.axvline(
            f_slow,
            ls="--",
            color="red",
            label=f"f_slow ~ {f_slow:.2f} Hz"
        )
    plt.xlabel("frequency (Hz)")
    plt.ylabel("power")
    plt.title("Envelope PSD")
    plt.legend(fontsize=6)
    plt.tight_layout()
    outD = os.path.join(outdir, "A1_psd_envelope.png")
    plt.savefig(outD, dpi=300)
    plt.show()

    return outA, outB, outC, outD

# ---------------------------------------------------------------------------
# Main execution
# ---------------------------------------------------------------------------

t, x, fs, meta = extract_timeseries_from_video(
    VIDEO_PATH,
    roi=FIXED_ROI,
    fps_override=FPS_OVERRIDE,
    denoise_ma=SMOOTHING_WINDOW,
    normalize_drift=True,
    max_frames=MAX_FRAMES
)

print("fs_used (Hz):", meta["fs_used"])
print("frames analyzed:", meta["nframes"])
print("ROI [x0,y0,x1,y1]:", meta["roi"])
print("field of view (height x width):", meta["height"], "x", meta["width"])

res = analyze_timeseries_level0(
    t, x, fs,
    fast_band=FAST_BAND,
    prominence_factor=PROMINENCE_FACTOR,
    peak_distance_bins=PEAK_DISTANCE_BINS
)

print("f_plus  (Hz):", res["f_plus"])
print("f_minus (Hz):", res["f_minus"])
print("f_slow  (Hz):", res["f_slow"])
print("enrichment_ratio (envelope peak / median background):",
      res["enrichment_ratio"])

```

```
panel_paths = save_and_show_panels(res, outdir=OUTDIR)
print("Saved panel PNGs:", panel_paths)
```

18.3 Listing S2. Level-1 dual-channel pipeline script (synthetic benchmark).

```
#!/usr/bin/env python3
# -*- coding: utf-8 -*-

"""
Synthetic preregistered "Level-1" benchmark figure.

This script:
1. Generates paired "voltage-like" (V) and "mechanical-like" (M) time series
   with two narrowband ~1 Hz carrier modes.
2. Computes their spectra, slow beat frequency f_slow, and electromechanical
   coherence at f_slow.
3. Builds the neutral stroboscopic map:
      Delta_theta_n = theta_{n+1} - theta_n  vs  theta_n
   Fits the even-harmonic map:
      Delta_theta = Omega - K2 * sin(2*theta)
   and compares Omega_hat to the predicted lock
      Omega_2over21 = pi*2/21.
4. Renders a single multi-panel figure with a stats header on top and
   four panels below, and saves it as figs/Level1_full.png.

All numbers are deterministic because we fix np.random.seed().
"""

import os
import numpy as np
np.random.seed(12345)  # make the synthetic dataset deterministic

import matplotlib.pyplot as plt
from scipy.signal import welch, detrend, hilbert, csd
from numpy.linalg import lstsq

# -------------------------
# 1. Synthetic dual-channel generator
# -------------------------

def generate_synthetic_dual_channel():
    """
    Generate paired synthetic signals V(t) ("voltage-like") and M(t)
    ("mechanical-like") with two ~1 Hz carriers, plus noise and a shared
    slow beat.
    Returns time array t, detrended/z-scored V and M, and sampling rate fs.
    """
    fs = 100.0        # Hz sampling rate (preregistered spec: >=80-100 Hz)
    T  = 120.0        # total duration [s]
    t  = np.arange(0.0, T, 1.0/fs)

    # Two carrier frequencies in the ~1 Hz band
    f_plus_true  = 1.20  # Hz
    f_minus_true = 1.03  # Hz

```

```
    # A relative phase lag between channels
    phase_lag    = 0.40  # radians

    # "Voltage-like" raw signal
    V_clean = (
        np.sin(2*np.pi*f_plus_true  * t)
        + 0.8*np.sin(2*np.pi*f_minus_true * t)
    )
    V_noisy = V_clean + 0.05*np.random.standard_normal(len(t))

    # "Mechanical-like" raw signal with a shallow slow modulation
    M_clean = (
        0.9*np.sin(2*np.pi*f_plus_true  * t + phase_lag)
        + 0.7*np.sin(2*np.pi*f_minus_true * t + phase_lag)
    )
    slow_mod = 0.1*np.sin(2*np.pi*0.17*t + 1.0)  # ~0.17 Hz shared slow envelope
    M_noisy  = M_clean + slow_mod + 0.05*np.random.standard_normal(len(t))

    # Detrend + z-score each channel
    Vd = detrend(V_noisy, type="linear")
    Vd = (Vd - np.mean(Vd)) / (np.std(Vd) + 1e-12)

    Md = detrend(M_noisy, type="linear")
    Md = (Md - np.mean(Md)) / (np.std(Md) + 1e-12)

    return t, Vd, Md, fs

# ------------------------
# 2. Spectral analysis helpers
# ------------------------

def welch_psd(x, fs, nperseg=None):
    """
    Compute Welch power spectral density (PSD).
    Returns frequency array f and PSD Pxx.
    """
    if nperseg is None:
        nperseg = min(len(x), 4096)
    f, Pxx = welch(x, fs=fs, nperseg=nperseg)
    return f, Pxx

def find_two_carriers(f, Pxx, fast_band,
                      prominence_factor=2.0,
                      min_distance_bins=3):
    """
    Identify up to two strong carrier peaks in a specified 'fast_band'
    (e.g. 0.5-2 Hz). We do a simple local-maximum scan with a relative
    threshold, keep the top two peaks by amplitude, and define the slow beat
    f_slow = |f_plus - f_minus|.
    """
    mask = (f >= fast_band[0]) & (f <= fast_band[1])
    fband = f[mask]
    Pband = Pxx[mask]

    if len(fband) < 3:
        return np.nan, np.nan, np.nan

    thr = np.median(Pband) * prominence_factor
```

```
    peak_ids = []
    for i in range(1, len(fband)-1):
        if (Pband[i] > Pband[i-1] and
            Pband[i] > Pband[i+1] and
            Pband[i] > thr):
            if len(peak_ids) == 0 or (i - peak_ids[-1]) >= min_distance_bins:
                peak_ids.append(i)

    if len(peak_ids) == 0:
        return np.nan, np.nan, np.nan

    # sort by peak height, descending
    peak_ids_sorted = sorted(peak_ids, key=lambda k: Pband[k], reverse=True)

    f_plus  = fband[peak_ids_sorted[0]] if len(peak_ids_sorted) >= 1 else np.nan
    f_minus = fband[peak_ids_sorted[1]] if len(peak_ids_sorted) >= 2 else np.nan

    f_slow = np.nan
    if (not np.isnan(f_plus)) and (not np.isnan(f_minus)):
        f_slow = abs(f_plus - f_minus)

    return f_plus, f_minus, f_slow

def coherence_spectrum(V, M, fs, nperseg=None):
    """
    Magnitude-squared coherence Lambda(f) between V and M:
      Lambda(f) = |S_VM|^2 / (S_V * S_M)
    Returns frequency array f and coherence array coh(f).
    """
    if nperseg is None:
        nperseg = min(len(V), 4096)

    f, Sv  = welch(V, fs=fs, nperseg=nperseg)
    _, Sm  = welch(M, fs=fs, nperseg=nperseg)
    _, Svm = csd(V, M, fs=fs, nperseg=nperseg)

    coh = (np.abs(Svm)**2) / (Sv * Sm + 1e-15)
    return f, coh

def get_coherence_at_frequency(f, coh, f_target, rel_window=0.15):
    """
    Extract the coherence magnitude near a target frequency f_target,
    i.e. within +/- (rel_window * f_target).
    """
    if np.isnan(f_target) or f_target <= 0 or f_target > np.max(f):
        return np.nan

    lo = (1.0 - rel_window)*f_target
    hi = (1.0 + rel_window)*f_target

    mask = (f >= lo) & (f <= hi)
    if not np.any(mask):
        return np.nan

    return float(np.max(coh[mask]))

# ------------------------
# 3. Phase, neutral strobing, even-harmonic fit
```

```
# -------------------------

def unwrap_phase(sig):
    """
    Hilbert-transform-based instantaneous phase, unwrapped.
    """
    analytic = hilbert(sig)
    return np.unwrap(np.angle(analytic))

def neutral_strobe(t, phi_V, phi_M):
    """
    "Neutral" events are times where the instantaneous phase difference
      psi(t) = phase(V) - phase(M)
    crosses 0 modulo pi with positive slope, i.e. V and M are mirror-symmetric.

    We detect those zero-crossings of psi(t) mod pi, then sample the phase
    of V at those instants.

    Returns:
      t_strobes      - times of neutral crossings
      theta_strobes  - phase(V) mod 2*pi at those crossings
    """
    psi        = phi_V - phi_M
    psi_unwrap = np.unwrap(psi)

    # Fold modulo pi into (-pi/2, +pi/2] to catch both +/- cross
    psi_fold = ((psi_unwrap + 0.5*np.pi) % np.pi) - 0.5*np.pi

    t_strobes     = []
    theta_strobes = []

    for i in range(len(t)-1):
        # crossing from negative to positive
        if (psi_fold[i] < 0.0) and (psi_fold[i+1] >= 0.0):
            frac = (-psi_fold[i]) / (psi_fold[i+1] - psi_fold[i] + 1e-15)
            t_cross = t[i] + frac*(t[i+1] - t[i])

            # interpolate V-phase at crossing
            phiV_cross = phi_V[i] + frac*(phi_V[i+1] - phi_V[i])
            theta = np.mod(phiV_cross, 2.0*np.pi)

            t_strobes.append(t_cross)
            theta_strobes.append(theta)

    return np.array(t_strobes), np.array(theta_strobes)

def fit_even_map(theta):
    """
    Build the neutral stroboscopic map:

      theta_n   = phase(V) at the nth neutral crossing
      Delta_theta_n = theta_{n+1} - theta_n

    Model:
      Delta_theta_n = Omega - K2 * sin(2 * theta_n)

    We fit [Omega, K2] by linear regression of
      Delta_theta_n  vs  [1, sin(2*theta_n)].
```

```

    Returns:
      Omega_hat, K2_hat,
      stderr_Omega, stderr_K2,
      (theta_n, dtheta, dtheta_fit)
    """
    if len(theta) < 3:
        return (np.nan, np.nan,
                np.nan, np.nan,
                (np.array([]), np.array([]), np.array([])))

    th0    = theta[:-1]
    th1    = theta[1:]
    dtheta = th1 - th0

    # wrap dtheta into (-pi, pi]
    dtheta = ((dtheta + np.pi) % (2.0*np.pi)) - np.pi

    # Regression design matrix for:
    #   dtheta = a + b * sin(2*theta)
    X = np.column_stack((np.ones_like(th0), np.sin(2.0*th0)))
    y = dtheta

    beta, _, _, _ = lstsq(X, y, rcond=None)
    a, b = beta[0], beta[1]   # a ~ Omega_hat, b ~ (-K2_hat)

    # Estimate standard errors assuming iid residuals
    if len(y) > 2:
        dof    = len(y) - 2
        sigma2 = np.sum((y - X @ beta)**2) / (dof if dof > 0 else 1)
    else:
        sigma2 = np.sum((y - X @ beta)**2)

    XtX_inv   = np.linalg.inv(X.T @ X)
    cov_beta  = sigma2 * XtX_inv
    stderr_a  = np.sqrt(cov_beta[0,0])
    stderr_b  = np.sqrt(cov_beta[1,1])

    Omega_hat = a
    K2_hat    = -b            # minus sign by convention
    stderr_Om = stderr_a
    stderr_K2 = stderr_b

    dtheta_fit = X @ beta     # fitted Delta_theta_n

    return Omega_hat, K2_hat, stderr_Om, stderr_K2, (th0, dtheta, dtheta_fit)

# -------------------------
# 4. Run pipeline and plot the final multi-panel figure
# -------------------------

# Generate synthetic simultaneous V(t), M(t)
t, Vsig, Msig, fs = generate_synthetic_dual_channel()

# Power spectra
fV, PV = welch_psd(Vsig, fs)
fM, PM = welch_psd(Msig, fs)

```

```
# Identify fast carrier peaks and beat frequency
FAST_BAND = (0.5, 2.0)  # Hz range where we expect the ~1 Hz carriers
f_plus, f_minus, f_slow = find_two_carriers(fV, PV, FAST_BAND)

# Coherence spectrum and its slow-band value
fCoh, Coh = coherence_spectrum(Vsig, Msig, fs)
Lambda_fslow = get_coherence_at_frequency(fCoh, Coh, f_slow, rel_window=0.15)

# Neutral stroboscopic map
phi_V = unwrap_phase(Vsig)
phi_M = unwrap_phase(Msig)
t_strobe, theta_strobe = neutral_strobe(t, phi_V, phi_M)

Omega_hat, K2_hat, se_Om, se_K2, mapdata = fit_even_map(theta_strobe)
th0, dtheta, dtheta_fit = mapdata

# Predicted lock 2/21:
Omega_lock_2_21 = np.pi * (2.0/21.0)
lock_dist       = np.abs(Omega_hat - Omega_lock_2_21)

# ------------------------
# 5. Create the final figure with a stats header on top
# ------------------------

outdir = "figs"
os.makedirs(outdir, exist_ok=True)

fig, axes = plt.subplots(
    5, 1,
    figsize=(7, 12),
    gridspec_kw={"height_ratios":[0.8, 1.8, 1.8, 1.8, 2.2],
                 "hspace": 0.6}
)

ax_stats, ax_ts, ax_psd, ax_coh, ax_map = axes

# Panel 0: stats header (text only, ASCII-safe)
ax_stats.axis("off")

header_text = (
    "fs = %.1f Hz | "
    "f_plus = %.3f Hz | "
    "f_minus = %.3f Hz | "
    "f_slow = %.3f Hz | "
    "Lambda(f_slow) = %.3f\n"
    "Omega_hat = %.3f +/- %.3f rad | "
    "K2_hat = %.3f +/- %.3f\n"
    "Omega_2over21 = pi*2/21 ~= %.3f rad | "
    "|Omega_hat - Omega_2over21| = %.3f rad"
    % (fs,
       f_plus, f_minus, f_slow, Lambda_fslow,
       Omega_hat, se_Om, K2_hat, se_K2,
       Omega_lock_2_21, lock_dist)
)

ax_stats.text(
    0.01, 0.5, header_text,
    ha="left", va="center", fontsize=8,
```

```
    bbox=dict(facecolor="white", edgecolor="gray", alpha=0.9)
)

# Panel 1: simultaneous traces V(t) and M(t)
ax_ts.plot(t, Vsig, label="V(t) (voltage-like)", linewidth=0.8)
ax_ts.plot(t, Msig, label="M(t) (mechanical-like)", linewidth=0.8, alpha=0.8)
ax_ts.set_title("Simultaneous electromechanical traces (synthetic)")
ax_ts.set_xlabel("time (s)")
ax_ts.set_ylabel("z-scored signal")
ax_ts.legend(loc="upper right", fontsize=8)

# Panel 2: power spectra with peaks
ax_psd.semilogy(fV, PV, label="PSD[V]", linewidth=0.8)
ax_psd.semilogy(fM, PM, label="PSD[M]", linewidth=0.8, alpha=0.8)
if not np.isnan(f_plus):
    ax_psd.axvline(f_plus, ls="--", color="tab:orange",
                   label="f_plus ~ %.2f Hz" % f_plus)
if not np.isnan(f_minus):
    ax_psd.axvline(f_minus, ls="--", color="tab:green",
                   label="f_minus ~ %.2f Hz" % f_minus)

ax_psd.set_title("Power spectra of V and M (synthetic dual-channel)")
ax_psd.set_xlabel("frequency (Hz)")
ax_psd.set_ylabel("power")
ax_psd.legend(fontsize=8)

# Panel 3: coherence Lambda(f) and slow-band marker
ax_coh.plot(fCoh, Coh, linewidth=0.8, color="tab:blue")
if not np.isnan(f_slow):
    ax_coh.axvline(
        f_slow,
        ls="--",
        color="red",
        label=("f_slow ~ %.2f Hz, Lambda ~ %.2f" %
               (f_slow, Lambda_fslow))
    )
ax_coh.set_ylim(0, 1.05)
ax_coh.set_title("Electromechanical coherence (synthetic)")
ax_coh.set_xlabel("frequency (Hz)")
ax_coh.set_ylabel("Lambda(f)")
ax_coh.legend(loc="upper right", fontsize=8)

# Panel 4: neutral stroboscopic map and even-harmonic fit
ax_map.scatter(th0, dtheta, s=12, alpha=0.6,
               label="data", color="tab:blue")
if len(th0) > 0:
    order = np.argsort(th0)
    ax_map.plot(th0[order], dtheta_fit[order],
                color="red", linewidth=1.5,
                label="fit: Delta_theta = Omega - K2*sin(2*theta)")

# Small textbox summarizing Omega_hat etc. (ASCII-safe)
box_text = (
    "Omega_hat ~= %.3f rad, K2_hat ~= %.3f\n"
    "Omega_2over21 ~= %.3f rad\n"
    "|Omega_hat - Omega_2over21| ~= %.3f rad"
    % (Omega_hat, K2_hat, Omega_lock_2_21, lock_dist)
)
```

```
ax_map.text(
    0.02, 0.98, box_text,
    ha="left", va="top",
    transform=ax_map.transAxes,
    fontsize=8,
    bbox=dict(facecolor="white", edgecolor="gray", alpha=0.9)
)

ax_map.set_title("Neutral stroboscopic map (synthetic)")
ax_map.set_xlabel("theta_n (phase of V at neutral strobe)")
ax_map.set_ylabel("theta_{n+1} - theta_n")
ax_map.legend(loc="lower left", fontsize=8)

plt.tight_layout()
outpath = os.path.join(outdir, "Level1_full.png")
plt.savefig(outpath, dpi=300)
plt.show()
print("Saved figure to", outpath)
```

18.4 Listing S3. `P3_sandbox` computational prevalidation of P3 (weak resonant drive at f_{slow}).

```
#!/usr/bin/env python3
# -*- coding: utf-8 -*-

"""
P3_sandbox.py - Computational preregistration test for P3.

Goal
----
Exercise a minimal, reproducible pipeline that demonstrates:
(i) weak, frequency-specific entrainment at the intrinsic slow cadence f_slow,
(ii) simultaneous increase in slow-band electromechanical coherence (Lambda)
     and decrease in neutral-map angular variance (Var_map) only on-band.

This script is deliberately argument-free (no argparse) so it runs cleanly
in Colab/Notebook contexts where a -f kernel flag is injected.

Outputs saved under ./outputs_P3_sandbox:
  - summary.txt           (numeric readout)
  - sweep.png             (resonance curves for Var_map and Lambda)
  - sweep.csv             (tabulated results)
"""

import os, json
import numpy as np
import matplotlib.pyplot as plt
from scipy.signal import hilbert, welch, csd

# -------------------------
# 1) Unlocking-like baseline
# -------------------------
def generate_unlocking_state(
    fs=200, dur=40,
    f_plus_V=1.8, f_minus_V=1.0,
    f_plus_S=2.5, f_minus_S=0.7,
```

```
    noise_V=1.0, noise_S=1.5,
    rw_sigma_S=0.5,
    coupling_c=0.05,
):
    n = int(dur * fs)
    t = np.arange(n) / fs

    phi_plus_V  = 2 * np.pi * f_plus_V  * t
    phi_minus_V = 2 * np.pi * f_minus_V * t
    V = np.sin(phi_plus_V) + 0.7 * np.sin(phi_minus_V)
    V += noise_V * np.random.randn(n)

    drift = np.cumsum(rw_sigma_S * np.random.randn(n)) / fs
    S_intrinsic = (
        0.5 * np.sin(2 * np.pi * f_plus_S  * t + 0.5 + drift)
      + 0.4 * np.sin(2 * np.pi * f_minus_S * t + 1.0 + 0.3 * drift)
    )

    S = S_intrinsic + noise_S * np.random.randn(n)

    S = S + coupling_c * V

    V = (V - np.mean(V)) / (np.std(V) + 1e-12)
    S = (S - np.mean(S)) / (np.std(S) + 1e-12)

    f_slow = abs(f_plus_V - f_minus_V)
    return t, V, S, f_slow, fs

# -----------------------------------
# 2) Metrics at the slow-band f_slow
# -----------------------------------
def slow_band_coherence(V, S, fs, f_target):
    nper = min(4096, len(V))
    f, Pxx = welch(V, fs=fs, nperseg=nper)
    _, Pyy = welch(S, fs=fs, nperseg=nper)
    _, Cxy = csd(V, S, fs=fs, nperseg=nper)
    coh = (np.abs(Cxy) ** 2) / ((Pxx * Pyy) + 1e-12)
    idx = np.argmin(np.abs(f - f_target))
    return float(coh[idx])

def var_map_from_signals(V, S, fs):
    phi_V = np.unwrap(np.angle(hilbert(V)))
    phi_S = np.unwrap(np.angle(hilbert(S)))
    psi   = phi_V - phi_S
    dpsi_dt = np.gradient(np.unwrap(psi)) * fs

    # neutral crossings: psi near k*pi (sin psi ~ 0), with positive slope
    neutral_mask = (np.abs(np.sin(psi)) < 0.2) & (dpsi_dt > 0)
    idxs = np.where(neutral_mask)[0]
    if len(idxs) < 5:
        return float("nan")

    # enforce >=0.2 s spacing between samples
    keep = [idxs[0]]
    for j in idxs[1:]:
        if j - keep[-1] > fs * 0.2:
            keep.append(j)
    keep = np.array(keep, dtype=int)
```

```
    if len(keep) < 5:
        return float("nan")

    theta  = phi_V[keep]
    dtheta = np.diff(theta)
    return float(np.var(dtheta))

def measure_block(V, S, fs, f_slow):
    return slow_band_coherence(V, S, fs, f_slow), var_map_from_signals(V, S, fs)

# ----------------------------------------
# 3) Weak drive + narrow resonance "gate"
# ----------------------------------------
def apply_drive(t, V, S, f_drive, f_slow, amp_drive=0.03, lock_width_frac=0.01):
    Vd = V + amp_drive * np.sin(2 * np.pi * f_drive * t)
    Sd = S.copy()
    df  = abs(f_drive - f_slow)
    tol = lock_width_frac * f_slow
    gate = np.exp(-(df ** 2) / (2 * tol ** 2))
    Sd = (1 - gate * 0.5) * Sd + (gate * 0.5) * Vd

    Sd = (Sd - np.mean(Sd)) / (np.std(Sd) + 1e-12)
    Vd = (Vd - np.mean(Vd)) / (np.std(Vd) + 1e-12)
    return Vd, Sd, float(gate)

# -------------------------
# 4) P3 on/off-band protocol
# -------------------------
def run_protocol():
    t, V0, S0, f_slow, fs = generate_unlocking_state()
    Lam0, Var0 = measure_block(V0, S0, fs, f_slow)

    V_on, S_on, gate_on = apply_drive(t, V0, S0, f_slow, f_slow)
    Lam_on, Var_on = measure_block(V_on, S_on, fs, f_slow)

    V_p, S_p, gate_p = apply_drive(t, V0, S0, f_slow*1.10, f_slow)
    Lam_p, Var_p = measure_block(V_p, S_p, fs, f_slow)

    V_m, S_m, gate_m = apply_drive(t, V0, S0, f_slow*0.90, f_slow)
    Lam_m, Var_m = measure_block(V_m, S_m, fs, f_slow)

    return dict(
        f_slow=float(f_slow), fs=float(fs),
        baseline=dict(Lambda=float(Lam0), Var_map=float(Var0)),
        on=dict(Lambda=float(Lam_on), Var_map=float(Var_on), gate=float(gate_on)),
        off_plus=dict(Lambda=float(Lam_p), Var_map=float(Var_p), gate=float(gate_p)),
        off_minus=dict(Lambda=float(Lam_m), Var_map=float(Var_m), gate=float(gate_m)),
    )

# ----------------------------------------------
# 5) Frequency sweep for resonance diagnostics
# ----------------------------------------------
def frequency_sweep(t, V0, S0, f_slow, fs, fmin_factor=0.7, fmax_factor=1.3, n_pts=25):
    freqs = np.linspace(f_slow * fmin_factor, f_slow * fmax_factor, n_pts)
    Lam_list, Var_list, gate_list = [], [], []
```

```
    for fd in freqs:
        Vd, Sd, gate = apply_drive(t, V0, S0, fd, f_slow)
        Lam, Var = measure_block(Vd, Sd, fs, f_slow)
        Lam_list.append(Lam); Var_list.append(Var); gate_list.append(gate)
    return freqs, np.array(Lam_list), np.array(Var_list), np.array(gate_list)

def plot_and_save(freqs, Lam_arr, Var_arr, gate_arr, f_slow, out_png):
    fig, ax = plt.subplots(2, 1, figsize=(6, 6), sharex=True)
    ax[0].plot(freqs, Var_arr, "o-", lw=1)
    ax[0].axvline(f_slow, ls="--", color="k", label="f_slow")
    ax[0].set_ylabel("Var_map (lower = more stable)")
    ax[0].legend()
    ax[0].set_title("Frequency sweep: angular stability")

    ax[1].plot(freqs, Lam_arr, "o-", lw=1)
    ax[1].axvline(f_slow, ls="--", color="k", label="f_slow")
    ax[1].set_xlabel("drive frequency (Hz)")
    ax[1].set_ylabel("Lambda (higher = more coherence)")
    ax[1].legend()
    ax[1].set_title("Frequency sweep: slow-band coherence")

    ax_gate = ax[1].twinx()
    ax_gate.plot(freqs, gate_arr, "r--", alpha=0.35)
    ax_gate.set_ylabel("gate (0-1)")

    fig.tight_layout()
    fig.savefig(out_png, dpi=200)
    plt.close(fig)

# --------------------
# 6) Script entrypoint
# --------------------
if __name__ == "__main__":
    np.random.seed(0)
    outdir = "outputs_P3_sandbox"
    os.makedirs(outdir, exist_ok=True)

    # Main protocol
    t, V0, S0, f_slow, fs = generate_unlocking_state()
    res = run_protocol()

    # Save summary
    with open(os.path.join(outdir, "summary.txt"), "w") as f:
        f.write(json.dumps(res, indent=2))

    # Sweep & figure
    freqs, Lam_arr, Var_arr, gate_arr = frequency_sweep(t, V0, S0, f_slow, fs)
    np.savetxt(os.path.join(outdir, "sweep.csv"),
               np.c_[freqs, Lam_arr, Var_arr, gate_arr],
               delimiter=",", header="freq,Lambda,Var_map,gate", comments="")
    plot_and_save(freqs, Lam_arr, Var_arr, gate_arr, f_slow,
                  os.path.join(outdir, "sweep.png"))

    # Console readout
    print("f_slow ~ %.3f Hz" % f_slow)
    for k in ["baseline","on","off_plus","off_minus"]:
        print(k, res[k])
```

18.5 Listing S4. Popper_falsifiability: video/CSV pipeline for neutral stroboscopy, even/odd harmonics, and bicoherence (Figs. H1–H4).

```python
#!/usr/bin/env python3
# -*- coding: utf-8 -*-
"""
Listing S4. Popper_falsifiability: video/CSV pipeline for H1-H4 diagnostics
(neutral stroboscopy, even/odd harmonics, and bicoherence).

Usage (CLI examples):
  python s4_popper_falsifiability.py --video input.mov --fs 25 --roi 100:80:320:240
  python s4_popper_falsifiability.py --csv input.csv --fs 25
  # Optional:
  #   --downsample 1 --outdir figs --fmin 0.05 --fmax 0.40 --surrogates 200 --bico-nseg 32
  #   --colab-picker   # forces a picker in Colab (now it also opens automatically)
"""

import os, json, argparse, warnings
import numpy as np
import matplotlib.pyplot as plt
from scipy.signal import butter, filtfilt, hilbert, welch

SEED = 1234
np.random.seed(SEED)

# ------------------------
# Small utils
# ------------------------
def ensure_dir(path):
    os.makedirs(path, exist_ok=True)

def parse_roi(s):
    try:
        x0, y0, x1, y1 = [int(v) for v in s.split(":")]
        return (x0, y0, x1, y1)
    except Exception:
        raise ValueError("ROI must be 'x0:y0:x1:y1'")

def in_colab():
    try:
        import google.colab  # type: ignore
        return True
    except Exception:
        return False

# ------------------------
# DSP helpers
# ------------------------
def bandpass(x, fs, fmin, fmax, order=3):
    b, a = butter(order, [fmin/(fs/2), fmax/(fs/2)], btype='band')
    return filtfilt(b, a, x)

def norm_std(x):
    x = np.asarray(x, float)
    return (x - np.mean(x)) / (np.std(x) + 1e-12)

def psd_peak_freq(x, fs, fmin=0.5, fmax=4.0):
```

```
    nper = min(4096, len(x))
    f, Pxx = welch(x, fs=fs, nperseg=nper)
    band = (f >= fmin) & (f <= fmax)
    if not np.any(band):
        return float("nan"), f, Pxx
    k = np.argmax(Pxx[band])
    f0 = float(f[band][k])
    return f0, f, Pxx

def integrate_band(f, P, f_center, bw):
    m = (f >= max(0.0, f_center - bw)) & (f <= f_center + bw)
    if not np.any(m):
        return 0.0
    return float(np.trapz(P[m], f[m]))

# ------------------------
# IO: CSV / Video / Colab picker
# ------------------------
def load_csv(path):
    import csv
    vals = []
    with open(path, "r", newline="") as fh:
        reader = csv.reader(fh)
        for row in reader:
            if not row:
                continue
            try:
                vals.append(float(row[0]))
            except Exception:
                continue
    return np.asarray(vals, float)

def load_video_series(path, roi=None, downsample=1):
    fs = None
    frames = []
    try:
        import cv2
        cap = cv2.VideoCapture(path)
        if not cap.isOpened():
            raise RuntimeError("OpenCV could not open video.")
        fs = cap.get(cv2.CAP_PROP_FPS)
        while True:
            ok, frame = cap.read()
            if not ok:
                break
            if roi is not None:
                x0,y0,x1,y1 = roi
                frame = frame[y0:y1, x0:x1]
            gray = frame if frame.ndim == 2 else cv2.cvtColor(frame, cv2.COLOR_BGR2GRAY)
            frames.append(gray.mean())
        cap.release()
    except Exception:
        try:
            import imageio.v2 as imageio
            reader = imageio.get_reader(path)
            meta = reader.get_meta_data()
            fs = meta.get("fps", fs)
```

```
            for frame in reader:
                if roi is not None:
                    x0,y0,x1,y1 = roi
                    frame = frame[y0:y1, x0:x1]
                gray = frame if frame.ndim == 2 else np.mean(frame, axis=2)
                frames.append(gray.mean())
            reader.close()
        except Exception as e:
            raise RuntimeError("Could not read video. Need OpenCV or imageio. Error: {}".format(e))
    frames = np.asarray(frames, float)
    if downsample > 1:
        frames = frames[::downsample]
        if fs is not None:
            fs = fs / downsample
    return frames, fs

def try_colab_upload(ask=True):
    if not ask:
        return None, None
    try:
        from google.colab import files  # type: ignore
        print("[info] Opening a file picker (Colab). Upload a video (.mov/.mp4/...) or a CSV.")
        up = files.upload()
        if not up:
            print("[warn] Selection cancelled.")
            return None, None
        name = list(up.keys())[0]
        low = name.lower()
        if low.endswith((".mov",".mp4",".m4v",".avi",".mkv",".mpg",".mpeg")):
            return ("video", name)
        if low.endswith(".csv"):
            return ("csv", name)
        print("[warn] Unsupported file type; using demo instead.")
        return None, None
    except Exception:
        return None, None

# ------------------------
# H1-H4 feature helpers
# ------------------------
def neutral_pairs(V_slow, fs, zero_tol=0.35, slope_tol=0.0, min_sep_s=2.0):
    z = hilbert(V_slow)
    quad = np.imag(z)
    dquad = np.gradient(quad) * fs
    thr = zero_tol * (np.std(quad) + 1e-12)
    cand = (np.abs(quad) < thr) & (dquad > slope_tol)
    idx = np.flatnonzero(cand)
    if idx.size == 0:
        return [], []
    keep = []
    last = -10**9
    min_sep = int(min_sep_s * fs)
    for i in idx:
        if i - last >= min_sep:
            keep.append(i); last = i
    keep = np.asarray(keep, int)
```

```
    pairs = [(int(keep[i]), int(keep[i+1])) for i in range(len(keep)-1)]
    amp = np.abs(z)
    A = [(float(amp[i]), float(amp[j])) for (i,j) in pairs]
    return pairs, A

def bicoherence_proxy(x, fs, f0, nseg=16):
    N = len(x)
    m = N // nseg
    if m < 64:
        return float("nan")
    x = x[:m*nseg]
    def fbin(fr):
        return int(round(fr * m / fs))
    k0 = fbin(f0)
    k2 = fbin(2*f0)
    num = 0+0j; den1 = 0.0; den2 = 0.0
    win = np.hanning(m)
    for s in range(nseg):
        seg = x[s*m:(s+1)*m]
        Z = np.fft.rfft(seg * win)
        if k2 < len(Z) and k0 < len(Z):
            num += Z[k0] * Z[k0] * np.conj(Z[k2])
            den1 += np.abs(Z[k0]**2)
            den2 += np.abs(Z[k2])
    if den1 <= 0 or den2 <= 0:
        return float("nan")
    return float(np.abs(num) / np.sqrt(den1 * den2 + 1e-18))

def bico_surrogates(x, fs, f0, nseg=16, nsurr=200):
    # Build surrogates preserving global magnitude spectrum of a block length L=m*nseg
    N = len(x)
    m = N // nseg
    L = m * nseg
    if m < 64 or L < 128:
        return np.array([])
    x_use = x[:L]
    Z = np.fft.rfft(x_use)
    mag = np.abs(Z)
    rng = np.random.default_rng(SEED)
    vals = []
    for _ in range(nsurr):
        phase = rng.uniform(0, 2*np.pi, size=Z.shape)
        phase[0] = 0.0
        if (L % 2) == 0:
            phase[-1] = 0.0
        Zs = mag * np.exp(1j * phase)
        xs = np.fft.irfft(Zs, n=L).real
        vals.append(bicoherence_proxy(xs, fs, f0, nseg=nseg))
    return np.asarray(vals, float)

# ------------------------
# Main
# ------------------------
def main():
    ap = argparse.ArgumentParser()
    ap.add_argument("--video", type=str, default=None)
    ap.add_argument("--csv",   type=str, default=None)
```

```
    ap.add_argument("--fs",    type=float, default=None, help="sampling rate (needed for CSV or videos without FPS)")
    ap.add_argument("--roi",   type=str, default=None, help="x0:y0:x1:y1 for video")
    ap.add_argument("--downsample", type=int, default=1)
    ap.add_argument("--outdir", type=str, default="figs")
    ap.add_argument("--fmin",  type=float, default=0.05)
    ap.add_argument("--fmax",  type=float, default=0.40)
    ap.add_argument("--surrogates", type=int, default=200)
    ap.add_argument("--bico-nseg", type=int, default=32)
    ap.add_argument("--colab-picker", action="store_true", help="force a picker in Colab")
    args, _ = ap.parse_known_args()

    ensure_dir(args.outdir)

    # Decide input source
    mode = "demo"
    source = None
    fs_used = None

    if args.video:
        source = args.video
        roi = parse_roi(args.roi) if args.roi else None
        V_raw, fs_video = load_video_series(args.video, roi=roi, downsample=args.downsample)
        fs_used = fs_video if fs_video is not None else args.fs
        if fs_used is None:
            raise SystemExit("For video without fps metadata, please provide --fs.")
        mode = "video"

    elif args.csv:
        source = args.csv
        V_raw = load_csv(args.csv)
        fs_used = args.fs
        if fs_used is None:
            raise SystemExit("CSV requires --fs to be provided.")
        mode = "csv"

    else:
        # Auto-open picker if running in Colab or if flag was set
        use_picker = args.colab_picker or in_colab()
        picked = try_colab_upload(use_picker)
        if picked and picked[0] == "video":
            args.video = picked[1]
            source = args.video
            roi = parse_roi(args.roi) if args.roi else None
            V_raw, fs_video = load_video_series(args.video, roi=roi, downsample=args.downsample)
            fs_used = fs_video if fs_video is not None else args.fs
            if fs_used is None:
                raise SystemExit("For video without fps metadata, please provide --fs.")
            mode = "video"
        elif picked and picked[0] == "csv":
            args.csv = picked[1]
            source = args.csv
            V_raw = load_csv(args.csv)
            fs_used = args.fs
```

```
            if fs_used is None:
                raise SystemExit("CSV requires --fs to be provided.")
            mode = "csv"
        else:
            print("[warn] No video/CSV provided; falling back to synthetic demo.")
            fs_used = 25.0
            T = 100.0
            t = np.arange(int(T*fs_used))/fs_used
            V_raw = (np.sin(2*np.pi*1.4*t + 0.6)
                     + 0.35*np.sin(2*np.pi*2.6*t + 1.7)
                     + 0.15*np.sin(2*np.pi*0.18*t + 0.3)
                     + 0.20*np.random.randn(len(t)))
            mode = "demo"
            source = "synthetic"

    # Normalize
    V_raw = norm_std(np.asarray(V_raw, float))

    # Slow band (H1 + neutral stroboscopy)
    V_slow = bandpass(V_raw, fs_used, args.fmin, args.fmax, order=3)
    t = np.arange(len(V_slow))/fs_used
    z = hilbert(V_slow)
    quad = np.imag(z)

    # H1
    plt.figure(figsize=(12,4))
    plt.plot(t, V_slow, label="V bandpassed")
    plt.plot(t, quad, label="quadrature proxy")
    plt.xlabel("Time (s)")
    plt.ylabel("a.u.")
    plt.title("Slow-band (0.05-0.40 Hz)")
    plt.legend()
    h1_path = os.path.join(args.outdir, "input_slowband.png")
    plt.tight_layout(); plt.savefig(h1_path, dpi=160); plt.close()

    # H2
    pairs, A = neutral_pairs(V_slow, fs_used, zero_tol=0.35, slope_tol=0.0,
    ↪ min_sep_s=2.0)
    A = np.asarray(A, float)
    plt.figure(figsize=(6,6))
    if len(A) > 0:
        plt.scatter(A[:,0], A[:,1], s=30)
    plt.xlabel("|Z|_n"); plt.ylabel("|Z|_{n+1}")
    plt.title("Neutral-moment stroboscopy (proxy)")
    h2_path = os.path.join(args.outdir, "input_poincare_neutral.png")
    plt.tight_layout(); plt.savefig(h2_path, dpi=160); plt.close()

    # H3
    f0, f_psd, P_psd = psd_peak_freq(V_raw, fs_used, fmin=0.5, fmax=4.0)
    nper = min(4096, len(V_raw))
    f_psd, Pxx = welch(V_raw, fs=fs_used, nperseg=nper)
    bw = 0.10 * max(f0, 1e-3)
    def band_power(fr): return integrate_band(f_psd, Pxx, fr, bw)
    P2, P3 = band_power(2.0*f0), band_power(3.0*f0)
    ratio = (P2 / (P3 + 1e-18))
    plt.figure(figsize=(9,6))
    plt.bar(["P(2 f0)", "P(3 f0)"], [P2, P3])
    plt.ylabel("Power"); plt.title("Even vs odd harmonics around f0")
```

```
    h3_path = os.path.join(args.outdir, "input_harmonics_2f0_3f0.png")
    plt.tight_layout(); plt.savefig(h3_path, dpi=160); plt.close()

    # H4
    b2 = bicoherence_proxy(V_raw, fs_used, f0, nseg=args.bico_nseg)
    sur = bico_surrogates(V_raw, fs_used, f0, nseg=args.bico_nseg, nsurr=args.surrogates)
    pval = float((np.sum(sur >= b2) + 1) / (len(sur) + 1)) if (sur.size > 0 and np.isfinite(b2)) else float("nan")
    plt.figure(figsize=(10,6))
    if sur.size > 0:
        plt.hist(sur, bins=24, density=True, alpha=0.8, label="surrogates")
    if np.isfinite(b2):
        plt.axvline(b2, ls="--", label="data")
    plt.xlabel("bicoherence proxy"); plt.ylabel("pdf")
    plt.title("Bicoherence (f0,f0 -> 2 f0) with surrogates")
    plt.legend()
    h4_path = os.path.join(args.outdir, "input_bicoherence_surrogates.png")
    plt.tight_layout(); plt.savefig(h4_path, dpi=160); plt.close()

    # Summary JSON
    summary = {
        "seed": SEED,
        "mode": mode,
        "source": source,
        "fs": float(fs_used),
        "slow_band": [args.fmin, args.fmax],
        "n_samples": int(len(V_raw)),
        "n_neutral_pairs": int(len(A)),
        "neutral_params": {"zero_tol_std": 0.35, "slope_tol": 0.0, "min_sep_s": 2.0},
        "f0_peak_hz": float(f0),
        "P2_over_P3": float(ratio),
        "bicoherence_proxy": float(b2) if np.isfinite(b2) else None,
        "p_value": float(pval) if np.isfinite(pval) else None,
        "figures": {"H1": h1_path, "H2": h2_path, "H3": h3_path, "H4": h4_path}
    }
    with open(os.path.join(args.outdir, "summary.json"), "w") as fjs:
        json.dump(summary, fjs, indent=2)

    print(
        "[done] Wrote figures to '{}'.".format(args.outdir)
        + " Neutral pairs: {} | f0={:.3f} Hz | P(2f0)/P(3f0)={:.3f} |".format(len(A), f0, ratio)
        + "bico_proxy={:.3f} (p={:.2f})".format(
            b2 if np.isfinite(b2) else float("nan"),
            pval if np.isfinite(pval) else float("nan"))
    )

if __name__ == "__main__":
    with warnings.catch_warnings():
        warnings.simplefilter("ignore")
        main()
```

18.6 Listing S5. `Capture_kinetics`: Adler-flow simulation for slow-phase capture, coherence build-up, and scaling-law prevalidation (Fig. F1).

The Python script below reproduces Fig. F1. It simulates an Adler-like flow for the slow phase, computes a coherence proxy $\Lambda(t)$ with sliding-window smoothing, enforces a preregistered entry criterion (signal $< 15\%$ of the plateau for $\geq 5\,\mathrm{s}$), fits a single-pole approach to estimate the time constant τ, and reports $T_{\mathrm{lock}} = -\ln(1-0.8)\,\tau$. The grid is expanded across $(f_{\mathrm{slow}}, \kappa, \delta)$ with n replicates per cell; medians (and IQRs) are used per cell, and deterministic per-cell seeds based on $(f, \kappa, \delta, \mathrm{rep})$ ensure exact reproducibility. In our *in silico* validation, the lock time scaled with the predicted abscissa as $T_{\mathrm{lock}} \propto \left[f_{\mathrm{slow}}\sqrt{\kappa^2-\delta^2}\right]^s$. Across the expanded grid, ordinary least squares on the log–log data yielded $s = 1.17$ with $R^2 = 0.59$, while a weighted fit that accounts for heteroscedasticity using weights $\propto 1/\mathrm{IQR}^2$ gave $s = 0.71$ with $R^2 = 0.56$. Nonparametric bootstrap 95% confidence intervals were [1.05, 1.32] for OLS and [0.25, 1.06] for the weighted fit (see Supplementary File `capture_scaling_slope.txt`).

Listing 1: Minimal realistic assay for capture kinetics and scaling (Listing S5).

```
# Minimal in-silico prevalidation for capture kinetics
# Expanded grid + replicates + weighted regression + bootstrap CIs
# Saves PNG/CSV/TXT to a folder and also displays figures.
# Comments in professional English for inclusion in the paper.

import os, csv, math, numpy as np
import matplotlib as mpl; mpl.rcdefaults()
import matplotlib.pyplot as plt
from numpy.linalg import lstsq
import hashlib

# ---------- deterministic seeding (reproducible per grid cell)
   ----------
MASTER_SEED = 12345
def deterministic_seed(f, k, r, rep, master=MASTER_SEED):
    msg = f"{f:.9f}|{k:.9f}|{r:.9f}|{rep}|{master}".encode()
    h = hashlib.blake2b(msg, digest_size=8).digest()
    return int(np.frombuffer(h, dtype=np.uint64)[0] & np.uint64(0
       xFFFFFFFF))

# ---------- SDE (Adler-like phase model) ----------
def simulate_adler(fslow, kappa, delta, D=2e-4, dt=1/200, T=360,
   seed=None):
    """
␣␣␣␣Simulate␣an␣Adler-like␣SDE␣for␣a␣phase␣variable:
␣␣␣␣␣␣␣␣dphi␣=␣2*pi*fslow*(delta␣-␣kappa*sin(phi))*dt␣+␣sqrt(2*D)*
   dW
␣␣␣␣Returns␣the␣phase␣trajectory␣and␣the␣time␣step␣used.
␣␣␣␣"""
    rng = np.random.default_rng(seed)
    n = int(T/dt)
    phi = 2*np.pi*rng.random()
    phi_traj = np.empty(n, dtype=np.float64)
```

```
    drift = 2*np.pi*fslow
    sdt = math.sqrt(dt); rt2D = math.sqrt(2*D)
    for i in range(n):
        dphi = drift*(delta - kappa*np.sin(phi))*dt + rt2D*sdt*rng
           .normal()
        phi = (phi + dphi + np.pi)%(2*np.pi) - np.pi
        phi_traj[i] = phi
    return phi_traj, dt

# ---------- coherence proxy Lambda(t) ----------
def lambda_trace(phi, fs, W=10.0):
    """
␣␣␣␣Proxy␣for␣coherence␣rise:␣smooth␣cos(phi)␣with␣a␣W-second␣
   uniform
␣␣␣␣window␣to␣emulate␣a␣single-pole␣approach␣to␣a␣plateau.
␣␣␣␣"""
    import scipy.ndimage as nd
    x = np.cos(phi)
    L = max(1, int(W*fs))
    return nd.uniform_filter1d(x, size=L, mode="nearest")

# ---------- T_lock via exponential fit ----------
def tlock_from_exp(trace, fs, frac=0.8, entry_frac=0.15,
   entry_min_sec=5.0, fit_window_sec=20.0):
    """
␣␣␣␣Enforce␣entry␣criterion␣(trace␣must␣remain␣below␣entry_frac*
   plateau␣for␣>=␣entry_min_sec),
␣␣␣␣then␣fit␣a␣single-pole␣approach␣y(t)␣=␣P␣-␣A*exp(-t/tau)␣using
   :
␣␣␣␣␣␣␣␣ln(P␣-␣y)␣=␣ln(A)␣-␣t/tau
␣␣␣␣Return␣T_lock␣=␣-ln(1-frac)*tau,␣or␣np.nan␣if␣conditions␣are␣
   not␣met.
␣␣␣␣"""
    P = np.nanmedian(trace[-int(20*fs):])  # robust plateau proxy
    if not np.isfinite(P) or P == 0:
        return np.nan
    target_entry = entry_frac * P
    below = trace < target_entry
    run, t0_idx = 0, None
    for i, ok in enumerate(below):
        run = run + 1 if ok else 0
        if run >= int(entry_min_sec*fs):
            t0_idx = i
            break
    if t0_idx is None:
        return np.nan
    Tw = max(int(fit_window_sec*fs), 1)
    t = np.arange(t0_idx, min(len(trace), t0_idx+Tw)) / fs
    y = trace[t0_idx: min(len(trace), t0_idx+Tw)]
    Z = P - y
    mask = np.isfinite(Z) & (Z > 0)
```

```
    if mask.sum() < 30:
        return np.nan
    X = np.vstack([np.ones(mask.sum()), t[mask]]).T
    b, *_ = lstsq(X, np.log(Z[mask]), rcond=None)   # ln(Z) = b0 +
        b1 t
    b1 = b[1]
    tau = -1.0/b1 if b1 < 0 else np.nan
    if not np.isfinite(tau) or tau <= 0:
        return np.nan
    return float(-np.log(1.0 - frac) * tau)

# ---------- log-log fits ----------
def loglog_fit_ols(xs, ys):
    """Ordinary␣least-squares␣slope,␣intercept,␣R^2␣for␣y␣~␣x^s␣(
       log-log)."""
    lx, ly = np.log(xs), np.log(ys)
    A = np.vstack([np.ones_like(lx), lx]).T
    beta, *_ = lstsq(A, ly, rcond=None)
    intercept, slope = float(beta[0]), float(beta[1])
    yhat = A @ beta
    ss_res = float(np.sum((ly - yhat)**2))
    ss_tot = float(np.sum((ly - ly.mean())**2))
    r2 = 1.0 - ss_res/ss_tot if ss_tot > 0 else np.nan
    return slope, intercept, r2

def loglog_fit_wls(xs, ys, w):
    """Weighted␣least-squares␣on␣log-log␣with␣nonnegative␣weights␣
       w."""
    lx, ly = np.log(xs), np.log(ys)
    w = np.asarray(w, float)
    W = np.diag(w)
    A = np.vstack([np.ones_like(lx), lx]).T
    Aw = W @ A
    yw = W @ ly
    beta, *_ = lstsq(Aw, yw, rcond=None)
    intercept, slope = float(beta[0]), float(beta[1])
    yhat = A @ beta
    ly_bar = np.sum(w*ly)/np.sum(w)
    ss_res = float(np.sum(w*(ly - yhat)**2))
    ss_tot = float(np.sum(w*(ly - ly_bar)**2))
    r2 = 1.0 - ss_res/ss_tot if ss_tot > 0 else np.nan
    return slope, intercept, r2

def bootstrap_ci(xs, ys, fit_fn, w=None, n_boot=1000, seed=2025):
    """Nonparametric␣bootstrap␣95%␣CI␣for␣slope␣with␣fit_fn␣=␣OLS␣
       or␣WLS."""
    rng = np.random.default_rng(seed)
    n = len(xs)
    idx = np.arange(n)
    boots = []
    for _ in range(n_boot):
```

```
        sel = rng.choice(idx, size=n, replace=True)
        try:
            if w is None:
                s, _, _ = fit_fn(xs[sel], ys[sel])
            else:
                s, _, _ = fit_fn(xs[sel], ys[sel], w[sel])
            if np.isfinite(s):
                boots.append(s)
        except Exception:
            pass
    if len(boots) == 0:
        return np.nan, (np.nan, np.nan), np.array([])
    boots = np.array(boots, float)
    lo, hi = np.percentile(boots, [2.5, 97.5])
    return float(np.median(boots)), (float(lo), float(hi)), boots

# ---------- parameter grid ----------
SAVE_DIR = "./capture_kinetics_outputs"
os.makedirs(SAVE_DIR, exist_ok=True)

fslows = np.round(np.geomspace(0.07, 0.35, 6), 5).tolist()
kappas = np.round(np.geomspace(0.04, 0.2, 6), 5).tolist()
ratios = [0.20, 0.35, 0.50, 0.65, 0.75]     # avoid extreme edge
   near 1.0
REPLICATES = 16
NOISE_D    = 2e-4
T_OBS      = 360.0

records = []  # (f, k, r, delta, T_med, T_iqr, abscissa)

# ---------- run grid with deterministic seeds ----------
for f in fslows:
    for k in kappas:
        for r in ratios:
            delta = r*k
            tlocks = []
            for rep in range(REPLICATES):

                seed = deterministic_seed(f, k, r, rep)  #
                   deterministic per-cell seed
                phi, dt = simulate_adler(f, k, delta, D=NOISE_D,
                   dt=1/200, T=T_OBS, seed=seed)
                fs = int(1/dt)
                lam = lambda_trace(phi, fs=fs, W=10.0)
                tlocks.append(
                    tlock_from_exp(lam, fs=fs, frac=0.8,
                       entry_frac=0.15, entry_min_sec=5.0,
                       fit_window_sec=20.0)
                )
            tlocks = np.array(tlocks, float)
            T_med = float(np.nanmedian(tlocks))
```

```
            T_iqr = float(np.nanpercentile(tlocks, 75) - np.
               nanpercentile(tlocks, 25))
            x = 1.0/(f*np.sqrt(max(k*k - (r*k)*(r*k), 1e-12)))
            records.append((f, k, r, delta, T_med, T_iqr, x))

# ---------- save CSV ----------
csv_path = os.path.join(SAVE_DIR, "capture_kinetics_grid_median.
   csv")
with open(csv_path, "w", newline="") as fh:
    w = csv.writer(fh)
    w.writerow(["fslow","kappa","ratio","delta","Tlock_median","
       Tlock_IQR","abscissa"])
    w.writerows(records)

# ---------- Figure 1:  Lambda(t) example ----------
plt.figure()
plt.plot(lam)
plt.xlabel("samples")
plt.ylabel("coherence␣proxy")
plt.title(r"Example␣$\Lambda(t)$␣proxy")
plt.tight_layout()
fig1_path = os.path.join(SAVE_DIR, "
   capture_lambda_timeseries_realistic.png")
plt.savefig(fig1_path, dpi=220)
plt.show()

# ---------- log-log scaling (median per cell) ----------
xs  = np.array([r[-1] for r in records], float)
ys  = np.array([r[4]  for r in records], float)     # median
   T_lock
iqr = np.array([r[5]  for r in records], float)

mask = np.isfinite(xs) & np.isfinite(ys) & (xs > 0) & (ys > 0)
xs_f, ys_f, iqr_f = xs[mask], ys[mask], iqr[mask]

# OLS
s_ols, b0_ols, r2_ols = loglog_fit_ols(xs_f, ys_f)
med_ols, (lo_ols, hi_ols), _ = bootstrap_ci(xs_f, ys_f,
   loglog_fit_ols, n_boot=1000, seed=2025)

# WLS: weights = 1/(IQR**2) (proxy for precision), regularized and
    clipped
eps = np.maximum(1e-6, np.nanpercentile(iqr_f, 5))
w_raw = 1.0/np.maximum(iqr_f, eps)**2
w = w_raw / np.max(w_raw)
w = np.clip(w, 0.05, 1.0)
s_wls, b0_wls, r2_wls = loglog_fit_wls(xs_f, ys_f, w)
med_wls, (lo_wls, hi_wls), _ = bootstrap_ci(xs_f, ys_f,
   loglog_fit_wls, w=w, n_boot=1000, seed=3030)

# Plot + lines
```

```
plt.figure()
plt.loglog(xs_f, ys_f, 'o', alpha=0.8, label="grid medians")
xf = np.linspace(xs_f.min(), xs_f.max(), 300)
yf_ols = np.exp(b0_ols) * xf**s_ols
yf_wls = np.exp(b0_wls) * xf**s_wls
plt.loglog(xf, yf_ols, '-', label=fr'OLS slope {s_ols:.2f}, $R^2$ {r2_ols:.2f}')
plt.loglog(xf, yf_wls, '--', label=fr'WLS slope {s_wls:.2f}, $R^2$ {r2_wls:.2f}')
plt.xlabel(r'$[f_{\rm slow}\sqrt{\kappa^2-\delta^2}]^{-1}$')
plt.ylabel(r'$T_{\rm lock}$ (s)')
plt.legend()
plt.tight_layout()
fig2_path = os.path.join(SAVE_DIR, "capture_scaling_loglog_realistic.png")
plt.savefig(fig2_path, dpi=220)
plt.show()

# ---------- TXT with both fits + bootstrap CIs ----------
slope_txt_path = os.path.join(SAVE_DIR, "capture_scaling_slope.txt")
with open(slope_txt_path, "w") as fh:
    fh.write("Log-log scaling for T_lock vs [f_slow * sqrt(kappa^2 - delta^2)]^{-1}\n")
    fh.write(f"Cells used (medians): {xs_f.size}\n")
    fh.write("\nOLS fit:\n")
    fh.write(f"  Slope: {s_ols:.6f}\n  R^2: {r2_ols:.6f}\n")
    fh.write(f"  Bootstrap median slope: {med_ols:.6f}\n")
    fh.write(f"  Bootstrap 95% CI: [{lo_ols:.6f}, {hi_ols:.6f}]\n")
    fh.write("\nWLS fit (weights = 1/(IQR^2), clipped):\n")
    fh.write(f"  Slope: {s_wls:.6f}\n  R^2: {r2_wls:.6f}\n")
    fh.write(f"  Bootstrap median slope: {med_wls:.6f}\n")
    fh.write(f"  Bootstrap 95% CI: [{lo_wls:.6f}, {hi_wls:.6f}]\n")
    fh.write(f"\nReplicates per cell: {REPLICATES}\nNoise D: {NOISE_D}, Observation T (s): {T_OBS}\n")
    fh.write("Entry criterion: <15% of plateau for >=5 s; fit window: 20 s; "
             "plateau = median of last 20 s.\n")

print("Saved outputs to:", os.path.abspath(SAVE_DIR))
print(" -", os.path.basename(fig1_path))
print(" -", os.path.basename(fig2_path))
print(" -", os.path.basename(csv_path))
print(" -", os.path.basename(slope_txt_path))
```

19 Glossary of symbols

This appendix summarizes the main symbols used in the slow-phase locking analysis, the coherence readout Λ, and the phase-targeted entrainment protocol. Unless noted

otherwise, quantities are evaluated under neutral-moment strobing (even parity) and at the mesoscale wavenumber $k^* = \pi/\ell$.

Table 6: Dynamical / locking variables (core): slow cadence, slow-phase map parameters, and slow-band coherence.

Symbol	**Units**	**Meaning / operational definition**
$V(\mathbf{x}, t)$	arb. units	Bioelectric field / membrane potential readout (optical electrophysiology).
$\sigma(\mathbf{x}, t)$	Pa (stress)	Cortical / tensional stress field inferred from traction force microscopy, AFM, etc.
$u(\mathbf{x}, t)$	m	Latent in-plane cortical displacement from which σ is defined.
f_-, f_+	Hz	Carrier frequencies of the two weakly coupled underdamped *latent* modes in the fast band (typically 1–3 Hz).
f_{slow}	Hz	Slow interference cadence, $\lvert f_+ - f_- \rvert$; appears as a shared slow-band peak in V and σ.
r_{eff}	–	Carrier ratio $r_{\text{eff}} = \Omega_-/\Omega_+$ (often $\approx f_-/f_+$ when carriers are well resolved); used to estimate the slow forcing Ω.
Ω	rad	Effective slow-phase forcing in the even (mod π) map, estimated from neutral-moment stroboscopy; operationally $\Omega \simeq \frac{\pi}{2}(1 - r_{\text{eff}})$.
K_2	rad	Even-harmonic coupling strength in the slow-phase map, obtained by regressing $\Delta\theta_n$ onto $\sin(2\theta_n)$ at neutral moments.
θ_n	rad	Fast "+" carrier phase sampled at successive neutral moments (near-symmetric crossings with $\psi \equiv 0 \bmod \pi$ and positive slope); in the even convention $\theta \sim \theta + \pi$.
$\Delta\theta_n$	rad	One-step slow-phase increment, $\theta_{n+1} - \theta_n$ (unwrapped across successive neutral moments).
Λ	–	Slow-band electromechanical coherence, $\Lambda \equiv C_{V\sigma}(f_{\text{slow}}) \in [0, 1]$. High Λ: V and σ share the slow cadence; low Λ: drift / loss of coordination.

Table 7: Latent-mode parameters used in the fast-band generator (Eqs. 1–4).

Symbol	**Units**	**Meaning / operational definition**
α_1, α_2	s^{-1}	Damped decay rates of the two latent modes.
ω_1, ω_2	rad/s	Damped (unmixed) carrier angular frequencies of the latent modes.
J	s^{-1}	Complex coupling between the modes (magnitude sets the split/lock threshold).
h_{V1}, h_{V2}	–	Complex projection gains from latent modes to the V channel.
h_{S1}, h_{S2}	–	Complex projection gains from latent modes to the σ channel.

Symbol	Units	Meaning / operational definition
$\Omega_\pm$	rad/s	Observable damped carriers (imaginary parts of the exponents $s_\pm$); $f_\pm = \Omega_\pm/(2\pi)$.
$f_\pm$	Hz	Carrier frequencies.

Table 8: Cycle-resolved and slow-drift metrics from Appendix E: neutral-crossing windows around τ_n, pre-crossing drift $D_{\text{pre}}(n)$, and sliding-window trajectory $(\widehat{\Omega}_n, \widehat{K}_{2,n})$ used to assess repeated re-entry into the 2/21 tongue.

Symbol	Units	Meaning / operational definition
$\mathcal{A}_n, \mathcal{B}_n, \mathcal{C}_n$	s	Short windows around a neutral crossing τ_n (Appendix E). $\mathcal{A}_n$: approach; $\mathcal{B}_n$: the neutral crossing; $\mathcal{C}_n$: immediate relaxation. Used to compute local coherence and reset ratios.
$D_{\text{pre}}(n)$	rad/s	Pre-crossing slow-phase drift magnitude, $D_{\text{pre}}(n) = \langle \lvert\dot{\psi}_{\text{slow}}(t)\rvert \rangle_{t\in\mathcal{A}_n}$. Large values indicate accumulated phase error just before τ_n.
$\widehat{\Omega}_n, \widehat{K}_{2,n}$	rad	Sliding-window estimates of forcing and even-harmonic coupling from fits of $\Delta\theta_j = \Omega_n - K_{2,n}\sin(2\theta_j)$ over N_{win} successive crossings ending at τ_n.

Table 9: Cycle-resolved diagnostics: angular stability Var_{map}, neutral-crossing reset ratio R_{reset}, phase offset $\psi(t)$, and locked winding number ρ_π.

Symbol	Units	Meaning / operational definition
Var_{map}	rad^2	Variance of the neutral stroboscopic increment $\theta_{n+1} - \theta_n$; proxy for spindle-orientation noise.
R_{reset}	–	Reset ratio $R_{\text{reset}}(n) = \Lambda_{\text{local}}(\mathcal{B}_n)/\Lambda_{\text{local}}(\mathcal{A}_n)$ (Appendix E). > 1 indicates re-synchronization at the neutral crossing.
$\psi(t)$	rad	Instantaneous phase difference $\psi = \phi_V - \phi_\sigma$ between V and σ (Hilbert phases). $\psi \equiv 0 \bmod \pi$ with positive slope defines a neutral crossing.
ρ_π	–	Locked winding number in the even (mod π) convention; physiological plateau $\rho_\pi = 2/21$.

Table 10: Material / biophysical parameters and readouts: couplings, spectra, coherence, and geometric projections.

Symbol	Units	Meaning / operational definition
ℓ	m	Effective cortical (shell) thickness setting the mesoscale.
k^*	m^{-1}	Mesoscale wavenumber where carriers are evaluated: $k^* = \pi/\ell$.

Symbol	Units	Meaning / operational definition
D_V	m^2/s	Effective voltage diffusivity / gap-junctional spread parameter.
τ_m	s	Membrane (RC) charging time.
κ	N/m	Effective surface (area) elastic modulus / in-plane tension modulus of the cortex.
η	$N \cdot s/m$	Effective cortical surface viscosity (loss).
D_σ	m^2/s	Effective stress diffusion / mechanical spreading.
β_R, β_I	V/Pa (or eq.)	In-phase (β_R) and quadrature (β_I) components of mechanical→electrical coupling.
γ	m/V (or Pa/V)	Electrical→mechanical coupling gain (drive of V onto cortical displacement/stress).
ϕ_c	rad	Electromechanical coupling phase, $\phi_c = \arg(\beta_R + i\beta_I)$.
$\chi_\pm$	–	Stress-weighted projection factors (mode–geometry overlap) that map $U_\pm(\mathbf{x})$ onto the helical advance direction $h(\mathbf{x})$ (Sec. 14).
$C_{V\sigma}(f)$	–	Magnitude-squared coherence between V and σ at frequency f.
$S_V(f)$, $S_\sigma(f)$	arb. units	Power spectral densities (Welch) of V and σ.
$S_V^{\text{slow}}(f)$, $S_\sigma^{\text{slow}}(f)$	arb. units	Slow-band spectra near f_{slow}.
c, c'	m/s	Derived effective propagation speeds $c = \chi_+ \, v_+(k^*)$, $c' = \chi_- \, v_-(k^*)$ with $v_\pm = \omega_{\pm,r}(k^*)/k^*$; reported for continuity, not used to select tongues.

Table 11: Locking geometry and quantitative criteria (Sec. 8) together with experimental variables for phase-targeted entrainment (Appendices F–G).

Symbol	Units	Meaning / operational definition
Locking geometry and quantitative criteria (Sec. 8)		
$\Omega_{2/21}$	rad	Tongue center for the 2/21 lock in the even (mod π) map: $\Omega_{2/21} = \pi \cdot 2/21 \approx 0.2992$.
q	–	Denominator of the rational p/q (even map). "Low order" means $q \leq 6$.
d_Ω	rad	Distance in Ω to the nearest $q \leq 6$ tongue *center* (or to the overlapping *boundary* if local overlaps occur). Used in the P2 criterion.
σ_Ω	rad	Uncertainty of $\widehat{\Omega}$ from neutral-moment, cycle-resolved sampling (robust SE across windows).
$P_{2/21}$	–	Monte Carlo probability (under physiological priors) that (Ω, K_2) lies inside the 2/21 tongue; P2 requires $P_{2/21} \geq 0.30$.
p_{re}	–	Per-cycle re-entry fraction into the 2/21 tongue (Appendix E), estimated from the rolling trajectory $(\widehat{\Omega}_n, \widehat{K}_{2,n})$.
Experimental variables for phase-targeted entrainment (Appendices F–G)		

Symbol	Units	Meaning / operational definition
f_{drive}	Hz	Drive frequency set near f_{slow} (on-band) as predicted by (Ω, K_2).
f_{ctrl}	Hz	Off-resonant control: $f_{\text{ctrl}} = f_{\text{slow}}(1+\delta)$ with $\delta \in [0.10, 0.25]$, energy-matched.
parity	–	Stroboscopic parity (even: neutral-moment sampling; odd: full-cycle). Internal on/off control.
RMS	various	Root-mean-square amplitude of electrical field (mV/mm) or mechanical strain (%); same RMS for on-band and off-band.
duty	%	Duty cycle of stimulation blocks (e.g., 50–70%).
ROI	–	Region of interest chosen by neutral-moment stroboscopy (high local voltage/flow power).
N_{win}	–	Window length (number of successive neutral crossings) for sliding estimates $(\widehat{\Omega}_n, \widehat{K}_{2,n})$.

Acknowledgments

This manuscript was prepared with the assistance of AI-based editing and drafting tools. The author retains full responsibility for the analysis, interpretation, and any errors.

References

[1] S. H. Strogatz, *Nonlinear Dynamics and Chaos*, Westview Press (2018).

[2] V. I. Arnold, Small denominators and problems of stability of motion in classical and celestial mechanics, *Russian Mathematical Surveys* **18** (1963) 85–191.

[3] M. Levin, Bioelectric signaling: Reprogrammable circuits governing growth and form, *Cell* **184** (2021) 197–205.

[4] G. Shim, I. B. Breinyn, A. Martínez-Calvo, S. Rao, and D. J. Cohen, Bioelectric stimulation controls tissue shape and size, *Nature Communications* **15** (2024) 2938.

[5] J. Cervera, M. Levin, and S. Mafé, Multicellular adaptation to electrophysiological perturbations analyzed by deterministic and stochastic bioelectrical models, *Scientific Reports* **14** (2024) 27608.

[6] E. K. Paluch, I. M. Aspalter, and M. Sixt, The actin cortex as a force generator in animal cells, *Nature Reviews Molecular Cell Biology* **17** (2016) 733–747.

[7] L. G. Lippincott-Schwartz *et al.*, Cellular mechanisms of tissue morphogenesis, *Science* **362** (2018) eaat1551.

[8] B. B. Machta *et al.*, Mechanics and active fluctuations of the cell cortex, *Annual Review of Condensed Matter Physics* **10** (2019) 325–344.

[9] V. I. Arnol'd, Small denominators. I. Mappings of the circle onto itself, *Amer. Math. Soc. Transl. (2)* **46** (1965) 213–284. [Original: *Izv. Akad. Nauk SSSR Ser. Mat.* **25** (1961) 21–86.]

[10] A. Pikovsky, M. Rosenblum, J. Kurths, *Synchronization: A Universal Concept in Nonlinear Sciences*, Cambridge University Press, Cambridge (2001).

[11] R. K. Aaron, D. M. Ciombor, B. J. Simon, Treatment of nonunions with electric and electromagnetic fields, *Clinical Orthopaedics and Related Research* **419** (2004) 21–29.

[12] T. Gordon, N. Amirjani, D. C. Edwards, K. M. Chan, Brief post-surgical electrical stimulation accelerates axon regeneration and muscle reinnervation without affecting functional measures in carpal tunnel syndrome patients, *Experimental Neurology* **223** (2010) 192–202.

[13] H.-M. Lim, M.-H. Nam, Y.-M. Kim, Y.-K. Seo, Increasing odontoblast-like differentiation from dental pulp stem cells through increase of β-catenin/p-GSK-3β expression by low-frequency electromagnetic field, *Biomedicines* **9** (2021) 1049.